Geochimica et Cosmochimica Acta

JOURNAL OF THE GEOCHEMICAL SOCIETY

xecutive
Editors

C. W. CORRENS, *Göttingen.* E. INGERSON, *Austin, Texas.* L. R. WAGER, *Oxford.*

ditors

L. H. AHRENS, *Capetown.* S. R. NOCKOLDS, *Cambridge.* H. C. UREY, *La Jolla, Calif.*
JOHN VERHOOGEN, *Berkeley, Calif.* A. P. VINOGRADOV, *Moscow.*
W. A. WAHL, *Helsingfors.*

CONTENTS VOLUME 19, NO. 1 MARCH 1960

P. W. GAST: Alkali metals in stone meteorites 1
R. E. MARINGER: Ablation deposits on iron meteorites 5
H. W. FAIRBAIRN, W. H. PINSON, P. M. HURLEY and R. F. CORMIER: A comparison of the ages of coexisting biotite and muscovite in some paleozoic granite rocks 7
W. G. ERNST: The stability relations of magnesioriebeckite 10
R. D. RUSSELL and R. M. FARQUHAR: Dating galenas by means of their isotopic constitutions—II 41
E. ANDERS: The record in the meteorites—II. On the presence of aluminium-26 in meteorites and tektites 53
E. A. VINCENT and L. I. BILEFIELD: Cadmium in rocks and minerals from the Skaergaard intrusion, East Greenland 63
H. FECHTIG, W. GENTNER und J. ZÄHRINGER: Argonbestimmungen an Kaliummineralien—VII. Diffusionsverluste von Argon in Mineralien und ihre Auswirkung auf die Kalium–Argon–Altersbestimmung 70
Book Reviews:
Osnovy Litologii i Geokhimii Kory Vyvetrivaniya (Fundamentals of the Lithology and Geochemistry of the Weathering Zone), by K. I. Lukashev. (Reviewed by W. D. Romey) 80
Clays and Clay Minerals: Proceedings of the Sixth National Conference on Clays and Clay Minerals. Edited by Ada Swineford. (Reviewed by E. C. Jonas) 81
Meeting Announcements 82
Papers to be published in future issues 83

PERGAMON PRESS NEW YORK • LONDON • PARIS • LOS ANGELES

GEOCHIMICA ET COSMOCHIMICA ACTA

EXECUTIVE EDITORS

PROF. C. W. CORRENS (1959) *Sedimentpetrographisches Institut der Universität, Lotzestr.* 13, *Göttingen, Germany*
PROF. E. INGERSON (1959–1960) *Department of Geology, University of Texas, Austin* 12, *Texas, U.S.A.*
PROF. L. R. WAGER, F.R.S. (1959–1961) *Department of Geology and Mineralogy, The University Museum, Oxford, England*

EDITORS

PROF. L. H. AHRENS (1959–1960) *Department of Chemistry, University of Capetown, Rondebosch, Cape Province, South Africa*
Dr. S. R. NOCKOLDS *Department of Mineralogy and Petrology, The University, Cambridge, England*
PROF. H. C. UREY, For. Mem. R. S. (1959) *University of California, La Jolla, California, U.S.A.*
Dr. JOHN VERHOOGEN (1959–1961) *Department of Geology, University of California, Berkeley, California, U.S.A.*
PROF. A. P. VINOGRADOV (1959–1961) *Vernadsky Institute, Moscow, U.S.S.R.*
PROF. W. A. WAHL (1959–1961) *Observatoriegaten* 8, *Helsingfors, Finland*

EDITORIAL ADVISORY BOARD

AMERICAN CONTINENT

A. F. BUDDINGTON, *Princeton*
D. GUIMÃRAES, *Belo Horizonte*
G. E. HUTCHINSON, *New Haven*
B. H. MASON, *New York*
F. WHIPPLE, *Cambridge*
R. WILDT, *New Haven*
H. S. YODER, *Washington*

EUROPE

T. F. W. BARTH, *Oslo*
L. CAPDECOMME, *Toulouse*
E. J. CONWAY, *Dublin*
P. ESKOLA, *Helsinki*
P. GALLITELLI, *Modena*
A. HADDING, *Lund*
O. HAHN, *Göttingen*
H. W. HARVEY, *Plymouth*
F. HEIDE, *Jena*
A. HOLMES, *Edinburgh*
W. Q. KENNEDY, *Leeds*
PH. H. KUENEN, *Gröningen*
S. LANDERGREN, *Stockholm*
F. MASHATSCHKI, *Vienna*
A. MUIR, *Harpenden*
J. ORCEL, *Paris*
E. RAGUIN, *Paris*
E. REINHARD, *Basle*
TH. G. SAHAMA, *Helsinki*
C. E. TILLEY, *Cambridge*
T. VOGT, *Trondheim*

FAR EAST

T. WATANABE, *Tokyo*

Publishing Office: Pergamon Press, Inc., 122 East 55th Street, New York 22, N.Y. (Plaza 3-9651)

Four issues per volume, three volumes per year

Subscription *per annum* (including postage) (A) $51.00; (B) For individual subscribers who write directly to the publisher certifying that the Journal is for their private use, $21.50. Members of the Geochemical Society, or non-members who occasionally publish papers in the Journal, $10.00 *per annum*.

Back numbers, $28.00 per volume

Single issues, $7.00 each

PERGAMON PRESS, INC.

122 EAST 55TH STREET, NEW YORK 22, N.Y. 4 & 5 FITZROY SQUARE, LONDON W.1

PRINTED IN NORTHERN IRELAND AT THE UNIVERSITIES PRESS, BELFAST

INTERNATIONAL SERIES OF MONOGRAPHS ON EARTH SCIENCES

General Editor: Professor EARL INGERSON

Volume 1

CONTRIBUTIONS IN GEOPHYSICS

In Honor of Beno Gutenberg

Editors: **Hugo Benioff, Maurice Ewing, Benjamin F. Howell, Jr. and Frank Press**

Publication of this volume was planned to coincide with Dr. Gutenberg's retirement, because of age, from the directorship of the Seismological Laboratory of the California Institute of Technology. The diverse nature of the topics chosen by the contributors is a measure of the breadth of Dr. Gutenberg's interests; and the wide geographic distribution of the contributors' homes indicates the range of his influence.

60s. net ($9.00)

Volume 3

PRINCIPLES OF GEOCHEMICAL PROSPECTING

TECHNIQUES OF PROSPECTING FOR NON-FERROUS ORES AND RARE METALS

by **I. I. Ginzburg**

Translated from the Russian by **V. P. Sokoloff**

This book constitutes the first effort to cover the entire subject of geochemical prospecting comprehensively, including hydrochemical, biogeochemical and geobotanical methods. It begins with a brief history of the development of the subject and a discussion of the principles on which it is based, followed by a generalized treatment of the subject of geochemical indicators.

70s. net ($11.50)

Volume 4

OVERVOLTAGE RESEARCH AND GEOPHYSICAL APPLICATIONS

Edited by **James R. Wait**

This volume contains the results of the first concerted effort to apply the overvoltage phenomenon to geophysical prospecting, made by the geophysical laboratories of the Newmont Mining Company.

Written primarily for exploration geophysicists, it will nevertheless be of value to all earth scientists.

55s. net ($9.00)

Volume 5

CLAYS AND CLAY MINERALS

Proceedings of the Seventh National Conference on Clays and Clay Minerals

Edited by **Ada Swineford**

State Geological Survey, University of Kansas

A wide variety of topics was covered at the Seventh National Conference. The proceedings stress regional clay mineralogy, the effect of saline water on clay minerals, genesis and identification of soil clays, and viscosity of clay suspensions.

60s. net ($8.50)

Titles in preparation include:

ORGANIC GEOCHEMISTRY

Edited by **Irving A. Breger**

PRINCIPLES OF METEORITICS

by **E. L. Krinov**

U.S.S.R. Academy of Sciences

Write for fully descriptive leaflets

PERGAMON PRESS

OXFORD LONDON NEW YORK PARIS

Headington Hill Hall, Oxford
122 East 55th Street, New York 22, N.Y.

4 & 5 Fitzroy Square, London W.1
24 Rue des Écoles, Paris V^e^

The Study of Elementary Particles by the Photographic Method

An account of the Principal Techniques and Discoveries illustrated by

AN ATLAS OF PHOTOMICROGRAPHS

by C. F. POWELL, P. H. FOWLER and D. H. PERKINS

H. H. Wills Physical Laboratory, University of Bristol

This book describes the development of the photographic method of recording the tracks of charged particles, including the technical methods employed in its application to the discovery of mesons, hyperons and anti-nucleons, and the elucidation of their properties.

The illustrations are on a lavish scale, and include many photographs of historical interest, together with others, hitherto unpublished, which show the great range of phenomena produced in the nuclear interactions of particles with energy in the range between 10^3 and 10^6 BeV.

Outstanding Nobel Prize-Winner Professor Powell and his co-authors have written this book in a style and at a level suitable for post-graduate students in physics, but much of the material would be useful to students in their final year of an Honours course.

Sections:

1 History of the method
2 Basic technical features of nuclear emulsions
3 Methods of measurement
Length and direction of tracks; the range-energy relation
Measurement of track density
4 Methods of measurement (*continued*)
Measurement of scattering
Other methods
5 Identification of charged particles
6 Electrons and gamma-rays
7 Mu-mesons
8 Pi-mesons
9 Heavy or kappa-mesons
10 Kappa-mesons (*continued*)
11 Hyperons and hypernuclei
12 Anti-protons
13 Disintegrations due to protons with energy between 100 and 30,000 MeV
14 Collisions of fast mesons and anti-nucleons with nuclei
15 Nuclear collisions at energies greater than 50 BeV
16 Heavy nuclei of the cosmic radiation

Appendices

Shear distortion and 'chopping' in emulsion
Half-lives of long-lived alpha-emitters
Scanning by unaided eye

Index

£12 10s. net ($40)

670 pages *numerous illustrations* 11½″ × 8½″

PERGAMON PRESS

OXFORD LONDON NEW YORK PARIS

Headington Hill Hall, Oxford
122 East 55th Street, New York 22, N.Y.
4 & 5 Fitzroy Square, London W.1
24 Rue des Écoles, Paris Ve.

Geochimica et Cosmochimica Acta, 1960, Vol. 19, pp. 1 to 4. Pergamon Press Ltd. Printed in Northern Ireland

5856-2 9A

Alkali metals in stone meteorites

P. W. GAST*
Lamont Geological Observatory,†
Columbia University, Palisades, N.Y.

(*Received* 6 *July* 1959)

THE elements potassium, rubidium and caesium form a group of geochemically similar elements. Because of this similarity and because both rubidium and potassium have radioactive isotopes useful in measuring geologic and cosmic time, there has been considerable interest in these three elements. The main object of the work reported here was to investigate rubidium and caesium abundances in meteorites, particularly in the calcium-rich achondrites.

A number of recent determinations of these elements are available; however, with the exception of Pasamonte, no data on the rubidium and caesium content of achondrites are available. There are some obvious disagreements even among the most recent measurements. First, the caesium content of chondrites reported by GORDON *et al.* (1958) is significantly higher than that reported by WEBSTER *et al.* (1958); also the rubidium content of Forest City determined by HERZOG and PINSON (1956) and SCHUMACHER (1957) seems higher than that of WEBSTER *et al.* (1958).

The measurements reported here were made by the method of stable isotope dilution. Tracer solutions of K^{41}, Rb^{87} and Cs^{137}, were calibrated against standard solutions of these elements. (Caesium-137 is radioactive with a 30 year half-life. In this application its radioactivity is incidental, its isotopic abundance was determined on a mass spectrometer just like that of rubidium and potassium.) Known amounts of these tracers were added to solutions of the samples. The alkali metals were precipitated with sodium tetraphenyl boron and separated from each other on an ion exchange column. A fraction of the potassium was combined with the total rubidium and analysed isotopically in a mass spectrometer with a surface emission ion source. Ion currents of 10^{-14} A of Cs^{137} could be obtained from less than 0·1 μc of Cs^{137}.

All individual determinations and blank determinations made in this study are given in Table 1. The uncertainties given arise from uncertainties in the blank and uncertainties in the isotope ratios. Where duplicate analyses were made, they are in good agreement. Previous determinations of potassium, rubidium, and caesium in these meteorite samples are also given in Table 1. It is important to note that with the exception of Pasamonte, these comparisons are made on different samples of the same meteorites. The average concentrations of rubidium and caesium in chondrites found here agree quite well with those found by WEBSTER *et al.* (1958).

* Present address, Department of Geology and Mineralogy, University of Minnesota, Minneapolis, Minn.

† Lamont Geological Observatory, Contribution No. 382.

Table 1. The potassium, rubidium and caesium content of chondrites and calcium-rich achondrites. When available, data of other workers are given for comparison. Numbers in parentheses refer to list of references.

	Potassium (p.p.m.)	Rubidium (p.p.m.)	Caesium (p.p.m.)	K/Rb	K/Cs
Chondrites					
Forest City*	820 ± 14	2·75 ± 0·04	106 ± 7	298	7750
ANHM 2406	840 (2)	2·9 (6)	100 (6)		
		3·5 (4)			
		3·9 (3)			
Beardsley†	917 ± 13	4·90 ± 0·06	193 ± 15	186	4700
Nininger 1349	895 ± 16	4·83 ± 0·06	913 (5)		
	1020 (1)				
Richardton†	818 ± 12	2·96 ± 0·035	88 ± 6	276	9300
Nininger 100	830 (1)				
Holbrook*	—	2·22 ± 0·04	146 ± 10	396	6000
ANHM 1162	880 (1)	2·3 (b)	489 (5)		
			280 (6)		
Modoc*	—	3·45 ± 0·06	90 ± 7	258	9850
ANHM 2443	890 (2)		80 (6)		
Achondrites					
Pasamonte‡	436 ± 13	0·21 ± 0·03	11·4 ± 1	2000	38,000
(white fraction)	413 ± 12	0·21 ± 0·02	11·0 ± 1		
	430 (7)	0·51 (3)	284 (5)		
	520 (2)				
Nuevo Laredo§	376 ± 13	0·38 ± 0·02	16 ± 3	990	15,000
	358 ± 16	0·36 ± 0·02	21 ± 1·5		
	470 (2)				
Sioux County†	322 ± 20	0·18 ± 0·06	11·8 ± 1	1250	27,500
Nininger 298	347 ± 12	0·29 ± 0·02			
Moore County**	187 ± 15	0·16 ± 0·03	5·2 ± 0·7	1200	36,000

Blank determinations (μg)	Potassium (μg)	Rubidium (μg)	Caesium (μg)
	16, 22, 18, 16	0·026, 0·019, 0·015	0·00035

* Furnished by Dr. B. MASON, American Museum of Natural History, N.Y.
† Furnished by H. H. NININGER, American Meteorite Museum, Sedona, Ariz.
‡ Furnished by Professor H. C. UREY, University of California, LaJolla, Cal.
§ Furnished by Dr. C. C. PATTERSON, California Institute of Technology, Pasadena, California.
** Furnished by Dr. E. P. HENDERSON, U.S. Nat. Museum, Washington, D.C.

(1) EDWARDS (1955).
(2) EDWARDS and UREY (1955).
(3) SCHUMACHER (1956).
(4) HERZOG and PINSON (1956).
(5) GORDON *et al.* (1958).
(6) WEBSTER *et al.* (1958).
(7) GEISS and HESS (1958).

With the exception of caesium in Holbrook there is also good agreement for the individual samples. The sample of Pasamonte was obtained from Professor H. C. Urey. It was labelled "Pasamonte, white fraction", and is part of the powder studied first by Edwards (1955), then by Schumacher (1956), and subsequently by Gordon *et al.* (1958). The new determinations should be directly comparable with their determinations. The rubidium and caesium contents found here are lower than those reported by the above authors by factors of 2·5 and 25, respectively. The potassium content is lower than that found by Edwards (1955), but agrees very well with that found by Geiss and Hess (1958). The potassium content of Nuevo Laredo is also lower than that found by Edwards (1955) while the potassium content of Moore County agrees with that found by Geiss and Hess (1958).

In their study of thirty-nine chondrites, Edwards and Urey (1955) found that one chondrite, Beardsley, had a distinctly higher potassium content than the others. Although the potassium content found here is not quite as high as that reported by them, the unusually high rubidium content and the high caesium content further suggests that Beardsley is an unusual chondrite.

There appears to be no correlation between the rubidium and caesium content among the five chondrites analysed; in fact, if Beardsley is excepted, the highest rubidium occurs with one of the lowest caesium values in Modoc and the lowest rubidium occurs with the highest caesium in Holbrook. In contrast to the lack of correlation among the chondrites, there is a good correlation between the rubidium and caesium contents of the four achondrites. The correlation between potassium and rubidium is not as good as the caesium–rubidium correlation.

A comparison of the K/Rb and K/Cs ratios in the chondrites and the achondrites shows that they are strikingly different. The average K/Rb ratio for the chondrites given in Table 1 is 280. Using the average of all rubidium contents given by Webster *et al.* (1958) and an average potassium content of 850 p.p.m. (Edwards, 1955), a ratio of 330 is found, the difference resulting mainly from the one very low K/Rb ratio, Beardsley, in Table 1 and the one high K/Rb ratio, Bluff, in the work of Webster *et al.* (1958). The average K/Rb ratio of the four achondrites in Table 1 is 1360. The average K/Rb ratio of igneous and metamorphic rocks is about 300 (Horstman, 1957). The highest ratio among the ninty-four samples analysed is 480. If certain types of pegmatities are ignored, the fractionation of the K/Rb ratios during igneous processes appears to be quite limited. Extremely high K/Rb ratios might conceivably be found in very early crystallizing fractions or as a result of succesive fractionations, but such early fractions would be relatively small compared to the total amount of material involved and would also have rather distinctive compositions. The achondrites do not fit this picture; the high aluminium, strontium and barium contents are in conflict with any hypothesis explaining the high K/Rb ratios in terms of igneous differentiation.

The average K/Cs ratio of the five chondrites in Table 1 is 7500, while that of Webster *et al.* (1958) is 9400. In view of the variability of the caesium content of chondrites these averages are in satisfactory agreement. Using an average ratio of 8500 for chondrites, the average K/Cs ratio of the four achondrites is 3·4 times higher than that of the chondrites. Although individual chondrites

(WEBSTER *et al.*, 1958) have K/Cs ratios higher than those found for the achondrites, the difference between the two types seems significant and related to the high K/Rb ratios in these objects.

The lower abundance of potassium, rubidium and caesium and the significant fractionation of the K/Rb and K/Cs ratios present an interesting problem. UREY (1957) has suggested that the low potassium content of the calcium-rich achondrites may be due to the loss of volatile compounds of these elements during superficial heating of larger objects. Such a process could be very effective in separating rubidium and caesium from potassium as a result of their different vapour pressures. Unfortunately, no measurements of the relative vapour pressures of these alkali metals or metal compounds in silicate mixtures are available. However, if the vapour pressures of the metals and of most simple compounds can be taken as an indication of the relative vapour pressures in silicates, it seems reasonable that rubidium and caesium would be volatilized to a greater degree than potassium. If this explanation is correct, the differences in relative abundance found here indicate a rather efficient fractionation process. Further work particularly on the relative volatility of these and other elements would be of particular interest. Perhaps this process may be of major importance in understanding the composition of the peculiar calcium-rich achondrites.

Acknowledgements—This work was supported by the National Science Foundation under Grant No. G3479. The co-operation of those people who furnished the samples for this study is gratefully acknowledged.

REFERENCES

EDWARDS G. (1955) *Geochim. et Cosmochim. Acta* **8,** 285.

EDWARDS G. and UREY H. C. (1955) *Geochim. et Cosmochim. Acta* **7,** 154.

GEISS H. and HESS D. C. (1958) *J. Astrophy. Soc.* **127,** 224.

GORDON B. M., FRIEDMAN L. and EDWARDS G. (1958) *Geochim. et Cosmochim. Acta* **12,** 170.

HERZOG L. F. and PINSON W. H. (1956) *Amer. J. Sci.* **259,** 555.

HORSTMAN E. (1957) *Geochim. et Cosmochim. Acta* **12,** 1.

SCHUMACHER E. (1956) *Helv. Chim. Acta* **36,** 538.

WEBSTER R. K. MORGAN and SMALES A. (1958) *Geochim. et Cosmochim. Acta* **15,** 150.

UREY H. C. (1957) Boundary conditions for theories of the origin of the solar system. *Physics and Chemistry of the Earth,* (Edited by AHRENS L., PRESS F., RANKAMA K. and RUNCORN S. K.) Vol. II. Pergamon Press, London.

Geochimica et Cosmochimica Acta, 1960, Vol. 19, pp. 5 to 6. Pergamon Press Ltd. Printed in Northern Ireland

Ablation deposits on iron meteorites*

R. E. MARINGER†
Metallurgical Engineering Divison, Battelle Memorial Institute

(*Received* 6 *July* 1959)

DURING the course of a larger study concerning the effects of aerodynamic heating suffered by iron meteorites during their passage through the atmosphere, it became necessary to assume a mechanism of ablation in order to calculate rates of heat flow through the meteorite surface. As ÖPIK (1958) has pointed out, it is believed that ablation of the larger meteorites can proceed by (1) direct vaporization, or by (2) the sweeping away of a molten surface layer. For purposes of analysis (MARINGER and MANNING, 1960) it is assumed that the latter mechanism predominates. There are some observational data which support this position.

Of eight irons examined during the course of this study, four (Grant, Costilla Peak, Keen Mountain, and Reed City) showed both visible structural alterations and hardness gradients near the meteorite surface, each of which can be definitely associated with the effects of aerodynamic heating. In addition, each of these irons displayed, at certain places on the surface, a metallic deposit which differed markedly from its substrate.

The deposit on the Costilla Peak was more abundant than on the other specimens. The extent to which it covered what is presumed (on the basis of flight marking and heat transfer calculations) to have been the trailing edge can be seen in the photograph of the slice shown in Fig. 1. It should also be noticed in this photograph that several of the visible cracks extend out to the meteorite surface. In most cases, there is no indication of any accelerated ablation at these points. This suggests that the cracks resulted from impact with the earth, and that since the cracks also appear to penetrate the ablation deposit, the deposit may have already solidified when impact occurred.

A higher magnification photograph of the deposit on Costilla Peak is shown in Fig. 2. The lamellar character of the deposit, and the abundance of entrapped oxides are clearly visible. This is true of the deposits found on each of the above-mentioned irons, although to a less obvious extent than on Costilla Peak. It is significant that, in each case, the deposit was found on a surface which had, on the average, the widest visible heat-affected zone for that particular meteorite. Since the widest zone indicates the lowest rate of heat transfer through the surface (MARINGER and MANNING, 1960) (i.e. less severe ablationary forces) it seems safe to assume that these deposits represent material from the frontal surface of the meteorite in flight which melted, was swept in waves across the surface by the flow of air around the specimen, and which froze in the position in which it was observed.

* This research was supported in whole or in part by the United States Air Force under Contract No. AF 33(616)-5080, monitored by the Aeronautical Research Laboratory, Wright Air Development Center.

† Assistant Chief, Metallurgical Engineering Division, Battelle Memorial Institute, Columbus, Ohio, U.S.A.

None of the remaining four irons (Social Circle, Kenton County, Odessa, and Misteca) showed any evidence of either aerodynamic heating, or of an ablation deposit. This suggests that the samples examined either represent meteorites which fragmented at a late stage in their flight through the atmosphere, or which have suffered rather severe corrosion or erosion since they fell.

The lamellar appearance, the abundance of oxide inclusions, and the location of these deposits do not appear to be consistent with an ablation mechanism occurring by direct vaporization. Therefore, at least during the final stages of flight, the ablation of iron meteorites appears to occur predominantly by the sweeping away of a molten surface layer.

References

Maringer R. E. and Manning G. K. (1960) Aerodynamic heating of the Grant Meteorite. *Geochim. et Cosmochim. Acta.* In press.

Öpik E. J. (1958) *Physics of Meteor Flight in the Atmosphere.* Interscience Tracts on Physics and Astronomy, No. 6. Interscience Publishers, New York.

Fig. 1. Slice from Costilla Peak meteorite. Note lamellar deposit along top edge of the slice (actual size).

Fig. 2. Ablation deposit on trailing edge of Costilla Peak meteorite. 20×.

Geochimica et Cosmochimica Acta, 1960, Vol. 19, pp. 7 to 9. Pergamon Press Ltd. Printed in Northern Ireland

A comparison of the ages of coexisting biotite and muscovite in some paleozoic granite rocks†

H. W. Fairbairn, W. H. Pinson, P. M. Hurley and R. F. Cormier‡
Massachusetts Institute of Technology, Cambridge, Mass.

(*Received* 20 *July* 1959)

During the past few years age studies of mica carried out by the geochronology laboratory at MIT have included a number of examples where both muscovite and biotite have been measured from the same rock by the Rb–Sr method. We are compiling here all of these scattered data in order to compare the precision of individual analysis with the difference between the micas of a pair. Ten of the eleven examples are from Paleozoic granitic rocks along the Atlantic seaboard (Nova Scotia, New Hampshire, and Georgia) and one is from mica schist (Connecticut). Six K–A ages of biotite are included for comparison with the Rb–Sr ages.

The pertinent data are in Table 1. Errors have been computed following the general method outlined by Fairbairn (1956). A 5 per cent error is considered to be normal in our laboratory and the table shows only three examples less than this. Where $*Sr^{87}/Sr$ is low, precision is also low. The "average" error of the mica ages here is ± 6 per cent.

The age differences in the members of a pair vary from 0 to 12·5 per cent and average less than 5 per cent. In the Georgia group (first part of Table 1) the differences are consistently less than the individual precision errors (B3173 excepted). Since the K–A age for this biotite, however, is in the direction of the Rb–Sr muscovite age, this departure from the trend of the other Georgia analyses may not be meaningful.

With one exception (3128 Ship Harbour) the Nova Scotia group follows the Georgia group trend fairly well. The Ship Harbour analyses show the single outstanding reversal. The K–A age of the biotite agrees closely with the Rb–Sr age, thus supporting the 12·5 per cent discrepancy with the muscovite age. Finally, the estimated precision errors do not overlap for this mica pair. The difference in age for this pair of micas thus seems to require a geochemical rather than an analytical explanation.

The single New Hampshire mica pair (1985) shows a smaller age difference than the individual estimated errors. In contrast the Bolton schist (3376A, Connecticut) has an intra-pair difference in excess of individual estimated error. However, the K–A age of the biotite is approximately the mean of the Rb–Sr ages of the micas, so that the comparison of individual error and difference may have no real meaning.

† MIT. Age Study no. 14.
‡ Present address, St. Francis Xavier University, Antigonish, N.S.

Table 1. Analytic and age data for mica pairs in granitic rocks

Sample no. and locality	*Sr^{87}/Sr (%)	*Sr^{87}/Rb^{87}	Sr/Rb age (million years)	% difference between members of a pair	A/K age (million years)	A^{40}/K^{40}
B3172 Stone Mt., Ga.	12	0·00394	283 ± 5%	4·0		
M3172	1·5	0·00383	272 ± 11%			
B3173 De Kalb Co., Ga.	2·7	0·00405	293 ± 5%	6·6	300	0·0191
M3173	1·0	0·00435	313 ± 15%			
B3174 Lithonia Gneiss De Kalb Co., Ga.	5·7	0·00399	287 ± 5%	1·0		
M3174	2·0	0·00402	288 ± 7%			
B3177 Elberton, Ga.	13	0·00353	254 ± 5%	3·6	235	0·0147
M3177	2·3	0·00341	245 ± 6%			
B1985 Concord, N.H.	1·5	0·00432	304 ± 8%	4·5		
M1985	1·5	0·00443	318 ± 8%			
B3376A Bolton Schist Strickland Quarry, Conn.	3·7	0·00334	240 ± 6%	7·8	232	0·0144
M3376	1·8	0·00311	222 ± 5%			
B1712 St. Margaret Bay, N.S.	19	0·00483	346 ± 5%	4·1	337	0·0216
M1712	49	0·00463	332 ± 4%			
B2091 Shad Bay, N.S.	17	0·00537	385 ± 5%	3·2		
M2091	4·9	0·00518	373 ± 6%			
B3128 Ship Harbour, N.S.	22	0·00492	353 ± 5%	12·5	363	0·234
M3138	6·4	0·00555	400 ± 6%			
B1708 Larry's River N.S.	50	0·00470	338 ± 4%	5·2		
M1708	11	0·00449	321 ± 5%			
B2089 Queensport, N.S.	58	0·00515	370 ± 4%	0	366	0·0236
M2089	1·8	0·00515	370 ± 6%			

Decay constants:
$\lambda_{Rb} = 1{\cdot}39 \times 10^{-11} \times \text{year}^{-1}$; $\lambda_e = 0{\cdot}585 \times 10^{-10} \times \text{year}^{-1}$; $\lambda = 5{\cdot}30 \times 10^{-10} \times \text{year}^{-1}$.
Prefixes: M, muscovite, B, biotite; all samples are granite unless otherwise noted.

Inspection of the table shows six biotites to be "older" than the associated muscovite, four to be "younger", with one pair showing agreement. No geological conclusion is therefore possible from these data regarding a possible general sequence of development of the two micas. This feature, combined with the observations above on intra-pair differences and individual precision errors, leads us to assume, in general, cogenesis of these mica pairs with the single exception, already named, of 3128. This does not specify anything regarding absolute age of the rocks themselves, as we are well aware that age measurements of coexisting feldspar and zircon may yield higher values than those determined for the mica pairs. For example GRUNENFELDER and SILVER (1958) have shown by U–Pb analyses on zircon that the Elberton granite and Lithonia gneiss are at least 450 million years old (compare mica ages for these rocks in Table 1). TILTON *et al.* (1958) have demonstrated a still larger time gap between coexisting minerals in the Baltimore gneiss, Md. Our conclusion is simply that, within the limits of analytical precision obtainable in our laboratory, the muscovite and biotite of each pair appear to have been equally affected by a thermal event at the particular time indicated for each in the table. In this limited sense and for this latest episode in their thermal histories they are cogenetic, regardless of absolute age.

Acknowledgements—The analytical work was made possible by the Atomic Energy Commission, Division of Research, whose continued support is gratefully acknowledged. The assistance of various individuals and organisations in obtaining samples is greatly appreciated and individual acknowledgement is made elsewhere.

REFERENCES

FAIRBAIRN H. W. (1956) Computation of error in Rb–Sr age calculations. *Ann. Rep. U.S. Atomic Energy Comm.* Contract AT(30-1)-1381, p. 29.

GRUNENFELDER M. and SILVER L. T. (1958) Radioactive age dating and its petrologic implications for some Georgia granites. *Abstr. Geol. Soc. Amer.* p. 70.

TILTON G. R., WETHERILL G. W., DAVIS G. L. and HOPSON C. A. (1958) Ages of minerals from the Baltimore gneiss, Maryland. *Bull. Geol. Soc. Amer.* **69,** 1469–1474.

Geochimica et Cosmochimica Acta, 1960, Vol. 19, pp. 10 to 40. Pergamon Press Ltd. Printed in Northern Ireland

The stability relations of magnesioriebeckite

W. G. Ernst
Geophysical Laboratory, Carnegie Institution of Washington, Washington, D.C.

(*Received* 23 *July* 1959)

Abstract—Magnesioriebeckite, $o Na_2Mg_3Fe_2^{3+}Si_8O_{22}(OH)_2$, has been synthesized hydrothermally and its stability field determined. The physical parameters which determine experimental phase equilibria include the partial pressure of oxygen as well as the temperature and vapour (= total, largely H_2O) pressure.

The stability field of magnesioriebeckite is bounded by surfaces within a P_{O_2}–P_{vapour}–T volume. P_{vapour}–T diagrams represent projections along the P_{O_2} axis. Three P_{vapour}–T diagrams are presented for magnesioriebeckite, each determined using a different buffer. At low vapour pressure, magnesioriebeckite breaks down to a high-temperature assemblage consisting of one or two iron (+ Mg) oxides, an olivine, $Na_2O{\cdot}5(Mg,Fe)O{\cdot}12SiO_2$, acmite or $Na_2O{\cdot}2(Mg,Fe)O{\cdot}6SiO_2$, and vapour. At vapour pressures greater than about 200 bars, magnesioriebeckite melts incongruently to one or two iron (+ Mg) oxides, an olivine, $Na_2O{\cdot}5(Mg,Fe)O{\cdot}12SiO_2$, liquid and vapour. Above 300 to 500 bars vapour pressure, magnesioriebeckite melts incongruently to one or two iron (+ Mg) oxides, an olivine, an orthopyroxene, liquid and vapour.

Values of ΔH for reactions involving magnesioriebeckite have been calculated; heats of reaction are similar to those for the breakdown of other hydrous minerals. Optical properties of synthetic magnesioriebeckite vary in response to P_{O_2} and T. The effect of the partial oxygen pressure on the composition and stability relations of minerals synthesized in this study again illustrates the petrologic importance of this variable.

Results of the investigation indicate that magnesioriebeckite is stable at magmatic temperatures; the existence of an intermediate member of the magnesioriebeckite–riebeckite series as an authigenic mineral suggests that magnesioriebeckite is also stable at very low temperatures. Since it has a wide P_{vapour}–T range, the restricted natural occurrence of magnesioriebeckite results chiefly from the rare fulfillment of hypersodic chemical conditions.

Introduction

The alkali amphiboles can be classified in three mineral series: (1) richterite–ferrorichterite (soda tremolite), (2) eckermannite–arfvedsonite (kataphorite), and (3) glaucophane–riebeckite. Sundius (1946), Miyashiro (1957), and Boyd (1959) have recently considered the classification and genesis of the alkali amphiboles. In addition, studies by Misch (personal communication), Borg (personal communication) and Miyashiro and co-workers are in progress.

Four end members comprise the gluecophane–riebeckite series: (1) glaucophane, $o Na_2Mg_3Al_2Si_8O_{22}(OH)_2$; (2) ferroglaucophane, $o Na_2Fe_3^{2+}Al_2Si_8O_{22}(OH)_2$; (3) magnesioriebeckite, $o Na_2Mg_3Fe_2^{3+}Si_8O_{22}(OH)_2$; and (4) riebeckite, $o Na_2Fe_3^{2+}Fe_2^{3+}Si_8O_{22}(OH)_2$. The symbol o represents the vacant position in the amphibole structure (Warren, 1929). Miyashiro (1957, p. 62) collected analyses of members of this series and demonstrated that although ferroglaucophane has not been reported, extensive solid solution clearly exists among the three remaining end members. The chemical variation of relatively pure glaucophane–riebeckites is illustrated in Fig. 1. With the exception of some iron-rich riebeckites which are late crystallization products of silicic–alkalic igneous rocks, minerals of this series are found principally in low grade metamorphic rocks.

Magnesioriebeckite was selected for experimental study in order to determine stability relations for a typical alkali amphibole, and to ascertain the influence of

P_{O_2} on a hydrous ferric silicate. It is the first alkali amphibole and the first hydrous ferric silicate for which these relations have been determined.

Experimental Techniques

Both Tuttle-press (Tuttle, 1948) and cold-seal apparatus (Tuttle, 1949) were employed in this investigation. Each type of pressure vessel was made of Haynes alloy 25, and was of sufficient bore to permit the use of charge capsules of 4·5 mm outside diameter.

Temperature was measured with chromel–alumel thermocouples. Each apparatus was calibrated on the melting point of NaCl (800·4°C) or Na_2SO_4 (884·7°C). A new thermocouple

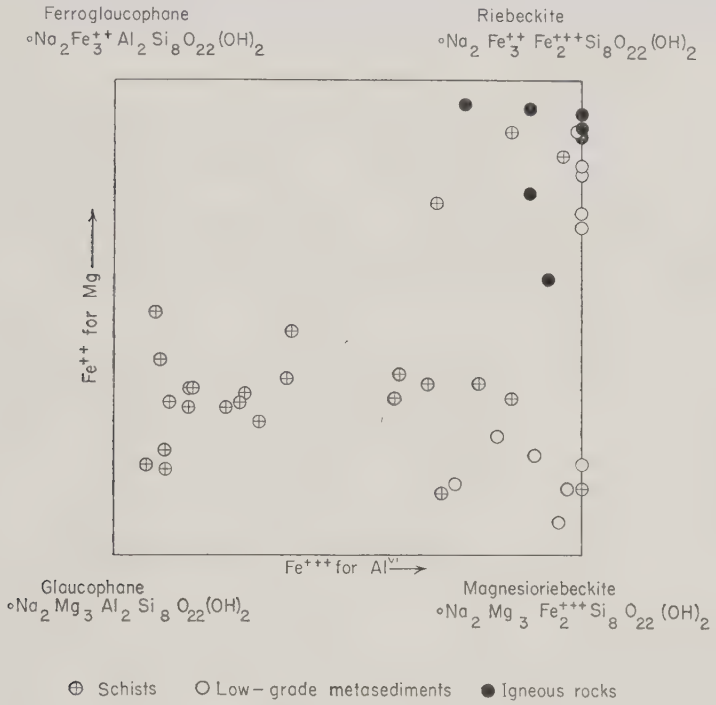

Fig. 1. Chemical variation in natural members of the glaucophane–riebeckite series (Al^{VI} = octahedrally co-ordinated aluminium).

was used for each experiment to minimize errors due to oxidation and contamination. Individual thermocouple readings were recorded every 6 min on a Minneapolis–Honeywell potentiometric recorder; however, temperatures were checked every day and prior to run termination with a Leeds and Northrup White potentiometer, reading to within 0·25°C. Temperature regulators were of the type developed by F. A. Mauer of the National Bureau of Standards and modified by J. L. England of the Geophysical Laboratory. They consist of a Wheatstone bridge, one arm of which is a variable resistance, another is a platinum sensing element within the furnace, and the other two arms have fixed resistances; an amplifier and motor driven variac are connected in series across the bridge. These regulators control the temperature of the pressure vessel to within ±2°C on runs lasting more than a month.

Pressure was continuously measured by a variety of gauges checked against a 14 in. Heise gauge taken as standard. Large reservoir tanks ensured relatively constant pressure; most fluctuations were less than ±10 bars.

Tuttle-press pressure vessels were quenched by an air blast. The water pressure was dropped to 1 atm in cold-seal bombs as the pressure vessels were removed from the furnaces. Both methods provided adequate quenches.

Many magnesioriebeckite runs were performed using mixtures of oxides. MgO, SiO_2 and Fe_2O_3 of high purity were supplied by J. F. Schairer of the Geophysical Laboratory. All compounds were heated to 1000°–1300°C previous to weighing. Sodium disilicate was prepared from SiO_2 and Fisher certified Na_2CO_3 by the method described by Schairer and Bowen (1955, p. 682; 1956, p. 131). Compounds were mixed in the desired proportion ($Na_2O{\cdot}3MgO{\cdot}Fe_2O_3{\cdot}8SiO_2$) in a motor-driven mullite or agate mortar under acetone for 1 hr. Synthetic magnesioriebeckite and high-temperature equivalent assemblages (grown from mix) were employed in a number of experiments.

The charges (approximately 30 mg of oxide mix and 5–15 mg H_2O) were sealed in platinum tubes by electric welding. Platinum takes iron into solid solution, but magnesioriebeckite runs were of short enough duration to make loss of iron to the container negligible (as shown by the occurrence of iron oxides in all high-temperature equivalent assemblages, indicating that phases were saturated with respect to Fe).

The temperature of the reaction talc = enstatite + quartz + vapour at 1000 bars vapour pressure was checked using both open and sealed tubes. Identical results were obtained, indicating that the strength of the platinum container is negligible under the conditions of these experiments, and that the total (= vapour) pressure on the charge is equal in magnitude to the pressure outside the capsule (gauge pressure).

Since the bulk composition contains iron, changes in partial pressure of oxygen influence the stability and composition of magnesioriebeckite, as well as the stabilities and compositions of iron-bearing phases of the high-temperature assemblages (e.g. see Eugster, 1959; Muan, 1958); accordingly, the buffer method of controlling P_{O_2} described by Eugster (1957) was adopted.

Proof that reactions involving magnesioriebeckite were reversible was obtained by rerunning synthetic magnesioriebeckite at temperatures higher than its stability limit, where it decomposed; likewise, high-temperature phase assemblages for the composition $Na_2O{\cdot}3MgO{\cdot}Fe_2O_3{\cdot}8SiO_2$ with excess water were rerun at low temperatures where they recrystallized to magnesioriebeckite.

Investigation of condensed phases was carried out in three stages. (1) The megascopic characters of the charge, buffer and container were examined with the aid of a 10-power hand lens. (2) Synthetic phases and buffers were studied microscopically using immersion oils of 0·002 refractive index interval. Refractive indices were determined for white light using a flat-stage microscope and are considered accurate to within ±0·002 to ±0·004, depending on grain size. Extinction angles were measured on a flat stage using sodium light. (3) X-ray analyses of charges (and opaque buffers) were performed using a Norelco diffractometer. Run products were examined with iron radiation between 5 and 60° 2θ. Patterns were compared with standard synthetic and natural minerals; reflection intensities of phases present afforded an approximate measure of their relative proportions.

Buffers

Theory of buffers

At a specified temperature (and total pressure) a system containing an element in two oxidation states in crystalline phases of constant composition is in equilibrium with a fixed oxygen pressure. A univariant assemblage of this sort can be used as a buffer to control P_{O_2}. Any tendency to increase or to decrease the oxygen pressure will result in changing the relative amounts of the solid buffer phases; only after one of the buffer phases has disappeared can P_{O_2} change at constant temperature.

Most igneous and metamorphic rocks appear to have formed at partial oxygen pressures close to or within the magnetite stability field. Therefore, the buffers haematite–magnetite (the highest P_{O_2} at any P_{total} and T where magnetite is stable), and magnetite–wüstite (the lowest P_{O_2} at any P_{total} and T where magnetite is stable) were selected along with the magnetite + silica–fayalite

buffer which lies within the magnetite field. A detailed discussion of the system Fe–Si–O and the influence of partial oxygen pressure on equilibria among iron-bearing phases has been presented by Eugster (1959).

The method of equilibrating the oxygen pressure of the buffer with the charge has also been described by Eugster (1957). At high temperatures and pressures, the charge reaches equilibrium with the buffer in a matter of minutes; at 800°C, P_{O_2} equilibration is effected in a few hours. Numerous runs performed at the same pressures and temperatures but for different lengths of time gave proof of experimental equilibrium. Identical results were obtained; if equilibrium had not been realized, run duration should have influenced the assemblage.

Table 1. Log P_{O_2} for several buffers at 1 atm total pressure

Temp. (°C)	(1) Haematite–magnetite	(2) Magnetite + silica–fayalite	(3) Magnetite-wüstite	(4) Magnetite–iron	(5) Wüstite–iron
427	−21·19	−28·8	—	−32·82	—
527	−16·74	−23·9	—	−27·60	—
560	−15·55	−22·5	−26·14	−26·14	−26·14
627	−13·28	−20·0	−23·16	—	−23·60
727	−10·51	−17·0	−19·55	—	−20·59
827	−8·25	−14·5	−16·58	—	−18·14
927	−6·36	−12·4	−14·11	—	−16·06
1027	−4·76	−10·7	−12·02	—	−14·35
1127	−3·39	−9·2	−10·23	—	−12·84

Calculation of P_{O_2} *at* 1 *atm total pressure*

Norton (1955) measured the dissociation at elevated temperatures of copper–oxygen and iron–oxygen buffer pairs using a mass spectrometer. His data for the reactions $3Fe_2O_3 = 2Fe_3O_4 + \frac{1}{2}O_2$, measured between 800° and 1400°C, and calculations for the reactions $Fe_3O_4 = 3FeO + \frac{1}{2}O_2$, $\frac{1}{2}Fe_3O_4 = \frac{3}{2}Fe + O_2$ and $FeO = Fe + \frac{1}{2}O_2$ are presented in Table 1 and in Fig. 2. Norton's data are consistent with the earlier work of Darken and Gurry (1945, 1946) except that the new haematite–magnetite data are more complete and indicate higher partial pressures of oxygen than those reported by Darken and Gurry. Norton's experimental values fall on straight lines in a ln P_{O_2} vs. $1/T_K$ plot; thus at high temperatures and low pressures oxygen behaves as an ideal gas.

The position and slope of the curve for the buffer reaction $Fe_3O_4 + \frac{3}{2}SiO_2 = \frac{3}{2}Fe_2SiO_4 + \frac{1}{2}O_2$ were determined using the P_{O_2} value on the magnetite + tridymite + fayalite liquidus at 1140°C found by Muan (1955, pp. 972, 973), and a 900°C value interpreted by Darken (1948) from investigations of Schenk *et al.* (1932). In the latter work, CO_2 gas was passed over the assemblage magnetite + tridymite + fayalite at constant temperature, and the equilibrium CO_2/CO ratio measured. While a range of values is presented, calculation showed that the spread has a negligible effect on the derived P_{O_2}. This computation was performed using

the equilibrium constants for the dissociation of carbon dioxide published by Wagman *et al.* (1945) graphically interpolated between 827° and 927°C. Values for the magnetite + silica–fayalite curve thus obtained are presented in Table 1 and Fig. 2. Due to the paucity of data, its position is uncertain, especially at low temperatures, so it is presented as a dashed P_{O_2}–T curve. The inversion of tridymite to quartz probably influences the oxygen pressure for this buffer. However, its effect is slight, and is well within the limits of error of the calculation.

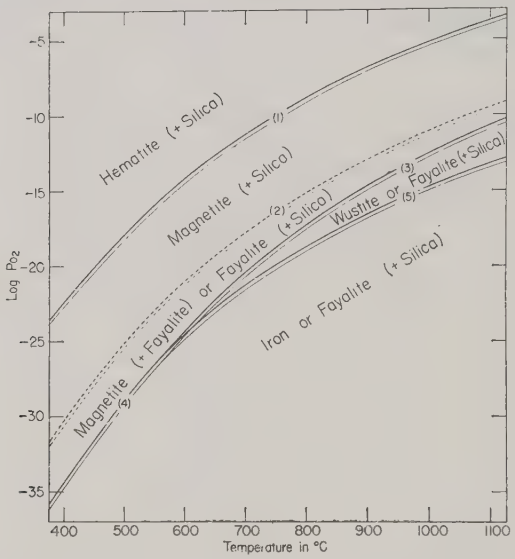

Fig. 2. Calculated P_{O_2}–T plot for several buffers at total pressures of 1 atm (heavy lines) and 2000 bars (light lines). Individual buffers are (1) haematite–magnetite, (2) magnetite + silica–fayalite, (3) magnetite–wüstite, (4) magnetite–iron, and (5) wüstite–iron.

Calculation of P_{O_2} *at high total pressure*

The influence of total pressure on the value of the oxygen partial pressure is minor. Experimental buffer reactions actually involve water, and may be written as follows:

$$\text{oxidized solid} + H_2 = \text{reduced solid} + H_2O$$

The activities of the solids are considered independent of concentration and are practically unaffected by increased temperature and total pressure (Glasstone, 1947, pp. 281–282), so the activity (fugacity) of the gas is fixed by the equilibrium constant. The substitution of fugacity for pressure allows the application of the ideal gas law to real gases. Fugacity (partial or total) is related to the corresponding pressure by the equation $f = \gamma P$, where γ, the fugacity coefficient, is a measure of the departure of real gases from ideal behaviour. The expression for the equilibrium constant (K_B) for each buffer at any temperature and P_{total} in terms of fugacity reduces to

$$K_B = \frac{f(H_2O)}{f(H_2)}$$

This expression may be multiplied by the equilibrium constant (K_W) for the dissociation of water:

$$K_B.K_W = \frac{f(H_2O)}{f(H_2)} \cdot \frac{f(H_2)f(O_2)^{\frac{1}{2}}}{f(H_2O)} = f(O_2)^{\frac{1}{2}}$$

If we now replace the right-hand term by one involving partial pressure and substitute logarithms, we obtain

$$\log K_B + \log K_W = \frac{\log \gamma_{O_2}}{2} + \frac{\log P_{O_2}}{2}$$

where γ_{O_2} is the fugacity coefficient of oxygen. The equilibrium constants K_W and K_B defined in terms of fugacities are independent of total pressure (Moore, 1955, pp. 76, 77) whereas the value γ_{O_2} is not. Accordingly, the relation between the partial oxygen pressure at high pressure (designated by superscript ′) to that at 1 atm pressure is:

$$\log K_B + \log K_W = \frac{\log \gamma_{O_2}}{2} + \frac{\log P_{O_2}}{2} = \frac{\log \gamma'_{O_2}}{2} + \frac{\log P'_{O_2}}{2}$$

or

$$\log P'_{O_2} = \log P_{O_2} - \log \gamma'_{O_2} + \log \gamma_{O_2}$$

In the temperature range of this investigation, oxygen has a fugacity coefficient of unity at 1 atm total pressure (Newton, 1935), so this expression reduces to:

$$\log P'_{O_2} = \log P_{O_2} - \log \gamma'_{O_2}$$

The high-pressure fugacity coefficients for oxygen were taken from values based on the law of corresponding states published by Newton. The data selected were those for the pure gas at the specified total pressure, in accordance with the "partial fugacity rule" (Newton, 1935, p. 302). It may be argued that fugacity coefficients should be selected which would obtain for the gas species subjected solely to its own pressure; this case results in the minimum P_{total} effect on partial pressures, since fugacity coefficients approach unity at low pressures. The "partial fugacity rule" gives the maximum pressure effect. The results of these calculations for several buffers are given in Table 2 and in Fig. 2. The partial oxygen pressures calculated are approximately one half order of magnitude lower at 2000 bars total pressure than at 1 atm total pressure.*

Calculation of partial hydrogen pressure

Similar computations indicate that near the lower P_{O_2} limit of the magnetite field, the partial pressure of hydrogen becomes appreciable (30 ± 20 per cent of the total pressure). The vapour (= total) pressure in this region must be considered as the sum of the partial pressures of hydrogen, oxygen, water and the condensed phases, but vapour pressures of the condensed phases and O_2 are exceedingly low throughout and can safely be ignored. In the haematite field, P_{H_2} is also negligible, and the vapour (= total) pressure may be considered as essentially P_{H_2O}.

* The influence of pressure on activities of condensed buffer phases alone is such that the change of P_{O_2} is of approximately equal magnitude but of opposite sign from that calculated above (H. G. Greenwood, Geophysical Laboratory, personal communication), so that the net effect of increased P_{total} on partial oxygen pressure is very small.

Experimental Results

Run data

Abbreviations used in this paper to designate phases are given in Table 3. Tables 4, 5 and 6 present results of hydrothermal investigations for the bulk composition $Na_2O{\cdot}3MgO{\cdot}Fe_2O_3{\cdot}8SiO_2$ with excess water and with oxygen pressure controlled by the buffers: (1) haematite–magnetite, (2) magnetite + silica–fayalite, and (3) magnetite–wüstite, respectively. Results of several experiments

Table 2. Calculated log P_{O_2} for several buffers at 2000 bars total pressure

Temp. (°C)	(1) Haematite–magnetite	(2) Magnetite + silica–fayalite	(3) Magnetite–wüstite	(4) Magnetite–iron	(5) Wüstite–iron
427	−21·58	−29·2	—	−33·21	—
527	−17·11	−24·2	—	−27·95	—
561	−15·86	−22·7	−26·50	−26·50	−26·50
627	−13·62	−20·4	−23·51	—	−23·94
727	−10·84	−17·3	−19·87	—	−20·91
827	−8·55	−14·8	−16·89	—	−18·44
927	−6·65	−12·7	−14·40	—	−16·34
1027	−5·03	−10·9	−12·29	—	−14·61
1127	−3·64	−9·4	−10·48	—	−13·09

Table 3. Abbreviations used to designate phases

Ac = acmite, $Na_2O{\cdot}Fe_2O_3{\cdot}4SiO_2$
Fe = iron
H = haematite
L = liquid (H_2O saturated silicate melt)
Ma = $Na_2O{\cdot}5(Mg,Fe)O{\cdot}12SiO_2$
Mf = magnesioferrite, $(Mg,Fe)O{\cdot}Fe_2O_3$
Mr = magnesioriebeckite, $Na_2O{\cdot}3MgO{\cdot}Fe_2O_3{\cdot}8SiO_2{\cdot}H_2O$
Mw = magnesiowüstite, (Mg,Fe)O
N = $Na_2O{\cdot}2(Mg,Fe)O{\cdot}6SiO_2$
Ol = olivine
Px = orthopyroxene
Q = quartz
V = vapour
(. . .) = parentheses enclose phases interpreted to be metastable
mix = oxide mixture
? = presence not definitely established

with P_{O_2} defined by a wüstite–iron buffer are given at the end of Table 6. At high pressures the charge was converted to between 90 and 100 per cent amphibole within the magnesioriebeckite field, but from 10 to 30 per cent of the high-temperature assemblages persisted metastably at low pressures. The occurrence of small amounts of quartz in a few runs suggests that one batch of mix was slightly off

Table 4. Results of investigations of the composition $Na_2O{\cdot}3MgO{\cdot}Fe_2O_3{\cdot}8SiO_2$ with excess water and with P_{O_2} defined by a haematite–magnetite buffer

Starting material	Temp. (°C)	P_{vapour} (bars)	Duration (hr)	Condensed phases
		Curve: H + Mf + Ol + Ma + Ac + Mr + V		
mix	827	34	44	H + Mf + Ol + Ma + Ac + Mr
mix	864	103	70	Mr (+ H + Mf + Ol + Ma + Ac)
mix	877	98	67	H + Mf + Ol + Ma + Ac
mix	895	198	14	Mr (+ H + Mf + Ol + Ma + Ac)
mix	902	205	19	H + Mf + Ol + Ma + Ac + Mr
mix	911	198	14	H + Mf + Ol + Ma + Ac
mix	914	250	8	H + Mf + Ol + Ma + Ac + Mr + L
		Field: H + Mf + Ol + Ma + Ac + V		
mix	813	1	356	H + Mf + Ol + Ma + Ac
mix	827	1	160	H + Mf + Ol + Ma + Ac
mix	860	1	200	H + Mf + Ol + Ma + Ac
mix	872	41	17	H + Mf + Ol + Ma + Ac
mix	881	51	20	H + Mf + Ol + Ma + Ac
mix	896	1	166	H + Mf + Ol + Ma + Ac
mix	899	141	17	H + Mf + Ol + Ma + Ac
mix	903	1	167	H + Mf + Ol + Ma + Ac
mix	914	100	43	H + Mf + Ol + Ma + Ac
mix	927	1	65	H + Mf + Ol + Ma + Ac
mix	954	1	47	H + Mf + Ol + Ma + Ac
		Curve: H + Mf + Ol + Ma + Ac + L + V		
mix	914	250	8	H + Mf + Ol + Ma + Ac + Mr + L
mix	913	151	62	H + Mf + Ol + Ma + Ac
mix	928	104	25	H + Mf + Ol + Ma + Ac
mix	929	166	6	H + Mf + Ol + Ma + L
mix	958	1	97	H + Mf + Ol + Ma + Ac
mix	963	1	48	H + Mf + Ol + Ma + Ac + L
mix	970	1	43	H + Mf + Ol + Ma + L
		Field: H + Mf + Ol + Ma + L + V		
mix	977	1	9	H + Mf + Ol + Ma + L
		Curve: H + Mf + Ol + Ma + Mr + L + V		
mix	911	261	7	Mr (+ H + Mf + Ol + Ma + Ac)
mix	914	250	8	H + Mf + Ol + Ma + Ac + Mr + L
mix	922	250	6	H + Mf + Ol + Px + Ma + L
		Field: Mr + V		
Mr	799	1850	40	Mr
mix	802	1950	5	Mr (+ H + Mf + Ol + Ma + Ac?)
Mr	808	500	18	Mr
mix	827	1850	40	Mr (+ H + Mf + Q?)
mix	828	1210	19	Mr
mix	842	245	43	Mr (+ H + Mf + Ol + Ma + Ac)
mix	853	1000	9	Mr (+ H + Mf + Q?)
mix	856	248	46	Mr (+ Q?)
Mr	858	1490	12	Mr (+ Q)
mix	860	980	64	Mr
mix	864	250	50	Mr (+ H + Mf + Ol + Ma + Ac)
Mr	864	1500	2	Mr

Table 4 (*contd.*)

Starting material	Temp. (°C)	P_{vapour} (bars)	Duration (hr)	Condensed phases
		Field: Mr + V (*contd.*)		
Mr	868	500	20	Mr (+ H + Mf + Q?)
Mr	869	1030	27	Mr
mix	876	730	119	Mr
Mr	879	1010	23	Mr
Mr	880	520	23	Mr
mix	886	250	49	Mr (+ H + Mf + Ol + Ma + Ac)
mix	890	750	52	Mr (+ H + Mf + Ol + Px + L)
mix	893	523	18	Mr (+ H + Mf + Ol + Ma + Ac)
mix	898	525	46	Mr (+ H + Mf + Ol + Px + L)
mix	900	261	8	Mr (+ H + Mf + Ol + Ma + Ac)
mix	900	738	41	Mr (+ H + Mf + Ol + Px + L)
		Curve: H + Mf + Ol + Px + Mr + L + V		
Mr	912	1000	20	Mr (+ H + Mf + Ol + Px + L)
mix	917	500	8	Mr (+ H + Mf + Ol + Px + L)
H + Mf + Ol + Px + L	922	750	18	Mr (+ H + Mf + Ol + Px + L)
Mr	924	990	14	H + Mf + Ol + Px + Mr + L
mix	925	505	10	H + Mf + Ol + Px + L
mix	925	762	6	H + Mf + Ol + Px + Mr + L
mix	925	1490	2	Mr (+ H + Mf + Ol + Px + L)
mix	932	1035	28	H + Mf + Ol + Px + L
Mr	933	740	23	H + Mf + Ol + Px + L
mix	933	1485	2	H + Mf + Ol + Px + Mr + L
mix	939	1490	2	H + Mf + Ol + Px + L
		Field: H + Mf + Ol + Px + L + V		
mix	940	1010	6	H + Mf + Ol + Px + L
Mr	944	1500	1	H + Mf + Ol + Px + L
mix	953	980	45	H + Mf + Ol + Px + L
		Curve: H + Mf + Ol + Px + Ma + L + V		
mix	922	250	6	H + Mf + Ol + Px + Ma + L
mix	929	251	6	H + Mf + Ol + Px + L

composition. This material was not employed in determination of the PT curves.

Magnesian end members of the phases $Na_2O{\cdot}5(Mg,Fe)O{\cdot}12SiO_2$ and $Na_2O{\cdot}2(Mg,Fe)O{\cdot}6SiO_2$ encountered in this study have been described by Schairer *et al.* (1954) in their discussion of the system Na_2O–MgO–SiO_2.

Location of curves

The data of Tables 4, 5 and 6 are shown on a plot of P_{vapour} and T in Figs. 3(a), 3(b) and 3(c), respectively. Each P_{vapour}–T diagram represents the intersections of phase boundary surfaces occurring within the P_{O_2}–P_{vapour}–T volume with the surface defined by a specific buffer and projected along the P_{O_2} axis. This may be more easily visualized by referring to the three-dimensional model in Fig. 5.

Each curve (representing the coexistence of specific high- and low-temperature assemblages) has been located at temperatures and pressures above those in which the low-temperature assemblage was obtained. This method is based on the

Table 5. Results of investigations of the composition $Na_2O{\cdot}3MgO{\cdot}Fe_2O_3{\cdot}8SiO_2$ with excess water and with P_{O_2} defined by a magnetite + silica–fayalite buffer

Starting material	Temp. (°C)	P_{vapour} (bars)	Duration (hr)	Condensed phases
		Curve: Mf + Ol + Ma + N + Mr + V		
Mr	848	152	46	Mr (+ Mf + Ol + Ma + N)
mix	856	150	46	Mf + Ol + Ma + N + Mr
		Field: Mf + Ol + Ma + N + V		
mix	857	1	108	Mf + Ol + Ma + N
mix	878	1	119	Mf + Ol + Ma + N
		Curve: Mf + Ol + Ma + N + L + V		
mix	876	147	65	Mf + Ol + Ma + N
mix	883	147	60	Mf + Ol + Ma + L
mix	901	1	46	Mf + Ol + Ma + N
mix	924	1	45	Mf + Ol + Ma + L
		Field: Mf + Ol + Ma + L + V		
mix	899	250	26	Mf + Ol + Ma + L
mix	911	253	21	Mf + Ol + Ma + L
mix	953	1	119	Mf + Ol + Ma + L
mix	961	1	17	Mf + Ol + Ma + L
mix	971	1	16	Mf + Ol + Ma + L
mix	978	1	7	Mf + Ol + Ma + L
mix	987	1	6	Mf + Ol + Ma + L (+ Px)
		Curve: Mf + Ol + Ma + Mr + L + V		
mix	882	250	26	Mr (+ Mf + Ol + Ma + L)
mix	889	254	30	Mf + Ol + Ma + L
		Field: Mr + V		
Mr	782	1900	20	Mr
mix	814	180	162	Mr (+ Mf + Ol + Ma + N)
mix	824	990	67	Mr (+ Mf + Q?)
mix	833	1850	45	Mr
Mr	842	154	45	Mr (+ Mf + Ol + Ma + N)
mix	848	1490	21	Mr
Mr (+ Mf + Q?)	849	996	22	Mr (+ Mf + Ol + Px + L)
mix	852	405	36	Mr (+ Q?)
mix	853	1490	21	Mr
Mr (+ Mf + Q?)	858	1000	23	Mr (+ Mf + Ol + Px + L)
Mr	860	404	60	Mr
Mr	868	404	60	Mr (+ Mf + Ol + Ma + L)
mix	874	1000	50	Mr
mix	894	1500	2	Mr (+ Mf + Ol + Px + L)
		Curve: Mf + Ol + Px + Mr + L + V		
Mf + Ol + Px + L	889	489	18	Mr (+ Mf + Ol + Px + L)
Mf + Ol + Px + L	893	908	25	Mr (+ Mf + Ol + Px + L)
Mr	895	398	62	Mr (+ Mf + Ol + Px + L)
Mr	897	760	16	Mr (+ Mf + Ol + Px + L)
mix	897	1000	17	Mr (+ Mf + Ol + Px + L)
mix	898	500	12	Mr (+ Mf + Ol + Px + L)
mix	901	1500	2	Mr (+ Mf + Ol + Px + L)
mix	904	480	26	Mf + Ol + Px + Mr + L
mix	905	1000	12	Mf + Ol + Px + Mr + L

Table 5 (*contd.*)

Starting material	Temp. (°C)	P_{vapour} (bars)	Duration (hr)	Condensed phases
		Curve: Mf + Ol + Px + Mr + L + V (*contd.*)		
Mr	906	398	64	Mf + Ol + Px + L
Mr	906	755	16	Mf + Ol + Px + L
mix	908	1500	2	Mf + Ol + Px + Mr + L
mix	910	500	21	Mf + Ol + Px + L
mix	912	1005	11	Mf + Ol + Px + L
Mr	914	1500	2	Mf + Ol + Px + L (+ Mr)
		Field: Mf + Ol + Px + L + V		
mix	912	385	19	Mf + Ol + Px + L
mix	917	480	26	Mf + Ol + Px + L
mix	920	993	7	Mf + Ol + Px + L
mix	925	993	7	Mf + Ol + Px + L
		Curve: Mf + Ol + Px + Ma + L + V		
mix	907	323	20	Mf + Ol + Px + Ma + L
mix	916	252	20	Mf + Ol + Ma + L
mix	926	253	22	Mf + Ol + Px + L
mix	945	288	19	Mf + Ol + Px + L
mix	946	162	22	Mf + Ol + Ma + L (+ Px)
mix	947	214	19	Mf + Ol + Px + Ma + L

observation that although high-temperature assemblages may persist indefinitely at low temperatures, the converse phenomenon is rare. Curves were located using oxide mixtures for the most part. The validity of this method has been substantiated by reversing the reaction; equilibrium assemblages are attained within a matter of hours, regardless of starting material. P_{vapour}–T curve sites are summarized in Table 7. Curve locations are considered accurate to ± 5°C.

All phases containing MgO contain some ferrous iron, the amount depending on the partial pressure of oxygen, the vapour (= total) pressure, and the temperature. For this reason magnesioriebeckite breaks down over a small temperature interval (approximately 20°C). Within this melting region the amphibole changes composition in a manner analogous to the melting of an intermediate olivine. As temperature increases, the amount of amphibole diminishes, and its composition becomes more magnesian. Curves bounding the stability field of magnesioriebeckite are drawn on the disappearance of amphibole.

Discussion of phase diagrams

The shape of the magnesioriebeckite P_{vapour}–T field in Fig. 3 is similar to those of other hydrous minerals. The steep dP/dT slope of the high-temperature stability limit above moderate pressures is due to an increased entropy change on melting, and to the solution of H_2O in the liquid phase (resulting in a larger $\Delta S/\Delta V$ term for reactions involving magnesioriebeckite and liquid). At low temperatures and vapour pressures, the high-temperature assemblage adjoining that of magnesioriebeckite consists of the phases haematite, magnesioferrite, olivine,

Table 6. Results of investigations of the composition $Na_2O{\cdot}3MgO{\cdot}Fe_2O_3{\cdot}8SiO_2$ with excess water and with P_{O_2} defined by a magnetite–wüstite buffer

Starting material	Temp. (°C)	P_{vapour} (bars)	Duration (hr)	Condensed phases
		Curve: Mf + Mw + Ol + Ma + N + Mr + V		
Mr	818	152	47	Mr (+ Mf + Mw + Ol + Ma + N)
Mr	831	154	45	Mf + Mw + Ol + Ma + N (+ Mr)
mix	851	248	40	Mr (+ Mf + Mw + Ol + Ma + N)
mix	863	250	26	Mf + Mw + Ol + Ma + N
		Field: Mf + Mw + Ol + Ma + N + V		
mix	839	150	46	Mf + Mw + Ol + Ma + N
mix	848	147	65	Mf + Mw + Ol + Ma + N
mix	865	147	60	Mf + Mw + Ol + Ma + N
mix	878	1	119	Mf + Mw + Ol + Ma + N
		Curve: Mf + Mw + Ol + Ma + N + L + V		
mix	872	254	30	Mf + Mw + Ol + Ma + N
mix	880	254	30	Mf + Mw + Ol + Ma + L
mix	883	162	21	Mf + Mw + Ol + Ma + N
mix	903	1	97	Mf + Mw + Ol + Ma + L
mix	903	162	21	Mf + Mw + Ol + Ma + N
mix	928	1	32	Mf + Mw + Ol + Ma + L
		Field: Mf + Mw + Ol + Ma + L + V		
mix	901	253	21	Mf + Mw + Ol + Ma + L
mix	909	252	21	Mf + Mw + Ol + Ma + L
mix	923	253	22	Mf + Mw + Ol + Ma + L
mix	960	1	12	Mf + Mw + Ol + Ma + L
mix	967	1	7	Mf + Mw + Ol + Ma + L
mix	977	1	16	Mf + Mw + Ol + Ma + L
		Curve: Mf + Mw + Ol + Ma + Mr + L + V		
Mr	877	396	36	Mr (+ Mf + Mw + Ol + Ma + L)
mix	878	504	24	Mr (+ Mf + Mw + Ol + Ma + L)
Mr (+ Mf + Mw + Ol + Px + L)	883	390	50	Mf + Mw + Ol + Ma + Mr + L
mix	884	500	9	Mr? (+ Mf + Mw + Ol + Ma + L)
mix	890	504	24	Mf + Mw + Ol + Px + L
		Field: Mr + V		
mix	800	1490	22	Mr (+ Q?)
mix	822	1010	60	Mr
mix	823	396	29	Mr (+ Mf + Mw + Ol + Ma + N)
mix	839	248	40	Mr (+ Mf + Mw + Ol + Ma + N)
mix	858	1000	50	Mr
Mr	860	1210	42	Mr
mix	862	1000	49	Mr
Mr	868	396	36	Mr (+ Mf + Mw + Ol + Ma + L)
mix	873	491	17	Mr (+ Mf + Mw + Ol + Ma + L)
mix	882	1000	9	Mr (+ Mf + Mw + Ol + Px + L)
mix	882	1500	3	Mr (+ Mf + Mw + Ol + Px + L)
mix	890	1500	2	Mr (+ Mf + Mw + Ol + Px + L)
		Curve: Mf + Mw + Ol + Px + Mr + L + V		
mix	878	504	24	Mr (+ Mf + Mw + Ol + Ma + L)
Mf + Mw + Ol + Px + L	883	908	25	Mr (+ Mf + Mw + Ol + Px + L)
mix	884	500	9	Mr? (+ Mf + Mw + Ol + Ma + L)
Mr	884	760	5	Mr (+ Mf + Mw + Ol + Px + L)
mix	889	1000	17	Mr (+ Mf + Mw + Ol + Px + L)
mix	890	504	24	Mf + Mw + Ol + Px + L
Mr	892	750	5	Mf + Mw + Ol + Px + L
mix	892	1420	2	Mr (+ Mf + Mw + Ol + Px + L)
mix	893	1505	2	Mr (+ Mf + Mw + Ol + Px + L)
mix	900	1005	10	Mf + Mw + Ol + Px + L
mix	900	1500	2	Mf + Mw + Ol + Px + Mr + L
Mr	904	1500	2	Mf + Mw + Ol + Px + L

Table 6 (*contd.*)

Starting material	Temp. (°C)	P_{vapour} (bars)	Duration (hr)	Condensed phases
		Field: Mf + Mw + Ol + Px + L + V		
mix	909	1005	8	Mf + Mw + Ol + Px + L
Mr	926	386	27	Mf + Mw + Ol + Px + L
		Curve: Mf + Mw + Ol + Px + Ma + L + V		
mix	878	504	24	Mr (+ Mf + Mw + Ol + Ma + L)
mix	884	500	9	Mr? (+ Mf + Mw + Ol + Ma + L)
mix	890	504	24	Mf + Mw + Ol + Px + L
Mr (+ Mf + Mw + Ol + Ma + L)	907	390	50	Mf + Mw + Ol + Ma + L
mix	915	392	23	Mf + Mw + Ol + Px + L
mix	945	250	29	Mf + Mw + Ol + Ma + L
mix	972	214	20	Mf + Mw + Ol + Px + L
		P_{O_2} defined by a wüstite–iron buffer		
mix	703	2000	85	Mr (+ Mw + Fe? + Ol + Ma + N)
Mr (+ Mw + Fe? + Ol + Ma + N)	854	1205	13	Mr (+ Mw + Fe? + Ol + Ma + L)
Mw + Fe? + Ol + Px + L	855	1200	20	Mr (+ Mw? + Fe? + Ol + Ma + L)

$Na_2O{\cdot}5(Mg,Fe)O{\cdot}12SiO_2$, acmite and vapour with P_{O_2} defined by a haematite–magnetite buffer; magnesioferrite, olivine, $Na_2O{\cdot}5(Mg,Fe)O{\cdot}12SiO_2$, $Na_2O{\cdot}2(Mg{\cdot}Fe)O.6SiO_2$, and vapour with P_{O_2} defined by a magnetite + silica–fayalite buffer; and magnesioferrite, magnesiowüstite, olivine, $Na_2O{\cdot}5(Mg,Fe)O{\cdot}12SiO_2$, $Na_2O{\cdot}2(Mg,Fe)O{\cdot}6SiO_2$, and vapour with P_{O_2} defined by a magnetite–wüstite buffer.

Incongruent melting curves for acmite or $Na_2O{\cdot}2(Mg,Fe)O{\cdot}6SiO_2$ (depending on the partial oxygen pressure), separate the low vapour pressure high-temperature assemblage adjacent the magnesioriebeckite field from the intermediate P_{vapour} high-temperature assemblage adjoining the magnesioriebeckite field. This latter assemblage consists of haematite, magnesioferrite, olivine, $Na_2O{\cdot}5(Mg,Fe)O{\cdot}12SiO_2$, liquid and vapour with P_{O_2} defined by a haematite–magnetite buffer; magnesioferrite, olivine, $Na_2O{\cdot}5(Mg,Fe)O{\cdot}12SiO_2$, liquid and vapour with P_{O_2} defined by a magnetite + silica–fayalite buffer; and magnesioferrite, magnesiowüstite, olivine, $Na_2O{\cdot}5(Mg,Fe)O{\cdot}12SiO_2$, liquid and vapour with P_{O_2} defined by a magnetite–wüstite buffer.

The incongruent melting curve for $Na_2O{\cdot}5(Mg,Fe)O{\cdot}12SiO_2$ separates these assemblages from the fields adjacent to the magnesioriebeckite field at high temperatures and high vapour pressures. In this region, haematite, magnesioferrite, olivine, orthopyroxene, liquid and vapour are stable with P_{O_2} defined by a haematite–magnetite buffer; magnesioferrite, olivine, orthopyroxene, liquid and vapour are stable with P_{O_2} defined by a magnetite + silica–fayalite buffer; and magnesioferrite, magnesiowüstite, olivine, orthopyroxene, liquid and vapour are stable with P_{O_2} defined by a magnetite–wüstite buffer.

The phase relations among the iron (+ Mg) oxides, olivine, orthopyroxene and liquid should be compared with the liquidus data of Muan and Osborn (1956, pp. 129, 130) for the system MgO–FeO–Fe_2O_3–SiO_2. Apparently addition of the components Na_2O and H_2O permits the stable coexistence of olivine, orthopyroxene, magnesioferrite and magnesiowüstite with melt in the present investigation. Muan and Osborn found pyroxene and magnesiowüstite mutually

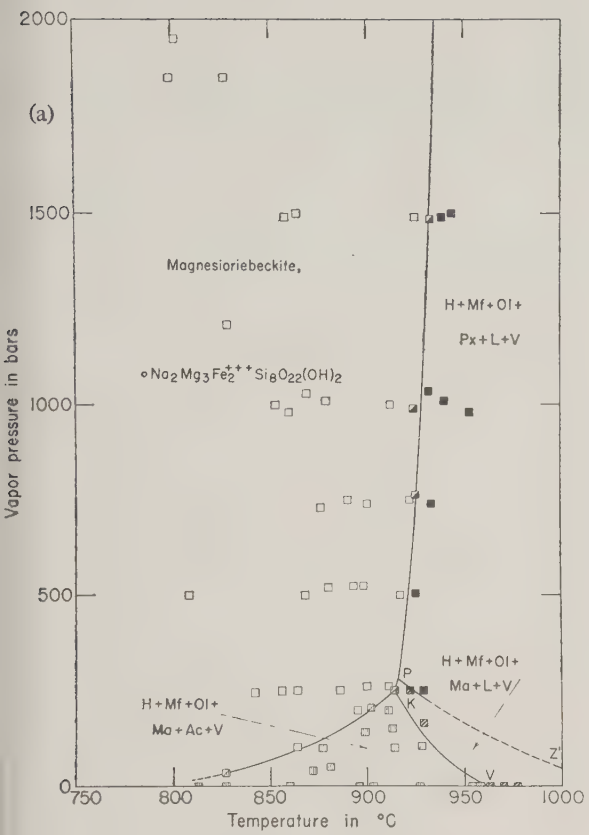

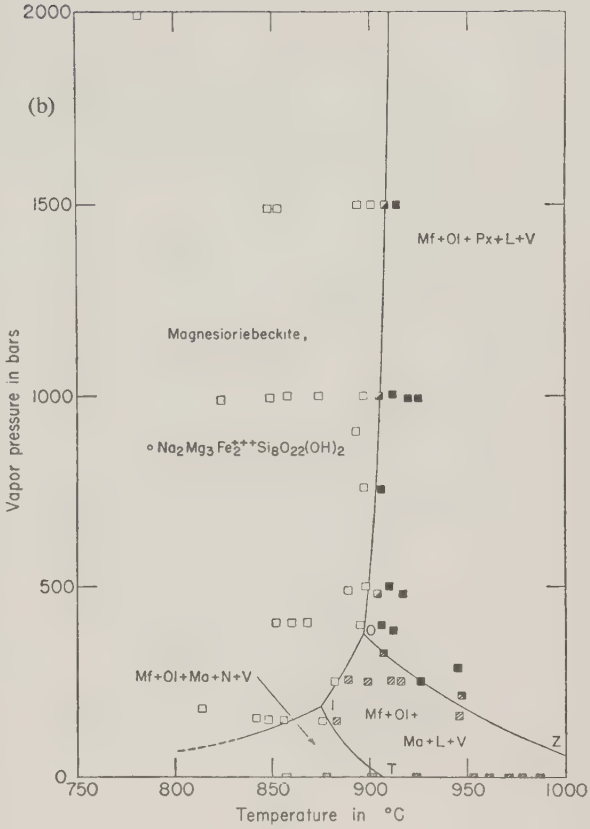

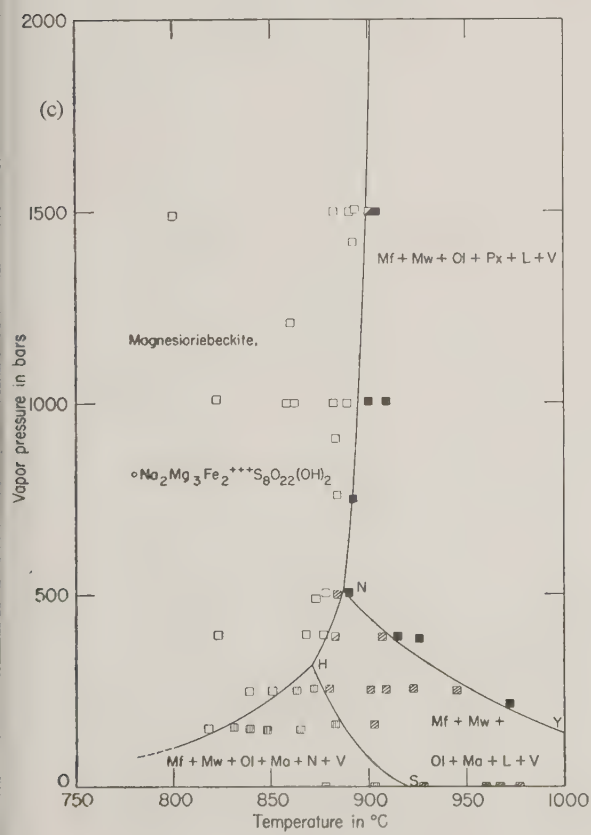

Fig. 3. P_{vapour}–T diagrams of the composition $Na_2O{\cdot}3MgO{\cdot}8SiO_2$ with excess water and with P_{O_2} defined by (a) haematite–magnetite, (b) magnetite + silica–fayalite, and (c) magnetite–wüstite buffers. Divided run symbols indicate presence of the low-temperature assemblage in trace amounts.

exclusive at liquidus temperatures in the system MgO–FeO–Fe_2O_3–SiO_2. These authors did not present subsolidus data, and at lower temperatures (corresponding to those of the magnesioriebeckite study), more similarity may be found between the two systems.

The P_{O_2}–T stability field of magnesioriebeckite at a constant vapour pressure of 2000 bars is plotted in Fig. 4. Iron in the amphibole is predominantly (but not exclusively) ferric, while much of the iron is bivalent in the high-temperature phases. During decomposition of magnesioriebeckite, there is a net transfer of

Table 7. P_{vapour}–T locations of curves presented in Figs. 3–5

Curve	P_{vapour} (bars)	Temp. (°C)
P_{O_2} *defined by a haematite–magnetite buffer*		
H + Mf + Ol + Ma + Ac + Mr + V	35	826 ± 5
	100	867 ± 5
	200	903 ± 5
	250	914 ± 5
H + Mf + Ol + Ma + Ac + L + V	1	963 ± 5
	125	930 ± 5
	250	914 ± 5
H + Mf + Ol + Ma + Mr + L + V	250	914 ± 5
	280	916 ± 5
H + Mf + Ol + Px + Ma + L + V	(230)	(930 ± 15)
	280	916 ± 5
H + Mf + Ol + Px + Mr + L + V	280	916 ± 5
	500	921 ± 5
	750	925 ± 5
	1000	928 ± 5
	1500	932 ± 5
	(2000)	(935 ± 5)
P_{O_2} *defined by a magnetite + silica–fayalite buffer*		
Mf + Ol + Ma + N + Mr + V	150	860 ± 5
	185	875 ± 5
Mf + Ol + Ma + N + L + V	1	908 ± 5
	140	880 ± 5
	185	875 ± 5
Mf + Ol + Ma + Mr + L + V	185	875 ± 5
	250	884 ± 5
	375	897 ± 5
Mf + Ol + Px + Ma + L + V	190	946 ± 5
	250	925 ± 5
	325	907 ± 5
	375	897 ± 5
Mf + Ol + Px + Mr + L + V	375	897 ± 5
	400	897 ± 5
	500	899 ± 5
	750	903 ± 5
	1000	905 ± 5
	1500	908 ± 5
	(2000)	(910 ± 5)

Table 7. (*contd.*)

Curve	P_{vapour} (bars)	Temp. (°C)
P_{O_2} *defined by a magnetite–wüstite buffer*		
Mf + Mw + Ol + Ma + N + Mr + V	150	824 ± 5
	250	856 ± 5
	315	871 ± 5
Mf + Mw + Ol + Ma + N + L + V	1	920 ± 5
	150	888 ± 5
	250	877 ± 5
	315	871 ± 5
Mf + Mw + Ol + Ma + Mr + L + V	315	871 ± 5
	400	879 ± 5
	510	887 ± 5
Mf + Mw + Ol + Px + Ma + L + V	230	960 ± 5
	400	908 ± 5
	510	887 ± 5
Mf + Mw + Ol + Px + Mr + L + V	510	887 ± 5
	750	891 ± 5
	1000	894 ± 5
	1500	898 ± 5
	(2000)	(901 ± 5)

Parentheses designate extrapolated value.

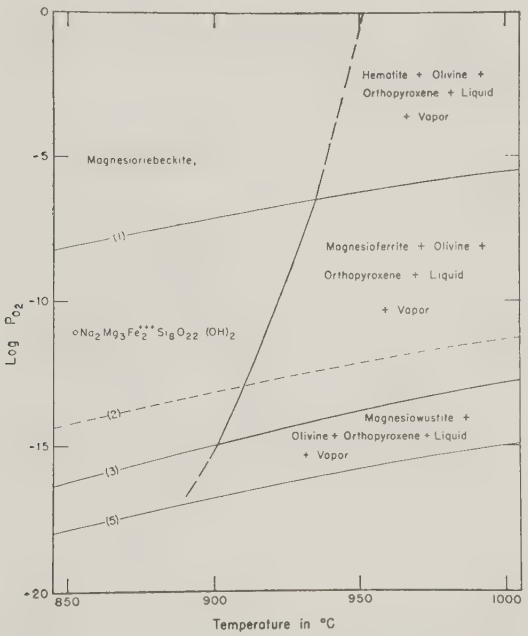

Fig. 4. P_{O_2}–T diagram of the composition $Na_2O3{\cdot}MgO{\cdot}Fe_2O_3{\cdot}8SiO_2$ with excess water at 2000 bars vapour pressure.

oxygen to the vapour phase. Therefore, elevated P_{O_2} favours expansion of the stability field of the more oxidized (small volume) magnesioriebeckite assemblage. Being a ferric mineral, magnesioriebeckite must be stable at partial oxygen pressures in excess of those defined by the haematite–magnetite buffer. Experimentation using the wüstite–iron buffer (the lower P_{O_2} limit of the wüstite field) indicates that magnesioriebeckite can exist at lower partial pressures of

Table 8. Compositions of phases at temperatures directly above the magnesioriebeckite field boundary at 1000 bars total pressure

Temp. (°C)	940	912	900
Log P_{O_2} (bars)	−6·35	−12·9	−14·87
Olivine	$Fo_{95\pm5}$	$Fo_{73\pm10}$*	$Fo_{65\pm10}$*
Orthopyroxene	$En_{98\pm2}$	$En_{79\pm3}$	$En_{73\pm3}$
Refractive index of glass	1·55 ± 0·01		1·53 ± 0·01

* Compositions determined by the method of Yoder and Sahama (1957). The amounts of olivine were small, so an internal X-ray standard was not used. Accordingly, olivine compositions have wide limits of error.

Table 9. Invariant points in the "system" magnesioriebeckite–water shown in Figs. 3 and 5

Point	*P*	*K*	*N*	*H*	*J*
Temp. (°C)	916	914	887	871	—
Log P_{O_2} (bars)	−6·62	−6·65	−15·08	−15·44	—
P_{vapour} (bars)	280	250	510	315	—
Phases	H	H	Mf	Mf	Mf
	Mf	Mf	Mw	Mw	Ol
	Ol	Ol	Ol	Ol	Ma
	Px	Ma	Px	Ma	Ac
	Ma	Ac	Ma	N	N
	Mr	Mr	Mr	Mr	Mr
	L	L	L	L	L
	V	V	V	V	V

oxygen than can magnetite (see last three runs of Table 6). In general, we should not expect ferric or ferrous silicates to occupy the same P_{O_2}–T stability fields as corresponding iron oxides. For example, the fayalite stability field extends to both higher and lower partial oxygen pressures than the wüstite field (Darken, 1948), as does that of annite (Eugster, 1959).

With the exception of haematite and possibly acmite, all condensed phases stable at temperatures above the magnesioriebeckite field contain important amounts of both MgO and FeO. For an example, the compositions of phases (including melt) at temperatures just above the magnesioriebeckite field boundary at 1000 bars total pressure are presented in Table 8. The magnesium–iron ratio in each phase is controlled by three variables—temperature, P_{O_2}, and bulk composition. As the temperature decreases all MgO–FeO-bearing phases become enriched in iron. With declining partial oxygen pressure, the high-temperature

stability limit of MgO–FeO-bearing phases is elevated,* causing a similar increment in iron content. As the partial oxygen pressure and temperature decline, the ferrous iron content of the condensed phase bulk composition increases, permitting the coexistence of iron-rich crystals and a highly ferrous melt (the decreasing index of the glass suggests that its Fe_2O_3/FeO ratio diminishes as P_{O_2} declines).

The FeO/MgO ratio of the condensed phases in the high-temperature assemblages at fixed P_{O_2}, P_{vapour} and T is lowest in the lowest melting crystalline phase, higher in the more refractory minerals, and highest in the liquid. (Bowen and Schairer, 1935a, p. 213, 1935b, pp. 550, 551, have briefly discussed this phenomenon, using as examples olivine, pyroxene and amphibole.) Consequently, at any given P_{O_2}, P_{vapour} and T for the investigated bulk composition, the partition of MgO and FeO among coexistent phases is such that the ratio FeO/MgO is lowest in $Na_2O{\cdot}2(Mg,Fe)O{\cdot}6SiO_2$, and successively higher in the phases $Na_2O{\cdot}5(Mg,Fe)O{\cdot}12SiO_2$, orthopyroxene, olivine, iron (+ Mg) oxide, and highest in the liquid.

Phase assemblages for the composition $Na_2O{\cdot}3MgO{\cdot}Fe_2O_3{\cdot}8SiO_2$ with excess water are shown on a plot of P_{O_2}, P_{vapour} and T in Fig. 5. The stability diagram has been shown in four stages of dissection. Solid lines within the P_{O_2}–P_{vapour}–T volume are experimentally determined curves: projection of these curves (there are three sets, one using each buffer) along the P_{O_2} axis onto a P_{vapour}–T face yields the relations presented in Figs. 3(a), 3(b) and 3(c). Dashed lines within the P_{O_2}–P_{vapour}–T volume are inferred phase relations at partial oxygen pressures both higher and lower than those with which magnetite can coexist. The top face of the diagram, *ABCD*, is a P_{O_2}–T section at 2000 bars vapour pressure, and is essentially a perspective view of Fig. 4.

Fig. 5(a) shows the P_{O_2}–P_{vapour}–T stability volume of magnesioriebeckite. The amphibole field is delineated from high-temperature assemblages of equivalent bulk composition by the magnesioriebeckite stability limit surface. Phase changes among the high-temperature assemblages are reflected on this surface as facets, which represent the P_{O_2}–P_{vapour}–T range for the equilibrium between magnesioriebeckite and specific high-temperature assemblages. (These facets are seen in cross section in Figs. 3 and 4.) At constant vapour pressure, the temperature of the magnesioriebeckite stability limit undoubtedly increases as P_{O_2} increases above that defined by a haematite–magnetite buffer. Magnesioriebeckite can exist stably at partial oxygen pressures as low as those of a wüstite–iron buffer, but it is certain that reduced P_{O_2} drastically lowers the temperature of its field boundary.

In Fig. 5(b), the incongruent melting surfaces of acmite, *WVUJKL*, and $Na_2O{\cdot}2(Mg,Fe)O{\cdot}6SiO_2$, *RSTUJIHG*, have been added. Along surface *WVUJKL*, the phases haematite and/or magnesioferrite (depending on the P_{O_2}) + olivine + $Na_2O{\cdot}5(Mg,Fe)O{\cdot}12SiO_2$ + acmite + liquid + vapour are in equilibrium. The generalized reaction involved in passing through this surface is acmite + vapour = haematite and/or magnesioferrite + liquid. Along surface *RSTUJIHG*, the

* Oxygen in equilibrium with ferrous compounds is consumed during melting in the P_{O_2} range investigated. Schematically, such reactions may be represented:

ferrous solid + O_2 = liquid

Hence, a diminished P_{O_2} tends to increase the high-temperature stability limit of FeO-bearing crystalline phases.

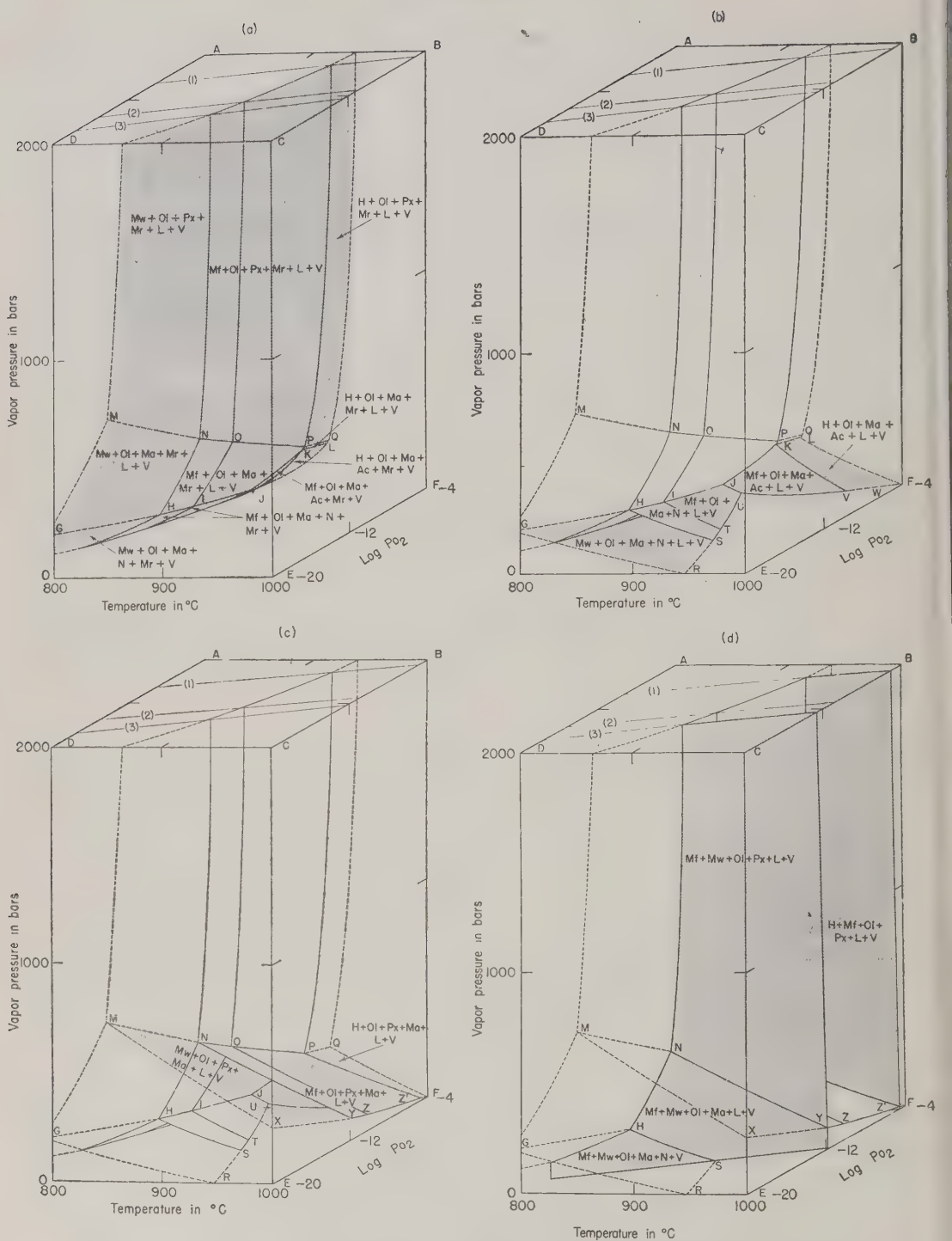
(a)
(b)
(c)
(d)
Vapor pressure in bars
Temperature in °C
Log Po2
Mw + Ol + Px + Mr + L + V
Mf + Ol + Px + Mr + L + V
H + Ol + Px + Mr + L + V
H + Ol + Ma + Mr + L + V
Mw + Ol + Ma + Mr + L + V
Mf + Ol + Ma + Mr + L + V
Mf + Ol + Ma + Ac + Mr + V
Mf + Ol + Ma + N + Mr + V
Mw + Ol + Ma + N + Mr + V
H + Ol + Ma + Ac + L + V
Mf + Ol + Ma + Ac + L + V
Mf + Ol + Ma + N + L + V
Mw + Ol + Ma + N + L + V
H + Ol + Px + Ma + L + V
Mw + Ol + Px + Ma + L + V
Mf + Ol + Px + Ma + L + V
Mf + Mw + Ol + Px + L + V
H + Mf + Ol + Px + L + V
Mf + Mw + Ol + Ma + L + V
Mf + Mw + Ol + Ma + N + V

Fig. 5. P_{O_2}–P_{vapour}–T stability volumes for the composition $Na_2O{\cdot}3MgO{\cdot}Fe_2O_3{\cdot}8SiO_2$ with excess water. (a) Magnesioriebeckite upper stability limit surface shaded. (b) Incongruent melting surfaces of acmite and $Na_2O{\cdot}2(Mg,Fe)O{\cdot}6SiO_2$ shaded. (c) Incongruent melting surface of $Na_2O{\cdot}5(Mg,Fe)O{\cdot}12SiO_2$ shaded. (d) High and low P_{O_2} magnesioferrite field boundary surfaces shaded.

phases magnesioferrite and/or magnesiowüstite (depending on the P_{O_2}) + olivine + $Na_2O{\cdot}5(Mg,Fe)O{\cdot}12SiO_2$ + $Na_2O{\cdot}2(Mg,Fe)O{\cdot}6SiO_2$ + liquid + vapour coexist. The principal reaction involved in passing through this surface is $Na_2O{\cdot}2(Mg,Fe)O{\cdot}6SiO_2$ + vapour = $Na_2O{\cdot}5(Mg,Fe)O{\cdot}12SiO_2$ + liquid. The 1 atm melting curves for acmite, *WVU*, and $Na_2O{\cdot}2(Mg,Fe)O{\cdot}6SiO_2$, *RSTU*, lie on the bottom face of the diagram (a P_{O_2}–T section parallel to face *ABCD* but at P_{vapour} = 1 atm). The high vapour pressure terminations of these incongruent melting surfaces occur at their intersections with the magnesioriebeckite field boundary along the curves *LKJ* and *GHIJ*. The stability of acmite decreases with diminishing P_{O_2}, whereas that of $Na_2O{\cdot}2(Mg,Fe)O{\cdot}6SiO_2$ decreases with increasing partial oxygen pressure. Thus, as indicated in Fig. 5(b), the two incongruent melting surfaces intersect along the curve *UJ*.

Fig. 5(c) shows the form of the incongruent melting surface of $Na_2O{\cdot}5(Mg,Fe)O{\cdot}12SiO_2$, *QPONMXYZZ'F*. Along this surface, phases in stable equilibrium are haematite and/or magnesioferrite, or magnesioferrite and/or magnesiowüstite (depending on the P_{O_2}), + olivine + orthopyroxene + $Na_2O{\cdot}5(Mg,Fe)O{\cdot}12SiO_2$ + liquid + vapour. The generalized reaction in passing through the surface is $Na_2O{\cdot}5(Mg,Fe)O{\cdot}12SiO_2$ + vapour = orthopyroxene + liquid. $Na_2O{\cdot}5(Mg,Fe)O{\cdot}12SiO_2$ is stable above 1000°C at 1 atm vapour pressure; accordingly, its incongruent melting surface intersects the side face *CBFE* (a P_{O_2}–P_{vapour} section at 1000°C). The high vapour pressure termination of this incongruent melting surface occurs at its intersection with the magnesioriebeckite field boundary along the curve *QPONM*. Since it contains ferrous iron in the P_{O_2}–P_{vapour}–T region investigated, increased oxygen pressure decreases the temperature of its stability limit. Accompanying this phenomenon, the FeO/MgO ratio in $Na_2O{\cdot}5(Mg,Fe)O{\cdot}12SiO_2$ decreases, so that at partial oxygen pressures greatly in excess of those defined by the haematite–magnetite buffer, the ferrous iron content of this phase is probably nil. This effect of P_{O_2} on the composition of (Mg,Fe)O-bearing silicates is similarly illustrated by the behaviour of olivine and orthopyroxene as previously described.

Finally, in Fig. 5(d) the two boundary surfaces which separate the fields of haematite, magnesioferrite, and magnesiowüstite have been added. Along these surfaces high-temperature assemblages of bulk composition equivalent to magnesioriebeckite contain coexistent haematite + magnesioferrite, and magnesioferrite + magnesiowüstite. The reactions involved in passing through these surfaces are haematite + MgO (from other phases) = magnesioferrite + O_2, and magnesioferrite (close to the composition of magnetite) + MgO (from other phases) = magnesiowüstite + O_2. The surfaces coincide with the P_{O_2}–P_{total}–T surfaces for the buffers haematite–magnetite and magnetite–wüstite, respectively, with low-temperature terminations along linear intersections with the magnesioriebeckite field boundary.

Thermodynamic Considerations

Application of phase theory to magnesioriebeckite P_{vapour}–T *curves*

The "system" magnesioriebeckite–water can be described by six components—Na, Mg, Fe, Si, H and O. Four invariant points were located in this study, two

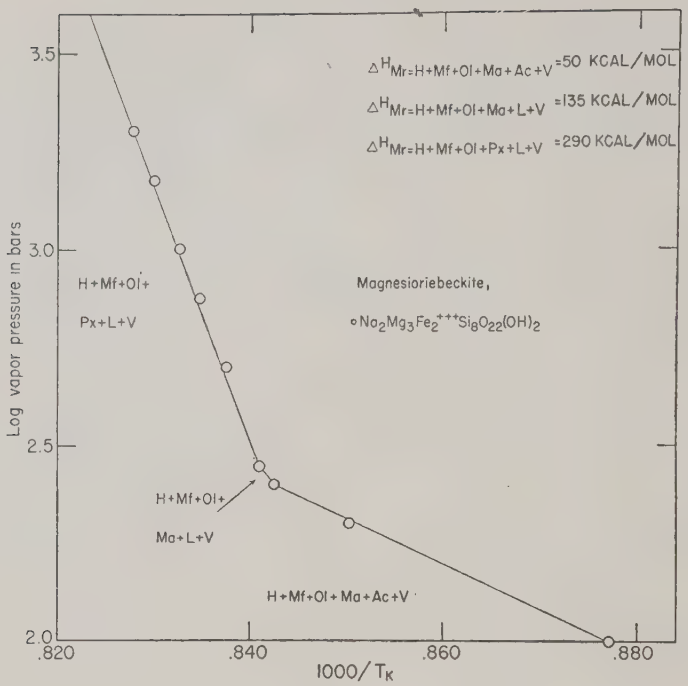
3.5
3.0
2.5
2.0
.820
.840
.860
.880
Log vapor pressure in bars
1000/ T_K
ΔH_Mr=H+Mf+Ol+Ma+Ac+V =50 KCAL/MOL
ΔH_Mr=H+Mf+Ol+Ma+L+V =135 KCAL/MOL
ΔH_Mr=H+Mf+Ol+Px+L+V =290 KCAL/MOL
H+Mf+Ol+
Px+L+V
Magnesioriebeckite,
°Na2Mg3Fe2+++Si8O22(OH)2
H+Mf+Ol+
Ma+L+V
H+Mf+Ol+Ma+Ac+V

(a)

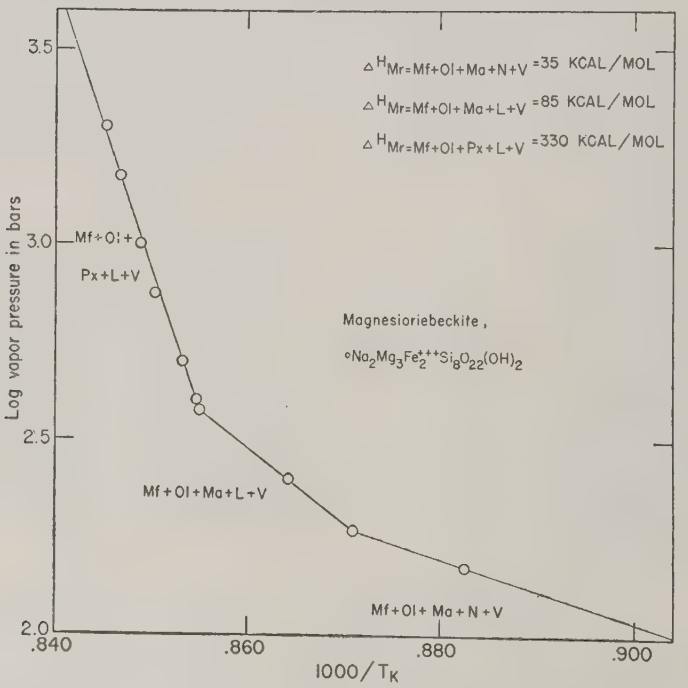
3.5
3.0
2.5
2.0
.840
.860
.880
.900
Log vapor pressure in bars
1000/ T_K
ΔH_Mr=Mf+Ol+Ma+N+V =35 KCAL/MOL
ΔH_Mr=Mf+Ol+Ma+L+V =85 KCAL/MOL
ΔH_Mr=Mf+Ol+Px+L+V =330 KCAL/MOL
Mf+Ol+
Px+L+V
Magnesioriebeckite,
°Na2Mg3Fe2+++Si8O22(OH)2
Mf+Ol+Ma+L+V
Mf+Ol+Ma+N+V

(b)

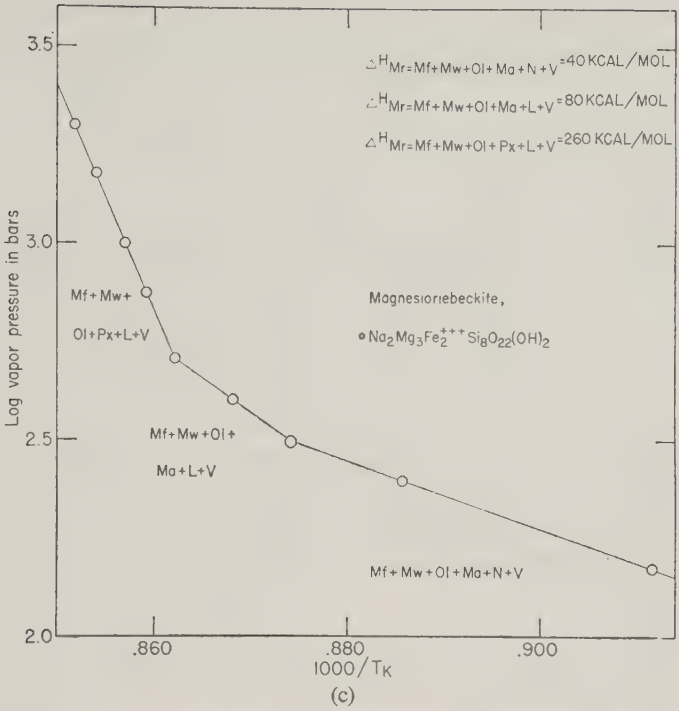

Fig. 6. Log P_{vapour}–$1/T_K$ plot of the magnesioriebeckite stability field with P_{O_2} defined by (a) haematite–magnetite, (b) magnetite + silica–fayalite, and (c) magnetite–wüstite buffers. Graphically derived heats of reaction for this method (integrated Clausius–Clapeyron equation) are also presented.

using a haematite–magnetite buffer and two using a magnetite–wüstite buffer (points P, K, N and H in Figs. 3 and 5). Co-ordinates of these points and phase assemblages are given in Table 9. A fifth invariant point, J, may be seen in Fig. 5(b) where the intersection of the incongruent melting surfaces of acmite and $Na_2O{\cdot}2(Mg,Fe)O{\cdot}6SiO_2$ meets the magnesioriebeckite field. $P = T$ co-ordinates of this point could not be determined for lack of a suitable P_{O_2} buffer.

Eight univariant curves terminate in an invariant point in a six-component system. Figs. 3(a) and 3(c) (the magnesioriebeckite P_{vapour}–T diagram using haematite–magnetite and magnetite–wüstite buffers, respectively) show three of these curves for each of two invariant points; two additional curves to each invariant point appear in Fig. 5. The remaining three univariant curves which lie within the amphibole field can be obtained only by appropriate changes of bulk composition or by elimination of the vapour phase. The location of curves not experimentally determined requires knowledge regarding the change of composition of all phases with P_{O_2}, P_{vapour} and T; this information is largely lacking. Complication also arises in the visualization of joins within an octahedron (each apex of which represents a component) for specific physical conditions.

Along the univariant curves shown in Figs. 3(a) and 3(c), seven phases are in equilibrium. Six phases appear in the divariant fields. In Fig. 3(b) (the magnesioriebeckite P_{vapour}–T diagram using a magnetite + silica–fayalite buffer)

one less phase is present throughout. The extra degree of freedom (which may be considered as oxygen content, FeO/Fe_2O_3 ratio or P_{O_2}) may be visualized in Fig. 5 as occurring between the P_{O_2}–T limits of the magnesioferrite field. In this region, the high-temperature phase assemblages can exist over a wide range of oxygen partial pressure, vapour (total) pressure, and temperature.

ΔH for reactions involving magnesioriebeckite

The decomposition curve of a hydrous mineral plotted against log P_{vapour} and $1/T_K$ may closely approximate a straight line (e.g. see Yoder and Eugster, 1955, p. 261). Such treatment assumes that (1) the vapour behaves as an ideal gas, (2) the heat of the reaction is independent of temperature, and (3) the volume change of the reacting solids is negligible. The slope of the straight line is $-\Delta H/2{\cdot}303R$. In Figs. 6(a), 6(b) and 6(c) the curves bounding the magnesioriebeckite stability field for partial oxygen pressures defined by the three buffers are plotted in this manner; the derived values of the heats of reaction are also given. Because of the assumptions required by this method, and small uncertainties in locating the magnesioriebeckite curves, such values of ΔH are probably accurate only to within $\pm$20 to 30 per cent. Since molar volumes of some of the phases are unknown, the more precise method of computing ΔS and ΔH by means of the Clapeyron equation cannot be used.

The calculated values of ΔH are comparable to those of reactions involving other hydrous minerals (Table 10). ΔH values for dehydration reactions are much smaller than for partial melting.

Description of Synthetic Magnesioriebeckite

Magnesioriebeckite optical data

Refractive indices and extinction angles of magnesioriebeckite are listed in Table 11. Fig. 7 illustrates the variation of N_X with partial oxygen pressure and temperature. Total pressure does not influence the optical properties of magnesioriebeckite. At a given temperature, high refractive index characterizes crystals grown at high partial pressure of oxygen, whereas at fixed P_{O_2} the refractive index of magnesioriebeckite varies inversely with temperature of crystallization. Equilibrium has been demonstrated by rerunning synthetic magnesioriebeckite at both higher and lower P_{O_2}. For example, the magnesioriebeckite produced at 800°C and log $P_{O_2} = -17{\cdot}50$ was rerun at 808°C and log $P_{O_2} = -8{\cdot}78$; magnesioriebeckite crystallized at 802°C and log $P_{O_2} = -9{\cdot}11$ was rerun at 854°C and log $P_{O_2} = -17{\cdot}68$. In both cases, new refractive indices were identical with those obtained for magnesioriebeckite grown directly from an oxide mixture at the same temperatures and partial oxygen pressures. Refractive indices of magnesioriebeckite are also independent of run duration, as may be seen from Table 11.

Indices of refraction are presumed to be a measure of the oxidation state of the iron in magnesioriebeckite, the lower the index, the smaller the Fe_2O_3/FeO ratio. Electrostatic neutrality of the structure is probably maintained: (1) through replacement of oxygen by hydroxyl (as suggested by Zussman (1955) for actinolite); (2) through partial filling of the vacant position by cations (H_3O + ?);

Table 10. Values for ΔH for reactions involving magnesioriebeckite compared with ΔH values for other hydrous minerals

Reaction	ΔH (kcal)	Reference
Mr = H + Mf + Ol + Ma + Ac + V	50	This paper
Mr = H + Mf + Ol + Ma + L + V	135	This paper
Mr = H + Mf + Ol + Px + L + V	290	This paper
Mr = Mf + Ol + Ma + N + V	35	This paper
Mr = Mf + Ol + Ma + L + V	85	This paper
Mr = Mf + Ol + Px + L + V	330	This paper
Mr = Mf + Mw + Ol + Ma + N + V	40	This paper
Mr = Mf + Mw + Ol + Ma + L + V	80	This paper
Mr = Mf + Mw + Ol + Px + L + V	260	This paper
Muscovite = sanidine + corundum + V	32	Yoder and Eugster (1955)
Tremolite = diopside + enstatite + Q + V	33	Boyd (1959)*
Brucite = periclase + V	10	MacDonald (1955)
Paragonite = albite + corundum + V	36	Eugster and Yoder (1954)*
Muscovite + Q = sanidine + mullite + V	49	Yoder and Eugster (1955)
2 analcite = nepheline + albite + 2V	56	Yoder (1954)*
Phlogopite = forsterite + leucite + O—$KAlSiO_4$ + V	69	Yoder and Eugster (1954)

* Personal communication.

Table 11. Optical properties of synthetic and natural magnesioriebeckite

Starting material	Temp. (°C)	P_{vapour} (bars)	Log P_{O_2} (bars)	Duration (hr)	N_X	N_Z	Extinction angle (°)
mix	876	730	−7·38	119	1·656 ± 0·002	1·674 ± 0·003	$Z \wedge c = 12 \pm 2$
mix	864	103	−7·50	70	1·657 ± 0·004	1·673 ± 0·004	$Y \wedge c = 4 \pm 4$
mix	856	248	−7·80	46	1·655 ± 0·003	1·668 ± 0·004	$X \wedge c = 9 \pm 2$ $Y \wedge c = 13 \pm 2$
mix	853	1000	−7·84	34	1·656 ± 0·002	1·674 ± 0·003	$Y \wedge c = 8 \pm 3$
mix	828	1210	−8·39	19	1·652 ± 0·002	1·672 ± 0·002	$X \wedge c = 12 \pm 3$ $Y \wedge c = 11 \pm 3$
Mr	808	500	−8·78	18	1·652 ± 0·002	1·670 ± 0·002	$Z \wedge c = 11 \pm 3$
mix	802	1950	−9·11	5	1·651 ± 0·003	1·671 ± 0·003	$Y \wedge c = 13 \pm 2$
mix	901	1500	−13·1	2	1·636 ± 0·004	1·651 ± 0·002	$Z \wedge c = 14 \pm 3$
mix	874	1000	−13·6	50	1·642 ± 0·002	1·657 ± 0·002	$Z \wedge c = 18 \pm 3$
mix	852	405	−14·0	36	1·641 ± 0·002	1·659 ± 0·003	$Z \wedge c = 18 \pm 2$
mix	848	1490	−14·2	21	1·640 ± 0·002	1·658 ± 0·002	$Z \wedge c = 21 \pm 2$
mix	814	180	−14·9	162	1·640 ± 0·002	1·658 ± 0·002	$Z \wedge c = 24 \pm 3$
Mf + Mw + Ol + Px + L	883	908	−15·23	25	1·637 ± 0·002	1·654 ± 0·002	$Z \wedge c = 18 \pm 2$
mix	858	1000	−15·87	50	1·637 ± 0·002	1·655 ± 0·002	$Z \wedge c = 17 \pm 3$
mix	839	248	−16·27	40	1·637 ± 0·004	1·657 ± 0·004	$Z \wedge c = 16 \pm 4$
mix	822	1010	−16·81	60	1·637 ± 0·002	1·655 ± 0·002	$Z \wedge c = 19 \pm 3$
mix	800	1490	−17·50	22	1·636 ± 0·002	1·658 ± 0·002	$Z \wedge c = 18 \pm 2$
Mr	854	1205	−17·68	13	1·633 ± 0·003	1·651 ± 0·003	$Z \wedge c = 14 \pm 3$
Miyashiro and Iwasaki (1957)			core rim		1·640 1·660	1·650 1·670	$Z \wedge c = 17$ $Y \wedge c = 28$
de Villiers (1949)					1·659	1·668	$X \wedge c = 9$–21

or (3) through minor solid solution with grunerite, $o\mathrm{Fe_7^{2+}Si_8O_{22}(OH)_2}$, or arfvedsonite, $\mathrm{Na_3Fe_4^{2+}Fe^{3+}Si_8O_{22}(OH)_2}$. In this third case, excess soda or silica and magnesia should occur in another phase. Such small quantities would be difficult to recognize since minor amounts of metastable phases are usually found with the magnesioriebeckite. However, yields of 98 to 100 per cent amphibole indicate that the amount of solid solution between magnesioriebeckite and a ferrous amphibole due to reduction of ferric iron is insignificant in the experimental investigation.

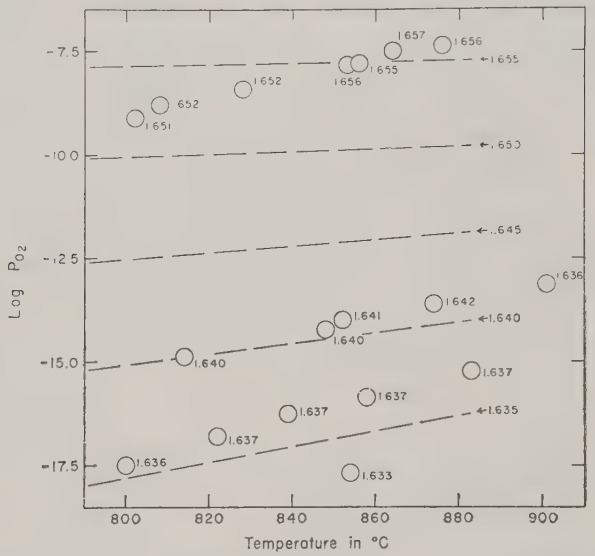

Fig. 7. Variation of N_X of magnesioriebeckite with P_{O_2} and T. (The sample run at 901°C, log $P_{O_2} = -13{\cdot}1$ crystallized within the magnesioriebeckite melting interval and is more magnesian than pure magnesioriebeckite.)

The seemingly anomalous optical properties of the amphibole shown in Fig. 7 at 901°C, log $P_{O_2} = -13{\cdot}12$ result from the fact that it crystallized within the previously mentioned melting interval of magnesioriebeckite and thus is more magnesian than the stable phase occurring below the magnesioriebeckite solidus surface. This surface lies approximately 20°C below the high-temperature amphibole field boundary.

Table 11 also illustrates a remarkable variability of extinction angle and sign of elongation among both natural and synthetic magnesioriebeckites. Obviously considerable care should be exercised in attempting to derive the chemical composition of iron-bearing amphiboles from their optical properties.

Magnesioriebeckite X-ray data

X-ray diffractometer patterns of magnesioriebeckite scanned between 5 and 60° 2θ using iron radiation are reproduced in Fig. 8. For the P_{O_2} range investigated, the synthetic magnesioriebeckite patterns are identical. A nonsystematic variance in peak height was observed, probably as a result of differences in grain size and orientation among the samples. For instance, in Fig. 8, reflections at 35·6° 2θ (301)

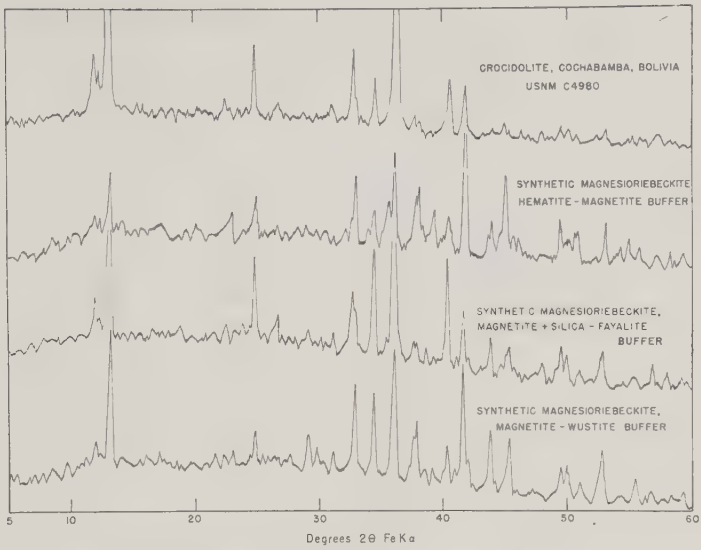

Fig. 8. X-ray diffractometer patterns for synthetic and natural magnesioriebeckite. The chemical analysis of USNM C-4980 is presented in Table 12.

and 39·2° 2θ ($\bar{1}41$) are well developed in a synthetic sample grown with P_{O_2} defined by a haematite–magnetite buffer while these reflections are indistinguishable from background radiation in a synthetic sample crystallized using a magnetite–wüstite buffer. The reflection at 12·4° 2θ could not be indexed employing the conventional amphibole space group criteria. The positions of the peaks agree well with natural magnesioriebeckite (crocidolite) from the Cochabama District, Bolivia (USNM C4980) obtained from Dr. G. Switzer of the U.S. National Museum. A new analysis of this material, which closely approximates the magnesioriebeckite end member is presented in Table 12.

Reflections of synthetic magnesioriebeckite were indexed by comparison with values calculated using the cell dimensions and space group ($I2/m$) given by Whittaker (1949) for another sample of Bolivian crocidolite. The sequence of reflections was then compared with that presented by Comeforo and Kohn (1954) for synthetic fluortremolite. The two patterns are quite similar. Since Comeforo and Kohn used the standard orientation of Bragg (1937, p. 190), $C2/m$, their indices were converted to those of the $I2/m$ orientation using the matrix of transformation

$$\begin{Vmatrix} h0l \\ 0k0 \\ 00\bar{l} \end{Vmatrix}$$

as explained by Buerger (1953, pp. 10–16).

Five reflections of synthetic magnesioriebeckite were measured using Lake Toxaway quartz as an internal standard (see Table 13). From these values, Q-values for individual reflections and the unit cell dimensions were calculated. Table 14 shows d-spacings, intensities, Q-values and 2θ values for synthetic magnesioriebeckite. In Table 15, lattice parameters and cell volume for the synthetic material are compared with data presented by Whittaker (1949) for

Table 12. New analysis of crocidolite from Cochabamba, Bolivia (USNM C-4980)

	Wt. (%)	Atomic proportions*			
SiO_2	55·44	Si	7·90		8·00
TiO_2	0·04	Ti	0·01		
Al_2O_3	0·22	Al	0·04	0·05	
Fe_2O_3	16·77	Fe^{3+}	1·79	1·74	4·98
FeO	5·23	Fe^{2+}	0·62		
MnO	0·09	Mn	0·01		
MgO	12·30	Mg	2·61		
CaO	2·17	Ca	0·33		2·22
Na_2O	6·76	Na	1·86		
K_2O	0·15	K	0·03		
H_2O+	0·55	Cl	0·01		0·30
H_2O-	0·05	F	0·03		
BaO	0·00	(H_2O+	0·26)		
Cl^-	0·08				
F^-	0·18				
	100·03				
Less O for Cl^- and F^-	0·09	Chemical analysis by H. B. Wiik.			
	99·94				

* Atomic proportions were calculated on the anhydrous basis of 23 oxygens, assuming $OH^- + F^- + Cl^- = 2{\cdot}00$ per formula unit (Miyashiro, 1957, p. 59).

Bolivian crocidolite. The latter sample has a smaller unit cell than synthetic magnesioriebeckite. The presence of additional ions in Whittaker's material may account for the difference in cell dimensions.

Geologic Application

Magnesioriebeckite occurs in schists in Japan (Miyashiro and Iwasaki, 1957; Seki, 1958) and the Ukraine (Polovinkina, 1924, 1953), in Bolivian and South African metasediments (Ahlfeld, 1943; de Villiers, 1949), and in marble in southern Australia (Jack, 1921; Wymond and Wilson, 1951; King, 1955). Milton (Milton and Eugster, 1959) described authigenic riebeckite from the Green River formation of the Colorado Plateau. Dr Milton supplied the writer with a sample of this material; optical data ($N_Y = 1{\cdot}64$, but variable, $X \wedge c \approx 5°$) suggest it is probably an intermediate member of the magnesioriebeckite–riebeckite series.

In most igneous and metamorphic rocks, soda and alumina are combined principally in plagioclase, and lime is concentrated in a calciferous amphibole and in other ferromagnesian minerals. Alkali amphiboles are not as common, and are thought to result: (1) from hypersodic and subcalcic bulk compositions, or (2) through physical conditions different from those commonly attained during regional metamorphism. Magnesioriebeckite is the first alkali amphibole for which P–T relations have been determined. Its high-temperature stability limit lies between those of tremolite and pargasite (Boyd, 1959). The authigenic occurrence

Table 13. Measurements of five X-ray reflections for synthetic magnesioriebeckite (space group $I2/m$)

Reflection	Number of readings	$2\theta_{ave.}$*	Standard deviation	Standard chart error of the mean
040	10	24·824	0·03218	±0·0102
231	4	32·901	0·02580	±0·0129
310	4	36·014	0·02373	±0·0119
251	4	41·665	0·01217	±0·0061
002	4	45·343	0·00648	±0·0032

* FeK_α = 1·9373 Å.

Table 14. X-ray powder data for synthetic magnesioriebeckite (space group $I2/m$)

Reflection	$2\theta_{obs}$*	Q_{calc}	Q_{obs}	ΔQ	I	d (Å)
020	11·96	0·012312	0·011574	−0·000738	11	9·298
110	13·16	0·014058	0·014004	0·000054	>100	8·453
040	24·824	0·049239	0·049239	0·000000	24	4·506
031	29·07	0·067283	0·067112	0·000171	23	3·860
231	32·901	0·085451	0·085475	−0·000024	65	3·420
240	34·35	0·093149	0·092925	0·000224	62	3·280
310	36·014	0·101856	0·101856	0·000000	90	3·135
321	37·85	0·112069	0·112098	−0·000029	41	2·987
051	38·66	0·116532	0·116745	−0·000213	14	2·926
330	40·37	0·126486	0·125708	0·000778	28	2·807
251	41·665	0·134700	0·134778	−0·000078	78	2·724
$\bar{2}31$	42·07	0·136926	0·137325	−0·000399	19	2·699
161	43·81	0·148501	0·148346	0·000155	31	2·596
002	45·343	0·158332	0·158332	0·000000	39	2·513
$\bar{2}51$	49·43	0·186175	0·186277	−0·000102	10	2·317
071	49·98	0·190412	0·190177	0·000235	17	2·293
$\bar{1}12$	51·04	0·198128	0·197819	0·000309	9	2·248
361	52·79	0·210567	0·210630	−0·000063	20	2·178
402	55·46	0·230992	0·230751	0·000241	15	2·082

* FeK_α = 1·9373 Å.

Table 15. Unit cell dimensions of synthetic and natural magnesioriebeckite

Synthetic magnesioriebeckite	Bolivian crocidolite, Whittaker (1949)
a = 10·04 Å b = 18·02 Å c = 5·28 Å β = 72·0° cell volume = 908·6 Å^3	a = 9·89 Å b = 17·95 Å c = 5·31 Å β = 72½° cell volume = 898·0 Å^3*

* Calculated by present writer.

of magnesioriebeckite–riebeckite and the high-temperature phase relations presented in this paper indicate that magnesioriebeckite is stable over a wide range of physical conditions in rocks of appropriate bulk composition (high soda, magnesia and ferric iron, and low alumina and lime).

The crocidolite (fibrous member of the series magnesioriebeckite–riebeckite) deposits of South Africa and Bolivia appear to have formed in rocks of favourable bulk compositions. Peacock (1928) and Hall (1930) considered metasomatic introduction of Na_2O, but concluded from field evidence that original sedimentary layers probably contained the necessary soda.

Small cross-fibre asbestos deposits in South Australia, composed of nearly pure magnesioriebeckite (crocidolite) and/or tremolite have been described by King (1955). The host rock is dolomitic, tremolite-bearing marble which locally contains magnesite. According to King, the asbestos is related to metasomatism involving tourmalinization and albitization. In a rock containing abundant calcium–magnesium carbonates, reaction with soda-rich fluids might be expected to yield soda tremolite instead of magnesioriebeckite. Assuming limited solid solution, an equilibrium reaction between these two amphiboles can be written:

$$MgCO_3 + CaMg(CO_3)_2 + o Na_2Mg_3Fe_2^{3+}Si_8O_{22}(OH)_2 = Na_2CaMg_5Si_8O_{22}(OH)_2 + Fe_2O_3 + 3CO_2$$

However, the partition of CaO between silicate and carbonate phases is in part dependent upon the P_{CO_2} (Danielsson, 1950). High partial pressure of carbon dioxide favours lime-bearing carbonates and CaO-poor silicates as illustrated by the above equation. Possibly magnesioriebeckite crystallized under conditions of soda metasomatism involving relatively high P_{CO_2} (or low temperature), while soda tremolite would have been favoured by lower partial pressures of carbon dioxide (or higher temperatures). The occurrence of tremolite in the same area suggests that some of the solutions may not have been hypersodic (or alternatively, either partial carbon dioxide pressure was quite low or relatively high temperature prevailed).

The authigenic riebeckite described by Milton and Eugster (1959) occurs in a sequence of evaporites of the Green River formation. The original connate fluids of these rocks were brines, judging from the abundance of soda-rich minerals; the presence of a member of the magnesioriebeckite–riebeckite series doubtless is a manifestation of the hypersodic nature of these fluids.

Miyashiro and Iwasaki (1957) have described a Japanese occurrence of magnesioriebeckite in an alkali-deficient, haematite-rich schist closely associated with glaucophane-bearing rocks. Albite is absent and Na_2O is principally contained in the amphibole. In this rock most of the Al_2O_3 is present in garnet and muscovite, chiefly in octahedral co-ordination; as Thompson (1947) observed, octahedral co-ordination of aluminium is favoured by high pressure. The present writer suggests that the lack of sodic plagioclase indicates its instability due to physical conditions characteristic of the glaucophane schist facies. The formation of magnesioriebeckite instead of glaucophane doubtless reflects the high Fe_2O_3 content of this rock. The problem of the glaucophane schist facies will be discussed more fully in a forthcoming paper.

Acknowledgements—The writer is especially indebted to F. R. Boyd of the Geophysical Laboratory who suggested the problem and supervised the experimental investigations. His constructive criticism and guidance are deeply appreciated. The writer also benefited greatly from many discussions with H. P. Eugster, D. R. Wones, H. S. Yoder, J. F. Schairer and N. Morimoto, all of the Geophysical Laboratory. To Professor A. C. Waters, of the Johns Hopkins University, who directed the pre-doctoral studies, thanks are also due.

Financial support of the investigation was derived from a National Science Foundation Terminal Year Fellowship and a 2-year Johns Hopkins Geophysical Laboratory Fellowship.

References

Ahlfeld F. (1943) Los yacimientos de crocidolita en las yungas de Cochabamba. *Notas Museo La Plata* **8** (*Geologia* No. 27), 355–371.

Bowen N. L. and Schairer J. F. (1935a) The system, MgO–FeO -SiO_2. *Amer. J. Sci.* **29,** 151–217.

Bowen N. L. and Schairer J. F. (1935b) Grunerite from Rockport, Massachusetts, and a series of synthetic fluor-amphiboles. *Amer. Min.* **20,** 543–551.

Boyd F. R. (1959) Hydrothermal investigations of amphiboles. In *Researches in Geochemistry.* John Wiley, New York.

Bragg W. L. (1937) *The Atomic Structure of Minerals.* Cornell Press, Ithaca.

Buerger M. J. (1953) *X-ray Crystallography.* John Wiley, New York.

Comeforo J. E. and Kohn J. A. (1954) Synthetic asbestos investigations—I. Study of synthetic fluor-tremolite. *Amer. Min.* **39,** 537–548.

Danielsson A. (1950) Das Calcit-Wollastonitgleichgewichte. *Geochim. et Cosmochim. Acta* **1,** 55–69.

Darken L. S. (1948) Melting points of iron oxides on silica; phase equilibria in the system Fe–Si–O as a function of gas composition and temperature. *J. Amer. Chem. Soc.* **70,** 2046–2053.

Darken L. S. and Gurry R. W. (1945) The system iron–oxygen—I. The wüstite field and related equilibria. *J. Amer. Chem. Soc.* **67,** 1398–1412.

Darken L. S. and Gurry R. W. (1946) The system iron–oxygen—II. Equilibrium and thermodynamics of liquid oxide and other phases. *J. Amer. Chem. Soc.* **68,** 795–816.

Eugster H. P. (1957) Heterogeneous reactions involving oxidation and reduction at high pressures and temperatures. *J. Chem. Phys.* **26,** 1760–1761.

Eugster H. P. (1959) Reduction and oxidation in metamorphism. In *Researches in Geochemistry.* John Wiley, New York.

Eugster H. P. and Yoder H. S. (1954) Stability and occurrence of paragonite. *Bull. Geol. Soc. Amer.* **65,** 1248.

Glasstone S. (1947) *Thermodynamics for Chemists.* Van Nostrand, New York.

Hall A. L. (1930) Asbestos in the Union of South Africa. *Geol. Surv. Union of South Africa,* Mem. 12.

Jack R. L. (1921) Report on the asbestos (crocidolite) deposits on sections 2A and 3A, hundred of Bright. *Dept. Mines, South Australia, Mining Rev.* No. 33.

King D. (1955) Investigation of asbestos deposits in the Robertstown and Truro Districts. *Dept. Mines, South Australia, Mining Rev.* No. 103, 58–73.

MacDonald G. J. F. (1955) Gibbs free energy of water at elevated temperatures and pressures with application to the brucite-periclase equilibrium. *J. Geol.* **63,** 244–252.

Milton C. and Eugster H. P. (1959) Mineral assemblages of the Green River formation. In *Researches in Geochemistry.* John Wiley, New York.

Miyashiro A. (1957) The chemistry, optics, and genesis of the alkali-amphiboles. *J. Fac. Sci., Univ. Tokyo* Sec. II, **11** (Pt. 1), 57–83.

Miyashiro A. and Iwasaki M. (1957) Magnesioriebeckite in crystalline schists of Bizan in Sikoku, Japan. *J. Geol. Soc. Japan* **63,** No. 747, 698–703.

Moore W. J. (1955) *Physical Chemistry.* Prentice-Hall, New York.

Muan A. (1955) Phase equilibria in the system FeO–Fe_2O_3–SiO_2. *J. Metals, Trans. A.I.M.E.* **203,** 965–976.

Muan A. (1958) Phase equilibria at high temperatures in oxide systems involving changes in oxidation states. *Amer. J. Sci.* **256,** 171–207.

Muan A. and Osborn E. F. (1956) Phase equilibria at liquidus temperatures in the system MgO–FeO–Fe_2O_3–SiO_2. *J. Amer. Ceram. Soc.* **39,** 121–140.

Newton R. H. (1935) Activity coefficients of gases. *Industr. Engng. Chem.* **27,** 302–306.

Norton F. J. (1955) Dissociation pressures of iron and copper oxides. *Rept. Gen. Electric Res. Lab.* No. 55-RL-1248.

Peacock M. A. (1928) The nature and origin of the amphibole asbestos of South Africa. *Amer. Min.* **13,** 241–285.

Polovinkina Y. I. (1924) On some interesting amphiboles from the rocks of Krivoi Rog. *Mem. Soc. Russe Min.* Ser. 2, **53,** 199–234.

Polovinkina Y. I. (1953) Cummingtonite and alkali amphiboles from Krivoi Rog. *Min. Sbornik, Lvov Geol. Soc.* No. 7, 167–186.

Schairer J. F. and Bowen N. L. (1955) The system K_2O–Al_2O_3–SiO_2. *Amer. J. Sci.* **253,** 681–746.

Schairer J. F. and Bowen N. L. (1956) The system Na_2O–Al_2O_3–SiO_2. *Amer. J. Sci.* **254,** 129–195.

Schairer J. F., Yoder H. S. and Keene A. G. (1954) Anhydrous silicate systems. *Carnegie Inst. Wash. Year Book* No. 53, 123–125.

Schenk R. von, Franz H. and Laymann A. (1932) Gleichgewichtsuntersuchungen über die Reduktions-, Oxydations-, und Kohlungsvorgänge beim Eisen—XI. *Z. anorg. allgem. Chem.* **206,** 129–151.

Seki Y. (1958) Glaucophanitic regional metamorphism in the Kanto Mountains. *Japan. J. Geol. and Geog.* 233–258.

Sundius N. (1946) The classification of the hornblendes and the solid solution relations in the amphibole group. *Sver. Geol. Unders. Arsb.* **40,** No. 4, 1–36.

Thompson J. B. (1947) Role of aluminum in rock-forming silicates. *Bull. Geol. Soc. Amer.* **58,** 1232.

Tuttle O. F. (1948) A new hydrothermal quenching apparatus. *Amer. J. Sci.* **246,** 628–635.

Tuttle O. F. (1949) Two pressure vessels for silicate-water studies. *Bull. Geol. Soc. Amer.* **60,** 1727–1729.

Villiers J. E. de (1949) Note on an unusual amphibole from Zesfontein, South West Africa. *Trans. Geol. Soc. South Africa* **51,** 77–80.

Wagman D. D., Kilpatrick J. E., Taylor W. J., Pitzer K. S. and Rossini, F. D. (1945) Heats, free energies, and equilibrium constants of some reactions involving O_2, H_2, H_2O, C, CO, CO_2, and CH_4. *J. Res. Nat. Bur. Stand.* **34,** 143–161.

Warren B. E. (1929) The structure of tremolite. *Zeit. Krist.* **72,** 42–57.

Whittaker E. J. W. (1949) The structure of Bolivian crocidolite. *Acta Cryst.* **2,** 312–317.

Wymond A. P. and Wilson R. B. (1951) An occurrence of crocidolite near Robertstown, South Australia. *Trans. Roy. Soc. South Australia* **74,** 44–48.

Yoder H. S. (1954) Zeolites. *Carnegie Inst. Wash. Year Book* No. 53, 121–122.

Yoder H. S. and Eugster H. P. (1954) Phlogopite synthesis and stability range. *Geochim. et Cosmochim. Acta* **6,** 157–185.

Yoder H. S. and Eugster H. P. (1955) Synthetic and natural muscovites. *Geochim. et Cosmochim. Acta* **8,** 225–280.

Yoder H. S. and Sahama Th. G. (1957) Olivine X-ray determinative curve. *Amer. Min.* **42,** 475–491.

Zussman J. (1955) The crystal structure of an actinolite. *Acta Cryst.* **8,** 301–308.

Geochimica et Cosmochimica Acta, 1960, Vol. 19, pp. 41 to 52. Pergamon Press Ltd. Printed in Northern Ireland

Dating galenas by means of their isotopic constitutions—II

R. D. Russell and R. M. Farquhar
Geophysics Laboratory, Department of Physics, University of British Columbia, Canada
and Geophysics Laboratory, Department of Physics, University of Toronto, Canada

(*Received* 5 *April* 1959; *revised August* 1959)

Abstract—Recently a rather large number of analyses of common lead samples has become available, and these in turn have led to a better understanding of the precise nature of the physical and geological processes resulting in the observed variations of lead isotope ratios. Specifically, there now appear to be three classes of leads, each of which has lead isotope ratios that vary in a remarkably simple pattern. These are meteoritic leads, anomalous leads, and leads from certain conformable lead ore deposits. The meteoritic leads and conformable leads both appear to have developed in surroundings where thorium and uranium had very similar properties, and in both cases the thorium to uranium ratio corresponds to a present value of $3{\cdot}73 \pm 0{\cdot}03$. This is taken to be evidence that both classes developed under predominantly reducing conditions. In contrast, the presence of thorium to uranium ratio present during the production of anomalous leads is extremely variable, suggesting an oxidizing environment. It has been suggested that all vein leads may be anomalous to some degree and therefore should be interpreted with this possibility in mind.

The methods for dating galenas proposed previously by the present writers are re-examined in view of these developments and it is shown that they may lead to more explicit information on the age and history of lead ores than has usually been obtained.

Introduction

A few years ago we became authors of a paper dealing with a method for estimating the ages of galenas for which the lead isotope ratios were known (Russell *et al.*, 1954). At the time that paper was written there appeared to be sufficient isotopic data available to justify the supposition that the isotopic behaviour of leads was rather regular and predictable and that the isotope ratios could be used to estimate the ages of the minerals. It also appeared that the relationships between the isotope ratios and ages of lead minerals were very imperfect and very large uncertainties were assigned to the age values obtained. These ranged as high as $\pm$800 million years.

Since the publication of the above paper there have been a number of developments that bear on this subject and it is worthwhile to reassess this problem in the light of our present knowledge. These developments have resulted to a considerable degree from the very extensive effort applied to dating galenas by F. G. Houtermans and his associates at the University of Bern, Switzerland, and by ourselves and others at the University of Toronto, Canada, as well as new discoveries in closely allied fields made by other scientists. They include the great advances in the understanding of the nature and behaviour of *anomalous* leads (Cahen *et al.*, 1958; Russell *et al.*, 1957; Farquhar and Russell, 1957), the recent determination of the ratios of the lead isotopes in meteorites (Patterson, 1956) and the recognition of a certain class of lead ores that may have had a simpler history than many vein leads and therefore may be easier to interpret (Stanton and Russell, 1959). It is the primary purpose of this paper to discuss the dating of galenas in the light of these developments.

There have been two procedures suggested for dating common leads, one by the present writers in the paper cited (Russell *et al.*, 1954) and that proposed by

Houtermans (Eberhardt *et al.*, 1955). The first was based on a mathematical treatment developed by Alpher and Herman (1951) and assumed that the lead isotopes had been produced in a single region uniform in lead, uranium and thorium, and which was common to all leads. Since this was clearly an oversimplification, the deviations of measured isotope ratios from those predicted by the simple theory had to be ascribed to the effects of more or less complex geological processes causing small, but more or less random deviations from the theory. The magnitude of these deviations was estimated and used to determine uncertainties for the ages calculated.

The method of Houtermans is based on the model used by Gerling (1942), Holmes (1946) and Houtermans (1946) for calculating the age of the earth in which it is assumed that the lead in each ore developed in particular source rocks —each characterized by particular thorium/lead-204 and uranium/lead-204 ratios. This model is much more flexible than the previous one, because the predicted isotope ratios are a function not only of the age of the sample, but of the relative abundances of uranium and thorium in the source rock for that particular ore. Ages calculated from these assumptions have often been called "model ages". This model assumes that the particular source rocks associated with each ore remained a closed system from a time approximately 4500 million years ago until the formation of the ore, and thus requires that the outer part of the earth be thought of as divided into a very large number of compartments among which there is negligible transfer of uranium, thorium and lead for periods of the order of thousands of millions of years. This is perhaps possible if the origin of the lead is well below the surface rocks (perhaps sub-crustal) but is a very difficult assumption in the case of surface rocks which are exposed to various geological processes. A much higher precision has been claimed for this method than for the method of Russell *et al.* and in many cases the results seem to have justified this.

Both groups recognize the importance of anomalous leads and it is implicitly assumed that such leads can be identified and will not be interpreted on the basis of the simple models described above. It is important to remember that anomalous leads themselves do not present a source of embarrassment in interpreting the isotope ratios of common leads, for when recognized, these leads can themselves be interpreted by other procedures and often provide more valuable information on the history of an ore deposit than could be obtained without them. It is their recognition that is sometimes difficult.

It will be seen in the remaining part of this paper that the present writers now assign a greater and more fundamental role to anomalous leads than has been ascribed to them before.

The Origin of Lead Ores

Now that the isotope ratios of a large number of lead ores have been studied (the order of 1000), it is possible to pick out three classes of leads for which the isotope ratios are apparently related in a remarkably regular fashion, although the nature of the regularity is different in each case. These classes are:

(1) Meteoritic leads
(2) Conformable leads.
(3) Anomalous leads.

The extreme importance of the isotope ratio determinations of meteoritic leads by PATTERSON (1956) has been widely acknowledged. Five analyses are available; two for lead in troilites separated from iron meteorites, and three for lead in stone meteorites. PATTERSON has given convincing reasons for supposing

Table 1. Isotopic compositions of lead in meteorites (after Patterson)

Meteorite	Lead composition		
	206/204	207/204	208/204
Nuevo Laredo, Mexico	50·28	34·86	67·97
Forest City, Iowa	19·27	15·95	39·05
Modoc, Kansas	19·48	15·76	38·21
Henbury, Australia (Troilite)	9·55	10·38	29·54
Canon Diablo, Arizona (Troilite)	9·46	10·34	29·44

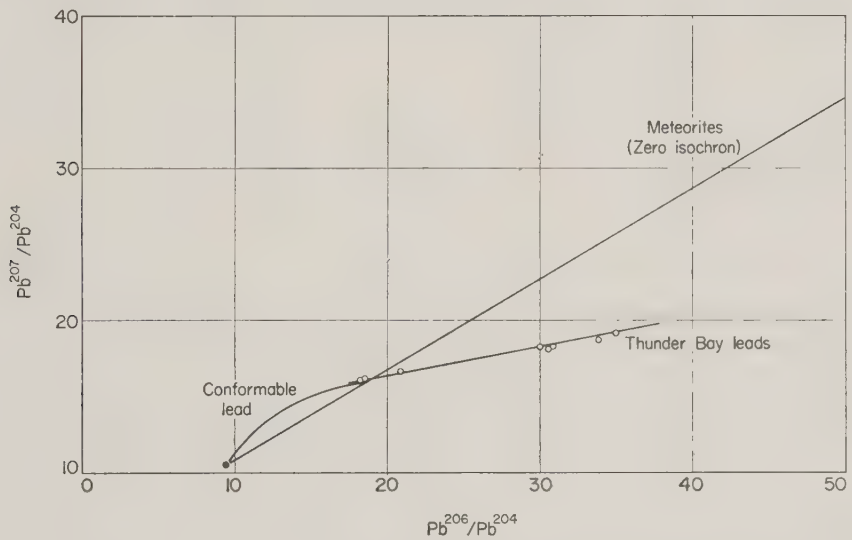

Fig. 1. The relationship between meteoritic lead isotope abundances and abundances of a typical suite of anomalous leads. The points shown represent anomalous leads from the Thunder Bay re ion, Ontario.

that these analyses represent leads grown since a common starting time in closed systems having quite different uranium/lead-204 and thorium/lead-204 ratios, and that the meteorites share with the earth a common origin time t_0 and common primeval lead abundance values. The meteoritic lead isotope ratios, which are given in Table 1. show a remarkable linear relationship. In Fig. 1 the ratios Pb^{207}/Pb^{204} and Pb^{206}/Pb^{204} are plotted and in Fig. 2 the ratios Pb^{208}/Pb^{201} and

Pb^{206}/Pb^{204} are plotted. The first straight line has a slope that is a function only of t_0 (with the assumptions stated) and gives a t_0 value of 4500 million years as previously reported by Patterson. The slope of the meteorite-lead line in Fig. 2 is insensitive to t_0, but depends critically on the relative thorium–uranium abundance. The fact that this plot is such a good straight line is rather remarkable

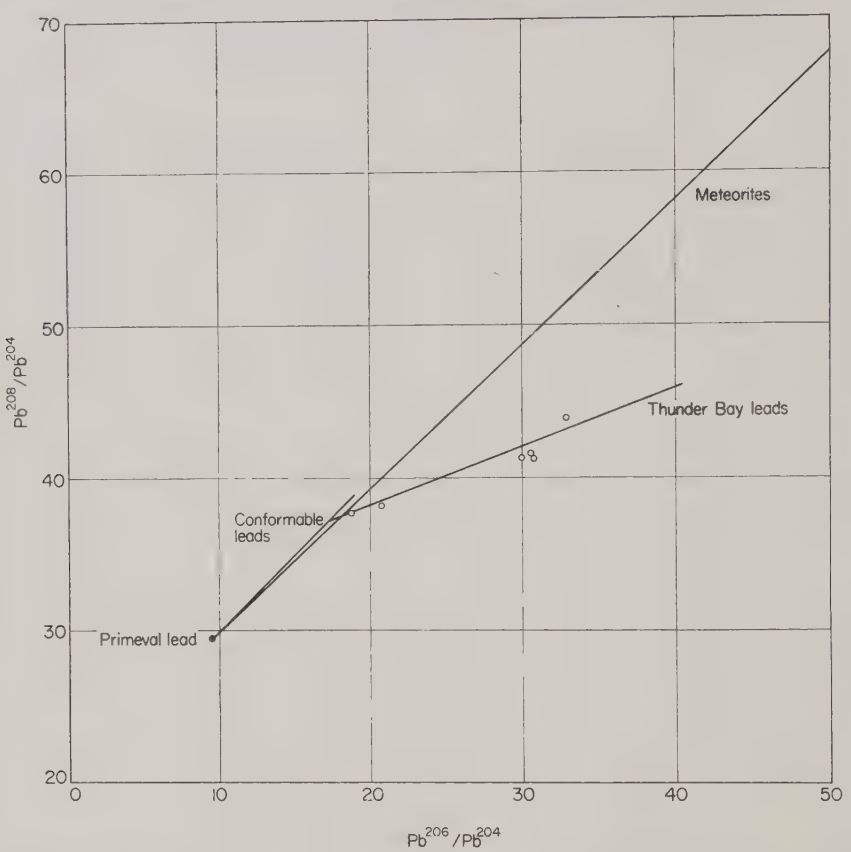

Fig. 2. The relationship between meteoritic lead isotope abundances, conformable lead isotope abundances and abundances of a typical suite of anomalous leads. The anomalous lead analyses show the largest scatter, and for clarity only these analyses are shown in detail.

and indicates that processes producing large fractionations of uranium relative to lead, produced no significant fractionation between uranium and thorium. The figure gives an atomic ratio Th^{232}/U^{238} equal to 3·72, referred to the present time.

Our attention has recently been attracted to the hypotheses of R. L. Stanton regarding the formation of a type of lead ore deposit of a conformable nature (Stanton and Russell, 1959; Stanton, 1958; Stanton, 1954a; Stanton, 1955b). These hypotheses, which will not be reviewed here in detail, deal with a classification of leads proposed by H. F. King, and of which Broken Hill Australia is the type example. Briefly they suggest that such deposits result from the replacement of iron in iron sulphide precipitated in off-reef facies associated with seaboard

volcanism. The precipitation of the iron sulphide lenses is the result of the rapid increase of sulphate-reducing bacteria in places where sulphate is abundant because of volcanic activity. The lead is presumed to have accompanied the volcanic ash as water-soluble halides, to have migrated in solution upwards through the ash deposited at the ocean bottom as the result of subsequent compaction, either replacing iron in iron-sulphide lenses if such are encountered or being lost to the oceans. These leads may have been derived from considerable depths below the

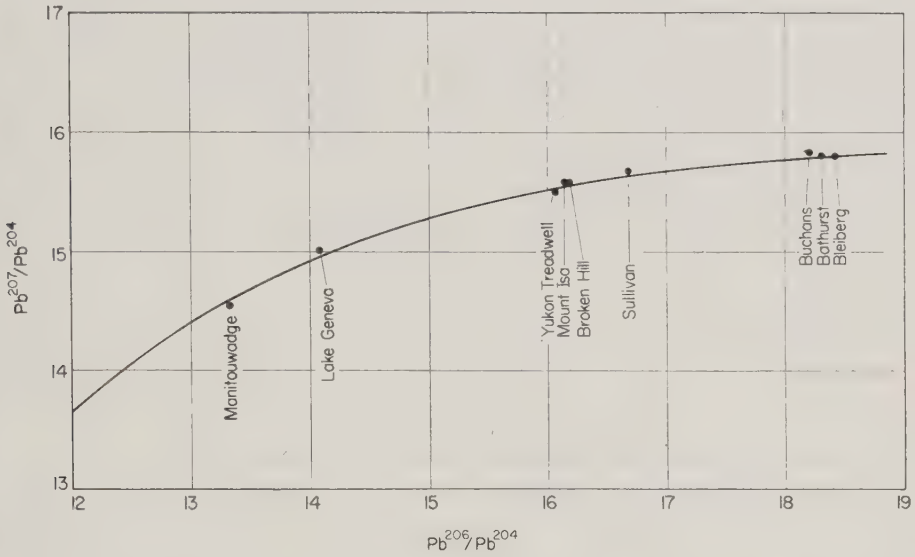

Fig. 3. Detail of Fig. 1, showing fit of conformable leads to their average curve.

surface by simple and short-term geological processes. In particular they may be of subcrustal origin and may represent mantle-lead except in the rare cases where the volcanic material passed through extremely radioactive materials (as may be the case, for example, at Vesuvius). Stanton and Russell have shown that such leads fit a single growth curve within the limits of precision of the measurements and thus may have all been developed in a single homogeneous region. The scatter in their abundances about a single growth curve is an order of magnitude less than that obtained when vein leads are included in the plot. The supposition is that lead migrates through some thickness of pre-existing rock to form *vein* leads and therefore has had at least the *possibility* of becoming anomalous by picking up excess radiogenic leads from these rocks. Examples of these conformable leads are plotted in Figs. 1 and 2 and also in expanded scale in Figs. 3 and 4.

The remarkable fact that the Pb^{207}/Pb^{204} and Pb^{206}/Pb^{204} fit a single growth curve extremely well, suggests the possibility that all these leads were produced in a single homogeneous region. However, the excellent regularity of the Pb^{208}/Pb^{204} vs. Pb^{206}/Pb^{204} graph (Fig. 4) is even more remarkable. This shows that the source materials for these leads were not only uniform in uranium relative to lead, but also in thorium relative to lead. The present ratio of thorium relative to

uranium can easily be calculated from this graph and gives a value of 3·74. The details of this calculation are given below.

Anomalous leads were first interpreted numerically by Russell *et al.* (1954) who studied samples from the Sudbury, Ontario, district. In the paper cited it was suggested that anomalous leads represented mixtures of single "ordinary" or non-anomalous lead with variable amounts of a single radiogenic lead, and thus Pb^{206}/Pb^{204} and Pb^{207}/Pb^{204} should be related linearly. Since then this type of

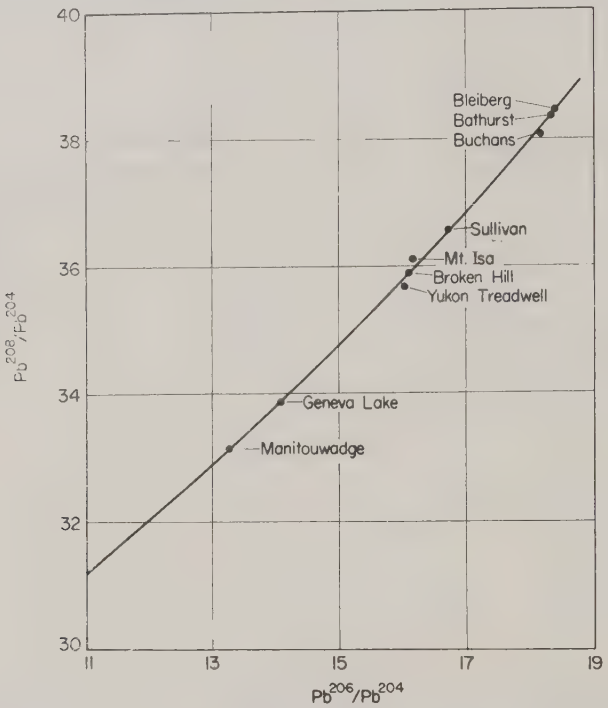

Fig. 4. Detail of Fig. 2, showing fit of conformable leads to their average curve.

relationship has been convincingly demonstrated for anomalous leads from the Thunder Bay region of Ontario (Farquhar and Russell, 1957). Analysis of anomalous leads show that the apparent ratio Th^{232}/U^{238} is extremely variable in the rocks producing the anomalous radiogenic component (e.g. 5·4 for Sudbury leads and 1·8 for Thunder Bay leads).

The following simple assumptions are sufficient to explain these features of observed lead isotope abundances. The condensation of primordial material to form parent bodies from which meteorites were derived, as well as the subsequent chemical and physical alterations resulting in the variety of meteorites observed today took place under conditions such that uranium existed in the quadrivalent state. In this oxidation state uranium compounds are very similar to thorium compounds and processes producing the observed variations in the lead/uranium ratios might produce little effect on the thorium/uranium ratio. The earth also condensed from similar material and the gross separation into core, mantle and crust also occurred under reducing conditions so that the thorium/uranium ratios

in its various parts were nearly identical to that ratio in meteorites. It was only in surface parts of the crust where oxidizing conditions developed that variations in the thorium/uranium ratio resulted. Conformable leads developed in regions of the earth below that at which oxidizing conditions prevail, and hence have isotope ratios produced in a uniform material with a thorium/uranium ratio equal to that of meteorites. Any addition to such leads of radiogenic lead produced in crustal rocks yields anomalous leads that may or may not be easily recognized as such.

The simplest, but certainly not the only method for satisfying the above assumptions is by asserting that surface leads are produced below the Moho and brought to the surface during orogenesis. This assumption is untenable if it is held that the uranium/lead ratio of the mantle is grossly different from the average for surface rocks, and this is often stated to be the case. However, there seems to be no real evidence for this statement, which now seems much less probable in view of PATTERSON's analyses of meteorites. VINOGRADOV (1955) has also presented evidence supporting his assertion that the lead/uranium ratio in meteorites is not as high as generally believed, while UREY (1956) has suggested that lead may be lithophile.

If these assumptions are true the concept of isochrons as applied to terrestrial leads is meaningless, although the zero isochron has significance in discussing meteoritic leads.

A Procedure for Dating Conformable Galenas

In line with the ideas outlined in the above paragraphs we have developed a method for dating galenas based on the following assumptions.

(1) The meteoritic lead isotope analyses are to be interpreted as PATTERSON suggests.

(2) All terrestrial lead develops isotope ratios by the accumulation of radiogenic lead in the mantle which is uniform in uranium, thorium and lead.

(3) Conformable leads as considered (and selected) by STANTON provide samples of mantle lead.

(4) All other lead ores, and particularly vein leads may have resulted from the migration of lead through crustal rocks of variable radioactivity and variable thorium/uranium ratios, and therefore have had the opportunity of becoming anomalous leads by picking up radiogenic lead developed in surface rocks.

(5) The observed scatter of the abundance of all ore leads about a single growth curve is solely the result of the inclusion of a large number of anomalous leads that have not been recognized as such.

After adopting these assumptions it is very easy to calculate the unique growth curve for lead in the earth's mantle. One end of the Pb^{207}/Pb^{204} vs. Pb^{206}/Pb^{204} growth curve lies at the point (9·50, 10·36) obtained by averaging Henbury and Canyon Diablo troilite lead isotope ratios. The other end of the same growth curve must lie on the zero isochron as defined by the meteoritic leads. Accepting PATTERSON's parameters for this isochron there results the equation

$$\frac{Pb^{206}}{Pb^{204}} = 1{\cdot}678\,\frac{Pb^{207}}{Pb^{204}} - 7{\cdot}87$$

Table 2. Comparisons of galena ages by various procedures
(All samples shown are conformable leads except Bleiberg, which is included to show that Houterman's *B*-type anomalous leads do not necessarily give "anomalous" ages by this method)

Location	Holmes Houtermans (million years)	Russell, Farquhar, Cumming			Russell, Stanton, Farquhar		
x *y* *z*		t_{206} (million years)	t_{208} (million years)	Ave (million years)	t_{6-7} (million years)	t_{8-4} million years)	Ave (million years)
Bleiberg, Austria (Mean of 2 samples 18·40 15·79 38·44	380	230	320	280	200	210	210
Bathurst, New Brunswick (Mean of 5 samples) 18·31 15·80 38·33	470	280	370	330	280	270	270
Buchans, Newfoundland 18·18 15·81 38·05	570	390	510	450	390	430	410
Sullivan Mine, B.C. North Star Mine, B.C. 16·68 15·67 36·59	1460	1150	1200	1170	1340	1250	1290
Mt. Isa, Australia (Mean of 10 samples) 16·17 15·58 36·10	1740	1390	1420	1410	1620	1520	1570
Broken Hill, Australia (Mean of 17 samples 16·14 15·58 35·88	1750	1410	1520	1460	1640	1630	1630
Yukon–Treadwell Mine Sudbury, Ontario 16·06 15·50 35·66	1740	1440	1620	1530	1640	1750	1690
Geneva Lake, Ontario (Mean of 2 samples) 14·08 15·02 34·10	2790	2320	2320	2320	2710	2570	2640
Manitouwadge, Ontario 13·32 14·54 33·15	3040	2630	2730	2680	2970	3060	3010

which modern mantle lead must satisfy. These conditions completely specify the growth curve except for a single parameter representing the present value of the U^{235}/Pb^{204} ratio. This can be chosen if the isotope ratio of *any* point on the curve is known (except of course the primeval lead composition which has already been specified). Table 2 lists the conformable leads discussed by Stanton and Russell. The final parameter for the growth curves was specified by insisting that the curve pass through the abundances of lead from the conformable deposit at Bathurst, New Brunswick. This choice was made because more analyses were available for this deposit than for the others, because it is a relatively young deposit and therefore it specifies the curve more precisely than an older sample, and because this deposit was studied personally by Stanton and therefore was identified positively by him as the type to which his hypotheses apply. In fact

the curve obtained fits all the samples well and this particular choice makes little difference to the equation for the curve, which in parametric form is

$$\left.\begin{aligned} \mathrm{Pb^{206}/Pb^{204}} &= 18.72 - 137{\cdot}8 \times 0{\cdot}0659(e^{\lambda t} - 1) \\ \mathrm{Pb^{207}/Pb^{204}} &= 15{\cdot}82 - 0{\cdot}0659(e^{\lambda' t} - 1) \\ \lambda &= 0{\cdot}1537 \times 10^{-9}\ \text{years}^{-1} \\ \lambda' &= 0{\cdot}9722 \times 10^{-9}\ \text{years}^{-1} \end{aligned}\right\} \quad (1)$$

This procedure for calculating the parameters of equations (1) does not require that the ages of the deposits be known. Having obtained these parameters it is quite straightforward to find an equation for Pb^{208}/Pb^{204} consistent with the observed isotope ratio for the conformable leads and equations (1). This is

$$\begin{aligned} \mathrm{Pb^{208}/Pb^{204}} &= 38{\cdot}80 - 34{\cdot}2(e^{\lambda'' t} - 1) \\ \lambda'' &= 0{\cdot}0499 \times 10^{-9}\ \text{years}^{-1} \end{aligned} \quad (2)$$

Figs. 3 and 4 illustrate the excellent fit of the conformable leads to these curves.

Equations (1) and (2) can then be used to estimate values for the age t of a galena of the conformable type. In principle it is possible to calculate t from the ratio of any two lead isotopes, but we have chosen Pb^{206}/Pb^{207} (which age we call t_{6-7}) and from the value Pb^{208}/Pb^{204} (which age we call t_{8-4}). Tables 3 and 4 give values of t_{6-7} and t_{8-4} as functions of the corresponding isotope ratio.

Ages calculated for the conformable leads studied are given in Table 2, where they are compared with values obtained by other methods. While this paper will not enter a detailed discussion of the age values, it is worthwhile noting that the Bathurst ores are overlain by Pennsylvanian sediments, suggesting a minimum age of 230 million years and that the oldest rocks nearby are Ordovician, suggesting an upper limit of 350–400 million years. Here our method seems to give a very satisfactory result. On the other hand the value for Sullivan seems older than previous geological estimates suggest as do in fact ages estimated for that deposit by all methods. In this regard it is interesting to note that the Coeur d'Alene district, Idaho, has given a number of well authenticated ages of similar magnitude.

A final point is that the ages obtained can be shifted somewhat up or down by assuming a slightly different zero isochron. We have preferred to use the zero isochron chosen by Patterson, as an impartial choice, but this may not be the best one. In particular if Patterson's zero isochron had been chosen by Houtermans in setting up his "model age" graphs, he would have obtained ages much less satisfactory than he has obtained with an arbitrarily selected zero isochron.

Vein and Anomalous Leads

It has already been pointed out that anomalous leads altered in crustal rocks will not conform to this simple theory and that all vein leads have had the possibility of becoming anomalous. The procedure for calculating age information about these leads varies somewhat from case to case.

In cases where a detailed study of anomalous leads has been made it may be possible to recognize the straight line relationships displayed by their abundances as was done, for example, in the case of Thunder Bay leads (Farquhar and

Table 3. The apparent age of a conformable lead ore, of the type described in the text, tabulated for various values of the Pb^{206}/Pb^{207} ratio. The age values are given in millions of years.

	0·000	0·002	0·004	0·006	0·008	0·010	0·012	0·014	0·016	0·018
0·90	3180	3154	3126	3099	3072	3045	3019	2994	2968	2943
0·92	2919	2895	2870	2846	2822	2789	2775	2751	2728	2705
0·94	2683	2660	2637	2615	2592	2570	2548	2525	2502	2479
0·96	2457	2435	2413	2390	2368	2346	2324	2301	2279	2258
0·98	2237	2215	2194	2172	2150	2129	2107	2085	2063	2042
1·00	2021	2000	1978	1957	1936	1915	1894	1873	1851	1830
1·02	1809	1788	1767	1746	1725	1704	1683	1662	1640	1619
1·04	1598	1577	1556	1535	1514	1493	1471	1450	1428	1406
1·06	1385	1363	1341	1320	1298	1277	1256	1234	1212	1190
1·08	1268	1146	1125	1103	1081	1059	1037	1015	993	971
1·10	949	927	905	883	861	839	817	795	773	751
1·12	729	707	685	662	640	618	596	573	551	528
1·14	505	483	460	437	414	391	368	345	323	300
1·16	276	253	229	206	183	159	136	112	89	65
1·18	41	18	−6	−30	−54	−78	−102	−126	−150	−174

Table 4. The apparent age of a conformable lead ore, of the type described in the text, tabulated for various values of the Pb^{208}/Pb^{204} ratio. The age values given are in millions of years.

	0·00	0·10	0·20	0·30	0·40	0·50	0·60	0·70	0·80	0·90
30	4583	4536	4489	4442	4395	4348	4300	4253	4205	4158
31	4111	4063	4015	3967	3919	3871	3823	3774	3726	3677
32	3628	3579	3530	3481	3432	3382	3333	3283	3233	3183
33	3133	3083	3033	2982	2931	2880	2829	2778	2727	2675
34	2626	2574	2523	2471	2419	2370	2315	2263	2210	2158
35	2105	2052	1999	1946	1993	1839	1786	1733	1679	1625
36	1571	1517	1463	1409	1355	1301	1246	1191	1136	1081
37	1026	970	914	858	802	746	690	634	577	520
38	463	386	329	291	233	175	117	59	0	−59
39	−117	−176	−235	−295	−355	−415	−475	−535	−596	−657

Russell, 1957) and Broken Hill leads (Russell *et al.*, 1957). The procedures then used are well described in the second paper which shows that the slope of the line along which the analyses follow can be used to give an upper limit to the time of deposition of the lead ores and also an upper limit to the age of the surface rocks producing the anomalous additions of radiogenic lead.

In particular cases where the line can be determined precisely either in the case of:

$$\frac{Pb^{207}}{Pb^{204}} \text{ vs. } \frac{Pb^{206}}{Pb^{204}} \quad \text{or} \quad \frac{Pb^{208}}{Pb^{204}} \text{ vs. } \frac{Pb^{206}}{Pb^{204}}$$

it may be possible to extrapolate the line and get a good intersection with the conformable lead growth curve and hence determine the time of derivation of the lead from the earth's mantle with good precision.

In the case of a vein lead it may often be very difficult to determine whether it is anomalous or not and in some cases where a group of such leads is studied from the same location, the variation in abundances may be so small that it is impossible to determine a best straight line for them. In this case only approximate age information can be obtained. This is done by noting that the minimum possible slope for a line representing anomalous leads is 0·0459 and the maximum probable slope is 0·804. The first figure comes from the present ratio in which lead-207 and lead-206 are being produced. The second figure represents the ratio of the rates of production of these isotopes 3500 million years ago. We have at present no evidence that rocks older than this age have been preserved. By making use of these limiting values for the slope and extrapolating from the anomalous lead abundances to the conformable lead growth curve, one can obtain a minimum age for the time at which this lead was derived from the earth's mantle. In some cases this can be determined rather precisely while in other cases experimental error leads to a very uncertain extrapolated value.

Conclusions

This paper has re-examined the proposal for dating galenas put forward 5 years ago by the present writers. In view of the considerable advances made in studying and interpreting the isotope ratios of common lead, modifications and improvements of the older procedure are suggested. It is suggested that conformable leads represent samples of lead extracted from the mantle as a result of rather simple geological processes and that their isotope ratios accurately specify the time at which the lead was derived from the mantle which in this case is nearly equal to the age of the sedimentary beds with which the conformable leads are associated. In the case of vein or anomalous leads these two times might be quite different and procedures have been suggested for putting limits on the time of derivation of the lead from the earth's mantle and for the time of emplacement of the lead in the form of lead minerals.

References

Alpher R. A. and Herman R. C. (1951) The primeval lead isotopic abundances and the age of the earth's crust. *Phys. Rev.* **84,** 1111–1114.

Cahen L., Eberhardt P., Geiss J., Houtermans F. G., Jedwab J. and Signer P. (1958) On a correlation between the common lead model age and the trace element content of galenas. *Geochim. et Cosmochim. Acta* **14,** 134–149.

Eberhardt P., Geiss J. and Houtermans F. G. (1955) Isotopic ratios of ordinary leads and their significance. *Z. Phys.* **134,** 91–102.

Farquhar R. M. and Russell R. D. (1957) Anomalous leads from the upper Great Lakes region of Ontario. *Trans. Amer. Geophys. Un.* **38,** 552–556.

Gerling E. K. (1942) Age of the earth according to radioactivity data. *C.R. Acad. Sci. USSR* **34,** 259–261.

Holmes A. (1946) An estimate of the age of the earth. *Nature, Lond,* **157,** 680–684.

Houtermans F. G. (1946) The isotope ratios in natural lead and the age of uranium. *Naturwissenschaften* **33,** 185–186; addendum, *Ibid.* 219.

Patterson C. C. (1956) Age of Meteorites and the earth. *Geochim. et Cosmochim. Acta* **10,** 230.

Russell R. D., Farquhar R. M., Cumming G. L. and Wilson J. T. (1954) Dating galenas by means of their isotopic constitutions. *Trans. Amer. Geophys. Un.* **35,** 301–309.

Russell R. D., Farquhar R. M. and Hawley J. E. (1957) Isotopic analyses of leads from Broken Hill, Australia. *Trans. Amer. Geophys. Un.* **38,** 557–565.

Stanton R. L. (1955a) Lower Paleozoic mineralization near Bathurst, New South Wales. *Econ. Geol.* **50,** 681–714.

Stanton R. L. (1955b) The genetic relationship between limestone volcanic rocks and certain ore deposits. *Aust. J. Sci.* **17,** 173–175.

Stanton R. L. (1958) Abundances of copper, zinc and lead in some sulphide deposits. *J. Geol.* **66,** 484–502.

Stanton R. L. and Russell R. D. (1959) Anomalous leads and the emplacement of lead sulphide ores. *Econ. Geol.* **54,** 558–607.

Urey H. C. (1956) Nuclear processes in geologic settings. *Nat. Acad. of Sci.—Nat. Res. Council* Publ. 400, p. 78.

Vinogradov A. P. (1955) *Lead Isotopes and their Geochemical Significance.* U.S.S.R. Academy of Science Press.

Geochimica et Cosmochimica Acta, 1960, Vol. 19, pp 53 to 62. Pergamon Press Ltd. Printed in Northern Ireland

The record in the meteorites—II

On the presence of aluminium-26 in meteorites and tektites*

E. Anders
The Enrico Fermi Institute for Nuclear Studies and Department of Chemistry
University of Chicago, Chicago, Illinois

(*Received* 11 *September* 1959)

Abstract—A search for cosmic-ray produced Al^{26} has been undertaken in meteorites and tektites, using γ–γ coincidence spectrometry. The sensitivity and specificity of this method were sufficient to permit non-destructive measurement of Al^{26} in a 70 g specimen of the Plainview chondrite; the specific activity found, $0{\cdot}058 \pm 0{\cdot}005$ positrons $min^{-1}\,g^{-1}$, agrees well with the value of Ehmann and Kohman. In the case of tektites, chemical separation of the aluminium fraction was required because of interference by the U and Th series. Although a very small amount of activity was found in the aluminium fraction from an australite, corresponding to an apparent Al^{26} content of $0{\cdot}005 \pm 0{\cdot}009$ positrons $min^{-1}\,g^{-1}$, and a "flight time" of $1{\cdot}1 \pm 2{\cdot}0 \times 10^5$ years, it is shown that even this low counting rate was due to some contaminant, rather than Al^{26}. Corrected for this contaminant, the counting rate becomes $0{\cdot}000 \pm 0{\cdot}009$ positrons $min^{-1}\,g^{-1}$, and the upper limit for the Al^{26} content of australites, $\leqslant 0{\cdot}022$ disintegrations $min^{-1}\,g^{-1}$ in contrast to the Ehmann and Kohman value of $0{\cdot}040 \pm 0{\cdot}011$. This limit corresponds to a "flight time" of $\leqslant 5 \times 10^5$ years. In view of this result, a terrestrial origin of tektites has once more become a possibility.

I. Introduction

In two recent papers, Ehmann and Kohman (1958a, 1958b) have reported the successful detection in meteorites and tektites of two cosmic-ray induced radioactivities: Al^{26} and Be^{10}. These results are of great potential value for the development of dating methods; moreover, if confirmed, they would constitute the most compelling evidence for an extraterrestrial origin of tektites. Unfortunately, the Geiger–Mueller counters used by Ehmann and Kohman did not permit identification of these nuclides by their radiation characteristics; instead, the identification had to be achieved by chemical means exclusively. Although both counting and chemical techniques were carried to an extraordinary degree of perfection, the activity levels were so low that the possibility of contamination by chemically similar activities during chemical processing could not be ruled out with absolute certainty. It was therefore thought desirable to verify these results by a technique that was highly sensitive and selective, and did not depend too heavily on chemical processing. These requirements are met by β–γ or γ–γ coincidence spectrometry. The advantages of β–γ coincidence techniques in low-level counting had already been demonstrated in an earlier paper (Anders, 1958). In the present work, γ–γ coincidence spectrometry was used.

II. Principle of the Method

Of the cosmic-ray induced activities detected by Ehmann and Kohman, the most abundant species, Al^{26}, is particularly well-suited for coincidence counting. In fact, its radiations are so characteristic that it is feasible to look for it in bulk

* This work was supported in part by the U.S. Atomic Energy Commission.

meteorite samples without any chemical processing. In its principal decay mode, comprising 84·6 per cent of all disintegrations, this nuclide emits a positron, followed by a γ-ray of 1·83 MeV (Rightmire *et al.*, 1959). Since the positron is promptly annihilated with the emission of two 0·51 MeV quanta, a total of three coincident photons are emitted per disintegration. When a sample containing Al^{26} is placed between the two counters of a γ–γ coincidence spectrometer, and the 0·51 MeV photons detected by the first counter are used to trigger the coincidence circuit, the resultant spectrum in the second counter will show the other

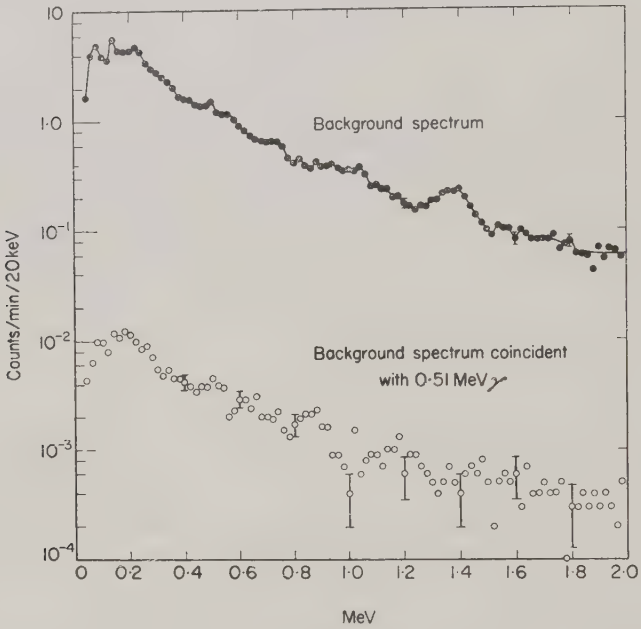

Fig. 1. Background reduction in γ–γ coincidence counting. The upper curve shows the total background of counter (2); counting time: 1000 min. The lower curve shows the background remaining in counter (2) when only events coincident with 0·51 MeV pulses in counter (1) are recorded. Counting time: 10,000 min.

0·51 MeV photon as well as the 1·83 MeV γ-ray. This method not only discriminates heavily against any other activities present (except positron emitters and a few nuclides with complex γ-ray spectra, such as ThC″), but also lowers the background considerably (Fig. 1). The reduction in background by factors of 200–400 is obtained at the expense of a loss in counting efficiency by factors of 5–10, depending on the energy interval, sample size, and the spacing between the counters. Further details on this point will be given in the next section.

III. Experimental Details

A. *Counting equipment and techniques*

The detectors used in the coincidence spectrometer were two thallium-activated sodium iodide crystals, 3·8 cm diameter × 5·1 cm thick, mounted on Dumont 6292 photomultiplier tubes. In order to improve the geometry, the usual 2·5 mm

layer of packed Al_2O_3 reflector between crystal and can was replaced by a thin coating of sprayed Al_2O_3. The resolution of the crystals for the 662 keV γ-ray of Cs^{137} was 9·0 and 8·4 per cent, respectively. Samples were always placed directly between the flat faces of the two crystals.

The entire assembly was surrounded by 10 cm of lead in a rectangular shield of interior dimensions 12 × 12 × 54 cm, lined with a graded X-ray adsorber of cadmium and copper. One of the counters was connected to a single-channel pulse height analyser (RIDL model 115), set to accept pulses in the interval from 470–550 keV. The output signal from this unit was fed into the coincidence

Table 1. Background reduction in γ–γ coincidence counting of positrons (Energy interval 470–550 keV)

Geometry	Sample area (cm^2)	Counter spacing (cm)	Background (counts min^{-1})		Counting yields for positrons* (%)		Figure of merit
			Total	Coinc.	Total	Coinc.	
I	0·5	0·15	5·2	0·020	16·5	3·56	12·1
II	7·9	0·48	5·2	0·019	12·5	2·00	7·0
III	18·5	1·1	5·4	0·016	6·50	0·465	1·7

* Counting yields were determined by means of a Na^{22} solution that had been calibrated by the National Bureau of Standards. For geometries II and III, $Na^{22}Cl$ of known specific activity was mixed with sufficient iron powder to give material of the same density and self-absorption characteristics as the sample. The mixture was then counted in lucite boxes of the same dimensions as the samples.

circuit of an RIDL model 3302 200-channel pulse-height analyser, so that only those pulses from the second counter were accepted and analysed that occurred in coincidence with the 510 keV pulses from the first counter. The signal from the second counter had to be passed through a 3 μsec delay line in order to match the delay in the relatively slow model 115 analyser.

Sample and background were counted alternately for 1000–1500 min intervals. Both analysers were recalibrated daily; the drift usually amounted to $\leq$0·2 and $\leq$1 per cent for the models 115 and 3302, respectively. Data were discarded whenever the drift exceeded 2 per cent.

Counting yields* and background data for several representative geometries are given in Table 1. The "figure of merit" in the last column is included to permit comparison of the "total gamma" and "coincidence" counting methods. It is given by the quotient $((S_2^2/B_2)/(S_1^2/B_1)$, where S is the counting yield, B the background rate, and the subscripts 1 and 2 refer to the "total" and "coincidence" methods, respectively (Loevinger and Berman, 1951; Freedman and Anderson, 1952). All ratios in Table 1 are greater than unity, clearly demonstrating the advantages of the coincidence technique. It should be noted, however, that the situation is unusually favorable for annihilation radiation, compared to γ-rays,

* Defined as the ratio of the number of counts to the number of positrons emitted by the sample. The energy interval 470–550 keV was used in both counters.

since *two* quanta with strong angular correlation are given off for every positron. On the other hand, the equipment used in the present study was not specifically designed for this experiment, and therefore did not realize the full potentialities of the method. Larger crystals, heavier shielding, and particularly anti-coincidence shielding could increase the sensitivity and signal-to-noise ratio substantially.

The same criterion may also be used to compare the coincidence technique with the counting method of Ehmann and Kohman. Their method has a higher figure of merit for samples smaller than 0·8 g, where self-absorption effects are small, but for heavier samples the coincidence method is superior.

B. *Materials*

The following materials were used in this investigation.

1. *Meteorites.* Plainview chondrite (no. 92.1216), obtained from Wards Natural Science Establishment, Rochester, New York. A 70·0 g slice, measuring 4·3 × 4·3 × 1·05 cm, was counted in geometry III without chemical processing. The background correction was determined by counting 44 g of powdered dunite in a polystyrene box of the same size as the specimen. The dunite was obtained through the courtesy of Dr. M. A. Van Dilla of the Los Alamos Scientific Laboratory.

Harrisonville chondrite (no. 12.11), obtained from Wards Natural Science Establishment. A 34 g slice of irregular shape, 0·8 cm thick, was counted. The results were quite similar to those for Plainview, and are not reported in detail.

2. *Tektites.* Three rizalite specimens (nos. Me 2426a, Me 2426b, Me 2437; total weight 30·2 g), obtained on loan from the Chicago Natural History Museum through the courtesy of Dr. S. K. Roy. The samples were put in a polystyrene box (inner dimensions 4·3 × 4·3 × 1·5 cm, total height 1·7 cm) and counted without chemical processing. The background correction was made by counting 48·9 g of powdered dunite in an identical box.

An australite specimen (no. A 181, 37·9 g) from Nullarbor Plain, Australia, obtained through the courtesy of Dr. H. H. Nininger, American Meteorite Museum, Sedona, Arizona. The specimen was processed chemically and 2·321 g of Al_2O_3, representing ~46 per cent of the total Al_2O_3 content, was counted in geometry II in a round lucite box (inner dimensions 3·2 cm diameter × 0·47 cm high, total height 0·55 cm). The background correction was made by counting 4·75 g of specially purified Al_2O_3 in the same geometry.

A composite sample of nineteen small australites and australite fragments, weighing 9·8 g, was made available to us through the courtesy of Professor A. Turkevich of the University of Chicago. He had obtained them from Sir William Penney. This sample was counted without chemical processing.

C. *Chemical procedure for the isolation of* Al^{26}

Because of the highly selective nature of the coincidence counting technique, the requirements for radiochemical purity were far less stringent than in the experiments of Ehmann and Kohman. Of the naturally occurring activities, only Tl^{208} and Bi^{214} were expected to interfere. The former (ThC″) emits γ-rays of 0·51 and 0·58 MeV in coincidence with each other and a 2·61 MeV γ-ray; the

first two and the degradation products of the latter (e.g. annihilation quanta from pair production, and Compton-degraded photons) combine to raise the coincidence counting rate in the vicinity of 0·51 MeV. The nuclide Bi^{214} (RaC), a member of the uranium series, interferes to a lesser degree due to coincidences between its γ-ray of 0·61 MeV and the degradation products of its 2·20 MeV gamma. Since the half-lives of both nuclides are short, it was only necessary to remove their long-lived parents, e.g. Th^{228} and Ra^{226}. The procedure was therefore designed so as to yield an aluminium fraction of moderate purity in a few simple steps; after that, this fraction could be freed from Th and Ra by such standard radiochemical techniques as $Fe(OH)_3$ and $BaSO_4$ scavenges.

The tektite was etched briefly in HCl and HF in order to remove any surface contamination. It was then ground to a powder and dissolved in a slight excess of 48% HF. The solution was evaporated to near dryness in the presence of sufficient HNO_3 to oxidize all iron to the (3+) state, the residue taken up in 10 *F* HCl and evaporated to dryness twice. In order to remove the remaining fluoride, the material was fumed to dryness with conc. H_2SO_4. The residue was leached with 1 *F* HCl, and the filtrate from this step poured into excess 6 *F* NaOH. The $Fe(OH)_3$ precipitate from this step was redissolved in HCl and reprecipitated in exactly the same manner. The two aluminate solutions were combined and the $Al(OH)_3$ precipitated by addition of HNO_3 to pH 8. The $Al(OH)_3$ was filtered, washed, and dissolved in 6 *F* HNO_3; iron and barium carriers were added, and the solution was once more made basic by addition of NaOH containing a small amount of sulphate ion. The mixed precipitate of $Fe(OH)_3$ and $BaSO_4$ removed any Th and Ra present. The aluminium hydroxide was again precipitated by addition of HNO_3, and was purified by two reprecipitations with ammonia. The final precipitate was ignited to Al_2O_3 at 1200°C, mounted and counted.

In order to avoid recontamination with Ra and Th from the reagents, the nitric acid was redistilled from Vycor, and the ammonia solution prepared from ammonia gas and deionized water. Only deionized water was used in the latter part of the procedure, and all reagents were purified by $BaSO_4$–$Fe(OH)_3$ scavenges whenever possible.

IV. Results

The coincidence spectrum of a 70 g slice of the Plainview chondrite is shown in Fig. 2.* The annihilation radiation peak at 0·51 MeV and the γ-ray peak of Al^{26} at 1·83 MeV are both present; the latter is rather less intense than the former because of the low efficiency of the 3·8 × 5·1 cm crystal for high-energy γ-rays. The slight displacement of the 1·83 MeV peak toward lower energies is due to a calibration error. The sum peak of 0·51 + 1·83 MeV lies outside the range investigated. In the small crystal used, its intensity should be very low, but it might easily dominate over the 1·83 MeV peak if a larger crystal were used.

No conclusive evidence is found for another possible cosmic-ray induced activity: $\sim 10^3$-year Ti^{44} in equilibrium with 4 hr Sc^{44}. The latter decays by emitting a positron in coincidence with a 1·16 MeV γ-ray. Though a slight excess

* The dunite sample used for the background correction was matched in volume but not density. Apparently this fact caused a slight overcorrection in the background, since the "net" counting rates between 0·6 and 1 MeV are mostly negative.

count was obtained at 1·1–1·2 MeV, the counting rate was too low to be significant. This nuclide should be produced with an abundance, lower by a factor of ten at least, than that of Al^{26}, so that its detection will require a more careful search involving chemical separation. The peak at 0·33 MeV, on the other hand, could not be assigned to any known natural radioactivity, as shown by comparison with the coincidence spectra of uranium and thorium minerals. It seemed to be present in two other meteorite spectra (Harrisonville and another Plainview sample), and might therefore conceivably be due to an unknown long-lived cosmic-ray produced

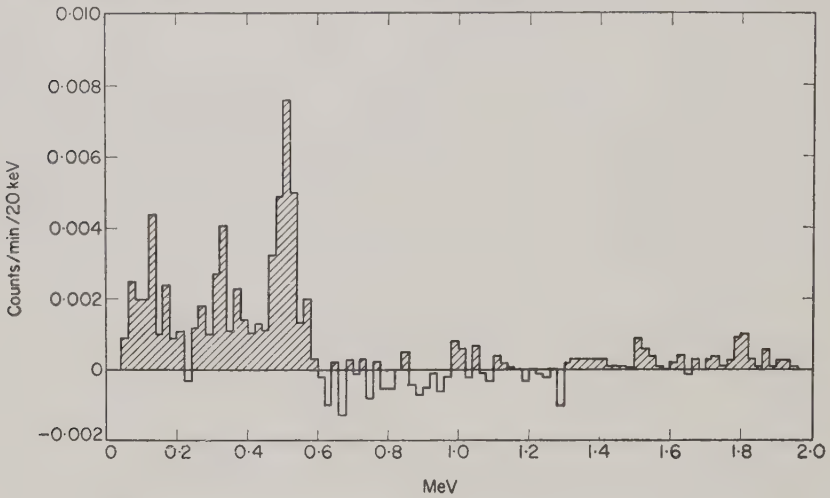

Fig. 2. Coincidence spectrum of Plainview chondrite. The peaks at 0·51 and 1·83 MeV are due to positron annihilation radiation and the principal gamma ray, respectively, of Al^{26}. Counting time: 10,000 min. For the background correction, 44 g of powdered dunite was counted in identical geometry.

positron emitter. However, it is not impossible that the 0·33 MeV peak was actually caused by statistical or instrumental effects. It would be premature to draw any conclusions without further evidence.

Other natural radioactivities seem to be absent from the spectrum. The 1·46 MeV γ-ray of K^{40} is almost completely suppressed since it is not coincident with any other γ-ray. (This suppression is also evident in the background spectrum in Fig. 1.) Neither is there any clear-cut evidence for the presence of the uranium and thorium series in the spectrum, as already pointed out by Van Dilla, *et al.* (1960). This fact is understandable in view of the rarity of these elements in chondrites ($1{\cdot}1 \times 10^{-8}$ gU/g and $3{\cdot}96 \times 10^{-8}$ gTh/g according to Hamaguchi *et al.* (1957) and Bate *et al.* (1959), respectively). In tektites, on the other hand, where the content of U and Th is more than a hundredfold higher, the coincidence spectrum is strongly dominated by the natural radioactive series (Fig. 3).

In the tektite spectrum, the peak between 0·5 and 0·6 MeV is a composite of the three previously mentioned γ-rays of ThC″ and RaC, while the peak between 0·2 and 0·3 MeV is due to γ-rays of the Th series and back-scattered γ-rays of higher energy. Clearly, it is impossible to infer from this spectrum the presence or absence of Al^{26} in tektites. A very similar spectrum was obtained from a

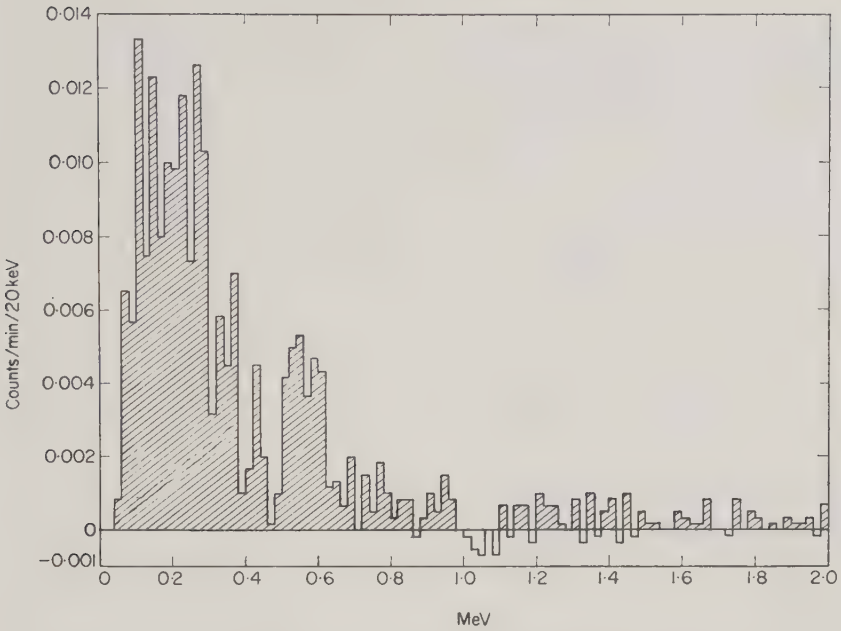

Fig. 3. Coincidence spectrum of three philippinites. All features of this spectrum may be attributed to the U and Th radioactive series. Counting time: 6000 min. For the background correction, powdered dunite was counted as above.

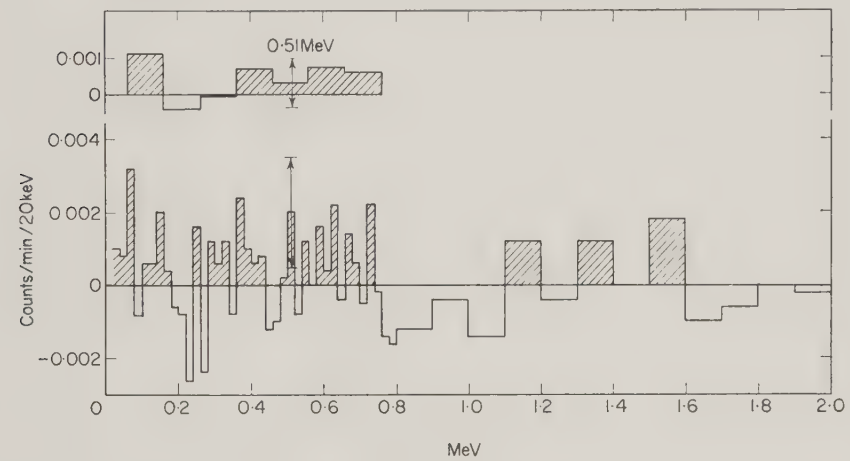

Fig. 4. Coincidence spectrum of the aluminium fraction from an australite. Counting time: 5000 min. As shown on the inset on the upper left, there is no evidence for a peak at 0·51 MeV, as would be expected if cosmic-ray produced Al^{26} had been present in this tektite. The slight positive counting rate in the region from 0 to 0·7 MeV is apparently due to the Compton continuum of some γ-ray emitter of terrestrial origin.

composite sample of 9·8 g of australite fragments. For comparison, the spectrum of the aluminium fraction separated from an australite is shown in Fig. 4.

There is considerable scatter in the experimental points, though the fluctuations are commensurate with the standard deviation indicated by the arrow. In order to minimize the scatter, a portion of the spectrum has been redrawn with lower

resolution on the inset to Fig. 4. Clearly, a slight positive counting rate is found near 0·51 MeV, but it is most significant that the counting rate is even higher in the adjacent channels. This fact implies that the counts at 0·51 MeV are part of the Compton continuum of a high-energy γ-ray, rather than annihilation radiation from Al^{26}. It is possible to prove this point by an independent line of reasoning, based on the data in Table 2.

Two counting rates were determined for each sample: the total γ counting

Table 2. Al^{26} in a meteorite and a tektite

Result	Plainview chondrite		Australite		Units
	Total 510 keV γ Counter (1)	510–510 coinc. Counter (2)	Total 510 keV γ Counter (1)	510–510 coinc. counter (2)	
Net counting rate	0·24 ± 0·03*	0·020 ± 0·0023	0·15 ± 0·04	0·0016 ± 0·0032	counts min^{-1}
Positron emission rate	3·7 ± 0·5	4·3 ± 0·5	—	0·08 ± 0·16	positrons min^{-1}
Specific positron activity	0·053 ± 0·007	0·062 ± 0·007	—	0·005 ± 0·009†	positrons min^{-1} g^{-1}

* Corrected for the Compton-degraded photons from K^{40} and the U and Th series.

† As shown in the text, the activity between 0·06 and 0·76 MeV cannot be due to positrons, but appears to be the Compton continuum of a higher energy γ-ray. Corrected for this effect, the positron specific activity becomes 0.000 ± 0.009 positrons min^{-1} g^{-1}.

rate in counter 1, and the coincidence rate in counter 2. From the counting yields given in Table 1, and other pertinent data in Section III, we can calculate two independent values of the specific positron activity for each sample. In the case of Plainview (counted in geometry III), the two net counting rates are in the ratio of 12:1, which agrees quite well with the 14:1 ratio of the two counting yields from the last row of Table 1. The final two values for the Al^{26} specific activity in Plainview, 0·053 ± 0·007 and 0·062 ± 0·007 positrons min^{-1} g^{-1}, agree well with each other. If we assume that the positron activity is entirely due to Al^{26}, we obtain apparent disintegration rates of 0·063 ± 0·008 and 0·074 ± 0·008 disintegrations min^{-1} g^{-1}, respectively. These values are somewhat higher than those of Ehmann and Kohman, 0·056 ± 0·006 and 0·052 ± 0·008, but the difference may be due to the contribution of another positron emitter (e.g. Sc^{44}), or to actual differences in the cosmic-ray exposure of the two Plainview specimens.

A very different picture is presented by the australite. Here the two net counting rates are in the ratio 94:1, compared to the value of 6·2:1 expected for geometry II. Obviously, the nuclide responsible for the "total γ" counts in counter (1) has a far lower coincidence rate with 0·51 MeV quanta in counter (2) than a positron emitter. This type of behavior is strongly suggestive of a nuclide that has a high-energy γ-ray in coincidence with another high-energy γ-ray, or with a γ-ray near 0·51 MeV. The latter possibility seems to be ruled out by the absence of a peak at 0·51 MeV in the coincidence spectrum.

If the average value of the continuum between 0.06 and 0.76 MeV is subtracted from the spectrum in Fig. 4, the net counting rate in the 510 keV channel becomes $0{\cdot}000 \pm 0{\cdot}009$ positrons $min^{-1}\,g^{-1}$, corresponding to an Al^{26} content of $0{\cdot}000 \pm 0{\cdot}0011$ disintegrations $min^{-1}\,g^{-1}$. Using the conventional $2\,\sigma$ criterion, one may derive an upper limit of 0.022 disintegrations $min^{-1}\,g^{-1}$ for the Al^{26} content of this australite. This result is in disagreement with the average value given by Ehmann and Kohman, $0.040 \pm 0{\cdot}011$, and would not appear to support their conclusion that australites contain Al^{26} at levels similar to that in stone meteorites. Of course, the present measurement is based on a single specimen, and it is not inconceivable that real variations in cosmic-ray exposure exist among australites. Further work will be needed to clarify this point.

Unfortunately, this result does not completely settle the puzzling question of the origin of tektites. It certainly removes the chief obstacle to a terrestrial origin (Spencer, 1933) for which Barnes (1940) and Urey (1957) have presented such impressive arguments, but does not in itself rule out an extraterrestrial, e.g. lunar origin (Nininger, 1943; O'Keefe, 1959). The latter hypothesis has been criticized on the grounds that the chemical composition of tektites is very similar to terrestrial sedimentary rocks, which are unlikely to have an exact counterpart on the moon. Barnes (1940) and Mason (1959) have pointed out that terrestrial igneous rocks exist that match the composition of tektites very closely, and in view of recent work on mineral differentiation in low gravitational fields (Fish *et al.*, 1960), it would seem prudent to remain very open-minded in regard to the composition of the lunar surface until actual samples have become available for study.

However, the evident absence of Al^{26} in australites imposes a few restrictions on such theories. The australites seem to be of quite recent origin, as implied by Reynolds' K–Ar ages for two specimens ($0{\cdot}44 \pm 0{\cdot}2$ and $0{\cdot}80 \begin{smallmatrix} +\,0{\cdot}5 \\ -\,0{\cdot}2 \end{smallmatrix}$ million years, respectively), so that any Al^{26} initially present should have decayed by less than a factor of 2. Hence the australites (or the particular specimen used in this study) must either have spent less than $5{\cdot}0 \times 10^5$ years in space, or were shielded from cosmic rays during their presumed extraterrestrial existence. The former alternative is at variance with the flight time of 10^7 years proposed by O'Keefe (1959), while the latter requires that the tektites travelled in a dense swarm stable against gravitational disruption by the sun. This possibility has been criticized by Urey (1955) on the grounds that it would lead to an areal distribution far denser than observed. It will be interesting to see how well these restrictions can be accommodated by current theories of an extraterrestrial origin of tektites.

Acknowledgement—I wish to thank Mrs. Elizabeth Viste for assistance in the experimental work and analysis of the data. I am also indebted to Drs. M. A. Van Dilla and E. C. Anderson for making their manuscript available to me in advance of publication, and for valuable criticisms that improved several aspects of this paper.

References

Anders E. (1958) Neutron activation cross section of Tc^{98}. *Phys. Rev.* **110,** 427–430.

Barnes V. E. (1940) North American Tektites. *Univ. Texas Publ* No. 3945, 477 pp.

Barnes V. E. (1958) Properties of tektites pertinent to their origin. *Geochim. et Cosmochim. Acta* **14,** 267–278.

Bate G. L., Huizenga J. R. and Potratz H. A. (1959) Thorium in stone meteorites by neutron activation analysis. *Geochim. et Cosmochim. Acta* **16,** 88–100.

Ehmann W. D. and Kohman T. P. (1958) Cosmic-ray-induced radioactivities in meteorites—I. Chemical and radiometric procedures for aluminium, beryllium and cobalt. *Geochim. et Cosmochim. Acta* **14,** 340–363.

Ehmann W. D. and Kohman T. P. (1958) Cosmic-ray-induced radioactivities in meteorites—II. Al^{26}, Be^{10} and Co^{60}, aerolites, siderites and tektites. *Geochim. et Cosmochim. Acta* **14,** 364–379.

Fish R. A., Goles G. G. and Anders E. (1960) The record in the meteorites—III. On the development of meteorites in asteroidal bodies. To be published.

Freedman A. J. and Anderson E. C. (1952) Low-level counting techniques. *Nucleonics* **10,** No. 8, 57–59.

Hamaguchi H., Reed G. W. and Turkevich A. (1957) Uranium and barium in stone meteorites. *Geochim. et Cosmochim. Acta* **12,** 337–347.

Loevinger R. and Berman M. (1951) Efficiency criteria in radioactivity counting. *Nucleonics* **9,** No. 1, 26–39.

Mason B. (1959) Chemical composition of tektites. *Nature, Lond.* **183,** 254–255.

Nininger H. H. (1943) Tektites and the moon. *Sky and Telescope* **2,** No. 4 and 5.

O'Keefe J. A. (1959) Origin of tektites. *Science* **130,** 97–98.

Reynolds J. H. (1960) Rare gases in tektites. To be published.

Rightmire R. A., Simanton J. R. and Kohman T. P. (1959) Disintegration scheme of long-lived aluminium-26. *Phys. Rev.* **113,** 1069–1077.

Spencer L. J. (1933) Origin of tektites. *Nature, Lond.* **131,** 117, 876; **132,** 571.

Urey H. C. (1955) On the origin of tektites. *Proc. Nat. Acad. Sci., Wash.* **41,** 27–31.

Urey H. C. (1957) Origin of tektites. *Nature, Lond.* **179,** 556–557.

Van Dilla M. A., Arnold J. R. and Anderson E. C. (1960) On natural and cosmic-ray induced radioactivities in meteorites. To be published.

Geochimica et Cosmochimica Acta, 1960, Vol. 19, pp. 63 to 69. Pergamon Press Ltd. Printed in Northern Ireland

Cadmium in rocks and minerals from the Skaergaard intrusion, East Greenland

E. A. Vincent and L. I. Bilefield
Department of Geology and Mineralogy, University Museum, Oxford

(*Received* 25 *November* 1959)

Abstract—Traces of cadmium have been determined by neutron activation analysis in a suite of rocks from the Skaergaard intrusion, East Greenland, and in the separated minerals from one of them. The original parent basic magma contained 0·13 p.p.m. Cd, and progressive fractional crystallization led slowly to a twofold increase in the ferrogabbros and a fourfold increase in the granophyres derived largely from the ultimate residual magmatic fractions. Cd does not appear to enter immiscible copper and iron sulphide droplets in the magma in preference to silicates and oxides, neither does it show any marked preference among the latter. Despite similar ionic radius and charge, Cd^{2+} does not follow Ca^{2+} in plagioclase and apatite, but is slightly concentrated in iron-rich pyroxene, olivine and titaniferous magnetite. Most of the Cd becomes concentrated in the residual magmatic liquids.

The values for Cd found by the neutron activation method in the standard rocks G–1 and W–1 were 0·06 p.p.m. and 0·33 p.p.m., respectively.

Introduction

Owing to the lack of sufficiently sensitive methods of analysis, little is known of the occurrence of cadmium in igneous rocks and their constituent silicate and oxide minerals, apart from the limited data provided by Sandell and Goldich (1943). In sulphide minerals, Cd is often sufficiently abundant to be estimated spectrographically, but this is seldom the case in ordinary igneous rocks, for which Sandell and Goldich used a colorimetric method, making no claim to great accuracy since they were working near the limit of sensitivity. Recently, Brooks *et al.* (1960) have determined Cd spectrographically in silicate rocks, together with other elements below the normal detection limit, after chemical pre-concentration from a large sample using anion exchange resins. The present paper reports the results of determinations of Cd made by a neutron-activation method, developed in this laboratory, on a series of rocks and minerals from the Skaergaard intrusion, East Greenland—a series which, although limited in number, is of unique interest in considering the behaviour of trace elements during the process of extreme fractional crystallization of a basic magma (Wager and Mitchell, 1951).

Analytical Method

Only a brief outline of the method will be given here, since it is hoped to publish a more detailed account elsewhere. Although it appears serviceable, the procedure adopted is probably capable of refinement; in particular, further research is desirable to achieve a consistently high chemical yield, since poor recovery of the added Cd carrier, with the fairly low counting rates observed (<100 counts/min) has sometimes led to a lower degree of precision than is often attainable in activation analysis.

Powdered rock samples (100–200 mg) are sealed in polythene tubes and irradiated for 1 week in the high-flux region ($\sim 10^{12}$ neutrons/cm^2 per sec) of the Harwell reactor BEPO. After irradiation, the sample is decomposed by sintering with Na_2O_2 at 480–500°C in a silica crucible; the cold cake is transferred to a beaker, $CdSO_4$ carrier solution ($\equiv$15 mg Cd) added and the whole evaporated twice nearly to dryness with HCl + HNO_3. After dilution, a few iron nails are added to precipitate metals of higher standard electrode potential, and these are filtered off,

along with silica. Cd is precipitated from the filtrate with trimethylphenyl ammonium iodide in the presence of holdback carriers, and after centrifuging and washing, the precipitate is redissolved in $H_2SO_4 + HClO_4$. The solution is diluted, holdback carriers and excess KBr added, and the Cd reprecipitated with brucine. The precipitate is centrifuged, washed and again redissolved in the acid mixture. Scavenges with ferric hydroxide and with silver iodide are then carried out on the solution, which is next acidified with H_2SO_4 and the Cd precipitated with β-naphthoquinoline in the presence of KI. After centrifuging and washing, the precipitate is redissolved in $H_2SO_4 + HClO_4$, and the Cd finally precipitated once more as the brucine complex. After standing, the precipitate is thoroughly washed with a dilute solution of the precipitants, then with water and ethanol–ether, finally slurried in ether and plated out on a weighed aluminium counting tray. The "brucinate" is dried under an infra-red lamp, weighed to determine the chemical yield ($Cd:[(CH_3O)_2C_{21}H_{20}O_2N_2]_2 \cdot CdBr_2 \cdot 2HBr = 0{\cdot}092$) and ^{115}Cd counted under a mica end-window Geiger–Muller counter.

Standards are prepared by irradiating very dilute solutions of cadmium acetate containing from *c.* 0·01 to 1 μg Cd (at higher concentrations, self-shielding becomes significant), which are subjected to a shortened form of the analysis used for the samples. The results are calculated from a comparison of counting rates of cadmium brucinate prepared from irradiated standards and from rock samples, corrected for the determined chemical yields.

Natural Cd comprises eight stable isotopes. On neutron irradiation under the conditions adopted here, the greatest part of the resultant activity is due to 2·3 day ^{115}Cd (~90 per cent) with a small or negligible contribution from 43 day ^{115m}Cd. The daughter isotope ^{115}In "grows in" during the decay of ^{115}Cd, giving rise to an increase in the counting rate of samples and standards for the first few hours after their final precipitation. Thereafter, parent ^{115}Cd and daughter ^{115}In decay with the half-life of the ^{115}Cd parent (2·3 days), so that counting rates of samples and standards are not compared until at least 24 hr after plating out, i.e. after equilibrium has been established between parent and daughter isotopes.

In the present work, radiochemical purity of the Cd separated from the rock samples was checked by plotting a decay curve; counting rates were usually too low to permit absorption curves to be constructed. Serious errors could be introduced into the analyses if spurious ^{115}Cd activity were produced from other elements in the sample during irradiation in the high neutron flux employed. The most likely nuclear reactions of this kind are $^{115}In \xrightarrow{n,p} {}^{115}Cd$; $^{118}Sn \xrightarrow{n,\alpha} {}^{115}Cd$; and $^{235}U \xrightarrow{n,f} {}^{115}Cd$. Experiments carried out using In, Sn and U monitors showed that the maximum percentage error which could be caused by the presence in the rock samples of any one of these elements in similar concentration to Cd is about 0·5 per cent, which is quite negligible for the present purposes. Experiments were also made to ensure that no serious self-absorption occurred within the plated-out brucinate precipitates within the source thickness range used.

Duplicate determinations of Cd generally agree within about 5-10 per cent of the amount present; a few of the analyses show a greater spread than this (Tables 2 and 3), but the precision is adequate for most geochemical purposes. It is difficult at present to assess the accuracy of the method, since, of the rocks we have analysed, independent determinations of Cd by other methods are available only for the international standard rock samples G–1 and W–1 (Table 1).

Agreement between these determinations is unsatisfactory, and while we have considered potential sources of systematic error in our activation method and do not think it likely that our results are in error by a large factor, further independent analyses are clearly required.

Results and Discussion

The results of the Skaergaard rock analyses are given in Table 2. The chilled marginal gabbro (4507) taken to represent the initial magma of the intrusion (Wager and Deer, 1939; Wager, Vincent and Smales, 1957) contains 0·13

Table 1. Determinations of cadmium in standard rock samples (p.p.m.)

Method	Granite, G–1	Diabase, W–1
(a) By neutron activation (this work)	0·054; 0·056 0·066 (Average 0·06)	0·30; 0·33; 0·34, 0·34 (Average 0·33)
(b) By polarographic analysis (Smythe and Gatehouse, 1955).	5 ± 2	4 ± 4
(c) By combined anion exchange enrichment and optical spectrography (Brooks, Ahrens and Taylor, 1960).	—	0·07, 0·09

p.p.m. Cd, a figure comparable with those reported by Sandell and Goldich (1943) who give an average of 0·18 p.p.m. Cd for eight samples of igneous rocks.

Cd remains low in the border group and gabbro picrite, and the rocks formed from at least the first 60-70 per cent of the magma to crystallize (the Hidden Layered Series) presumably contained rather less Cd than the liquid at corresponding stages. During the stages represented by the lower olivine gabbros and middle gabbros of the exposed part of the Layered Series, the Cd content of the rocks slowly rises, with some irregularities, reaching twice the initial value in the ferrogabbros and three or four times the initial value in the granophyres representing, at any rate in part, the latest differentiates. When the results are plotted against approximate percentages of the magma solidified (Fig. 1), their distribution is broadly on an hyperbola, characteristic of cases where insignificant amounts or constant small amounts of a trace element are precipitated in the crystal fractions, so that it becomes concentrated in the ultimate magmatic residues (Wager and Mitchell, 1951, p.177).

In detail, the Cd contents of the Skaergaard rocks show some irregularities. The two lower olivine gabbros, 5086 and 5087, for example, differ in Cd content by a factor of 2, although the rocks come from the same differentiation stage in the intrusion and do not differ greatly in mineralogical composition; it might be that they received different contributions of Cd from the relatively enriched interstitial liquids.

Three hortonolite ferrogabbros were analysed: an average example in respect of mineralogical composition (5181), and nearby felspathic (5321) and melanocratic facies (5196), the last carrying noteworthy amounts (*c.* 0·4 per cent) of accessory copper–iron sulphides representing a separate immiscible magmatic phase (Wager *et al.*, 1957). The rather similar results obtained for the average (0·40 p.p.m.) and the felspathic (0·33 p.p.m.) rocks suggest that Cd is not particularly concentrated in the plagioclase, where, on the basis of similar ionic radius and charge, it might have been expected to substitute for Ca^{2+}. This is borne out by finding only 0·15 p.p.m. Cd by direct analysis of the pure plagioclase separated from the average rock (Table 3). Goldschmidt, in contrast, found sufficient Cd for spectrographic detection in an anorthosite (Goldschmidt, 1954, p. 268).

The melanocratic rock (5196) with accessory copper sulphides has even less

Table 2. Cadmium in rocks of the Skaergaard intrusion

	Rock no. E.G.	Type	Height in intrusion (metres)	Cd concentration (replicate analyses) (p.p.m.)	Average Cd conc. (p.p.m.)	Remarks
Late Differentiates	5259	Transgressive acid granophyre	—	0·57; 0·59; 0·54	0·57	
	4489			0·44; 0·44	0·44	
Layered Series	4332	Basic hedenbergite granophyre	2590	0·27; 0·28	0·28	
	4328	Fayalite ferrogabbro, Upper Purple Band	2500	0·28; 0·27	0·28	Rock carries *c.* 2% by weight of iron sulphides
	5196	Hortonolite ferrogabbro, melanocratic band	1900	0·11; 0·12	0·12	Rock carries *c.* 0·4% by weight of copper sulphides
	5181*	Hortonolite ferrogabbro, average rock	1800	0·38; 0·43	0·40	Rock carries *c.* 0·03% by weight of copper sulphides
	5321	Hortonolite ferrogabbro, plagioclase cumulite	1750	0·34; 0·32	0·33	
	5052	Middle gabbro (olivine-free)	825	0·08; 0·09	0·09	
	5087	Lower olivine gabbro	280	0·20; 0·19	0·20	
	5086		280	0·08: 0·12	0·10	
Marginal rocks	4526	Gabbro picrite	—	0·08; 0·09	0·09	
	4443	Border group	—	0·11	0·11	
	4507	Chilled marginal gabbro	—	0·13; 0·11; 0·13	0·13	
		(≡ initial magma)	—	0·13		

* See also Table 3 for Cd in individual minerals.

Cd than the average and there was clearly no noteworthy concentration of the element in the early magmatic sulphide liquid. Moreover, still higher in the sequence the fayalite ferrogabbro (4328) carries about 2 per cent of iron sulphide droplets (marcasite after pyrrhotite: WAGER *et al.*, 1957), and here also the Cd content is not abnormally high. Though no direct analyses for Cd have been made on the Skaergaard sulphide minerals, it appears probable that Cd did not enter the relatively early-formed sulphide liquids in preference to the simultaneously crystallizing silicates and oxides.

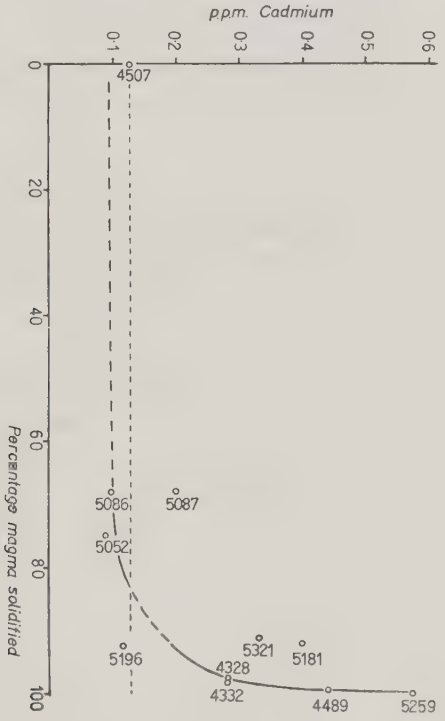

Fig. 1.

Pure (>99 per cent) concentrates of the principal mineral components of the average ferrogabbro 5181 were prepared, avoiding the use of Clerici's solution which may grossly contaminate samples so separated with various heavy metals. The contents of Cd determined in these individual minerals are given in Table 3.

The distribution of Cd between the various silicate and oxide phases is rather uniform and, as is also suggested by the total rock analyses, the behaviour of the element during magmatic fractionation shows no marked coherence with any major element: this is reminiscent of the distribution of gold among these same minerals (VINCENT and CROCKET, 1960). The results in Table 3 show, moreover, that the calcium-bearing minerals, plagioclase and apatite, actually contain less Cd than the ferromagnesian silicates and magnetite.

Knowing the approximate modal mineralogical composition of the rock, the contribution of each mineral to the total Cd present may be assessed, and it is found that the Cd contents of the individual minerals analysed only account for

Table 3. Cadmium in constituent minerals of average hortonolite ferrogabbro, 5181

Mineral	Wt. % of rock	Cd found (p.p.m.)	Mean Cd (p.p.m.)	Contribution to total Cd (p.p.m.)
Plagioclase, An_{40}	54	0·14; 0·16	0·15	0·081
Pyroxene, $Ca_{35}Mg_{34}Fe_{31}$	23	0·42; 0·44	0·43	0·099
Olivine, Fa_{60}	13	0·37	0·37	0·048
Titaniferous magnetite	4·5	0·31; 0·28	0·30	0·014
Ilmenite	5·5	0·12; 0·12	0·13	0·007
		0·14		
Whole rock			0·04	Σ 0·0249
[Apatite from rock 4312		0·15; 0·14	0·15]	

about 60 per cent of the Cd determined in the same rock by direct analysis. The discrepancy may be largely due to the relative concentration of Cd in the residual magmatic liquids, so that an appreciable proportion may be located in the outermost zones of silicates and oxides and in the interstitial accessory material, both of which would largely be lost in the process of crushing and separating the minerals for analysis.

At this particular horizon in the hortonolite ferrogabbros, apatite, having earlier been a product of crystallization of the interprecipitate liquids, enters the primary precipitate assemblage in quantity. Apatite separated from a nearby ferrogabbro (4312) contains but 0·15 p.p.m. Cd, the same as in the plagioclase of 5181. Goldschmidt remarks (1954, p.270) that apatite "is very likely to be a host of cadmium in magmatic rocks", but that is not the case here.

Apart from its tendency to become concentrated in the ultimate liquid magmatic fractions, Cd appears in the ordinary minerals of the gabbros to follow Fe rather than Ca, but any coherence is slight. Neither does Cd in the Skaergaard example show any marked chalcophile tendency, although at a relatively much later stage in magmatic evolution in general, the concentration of Cd with Zn in hydrothermal sulphides is well established. The final entry of Cd into predominantly covalently-bonded sulphides, and its complete lack of coherence with Ca in the Skaergaard rocks and minerals, emphasizes that ionic radius and charge are insufficient criteria for evaluating the geochemical behaviour of Cd. The second ionization potential of Cd^{2+} is much higher than for Ca^{2+} however, and this may go far towards explaining the differences. Cd in the Skaergaard minerals is slightly concentrated in the iron–pyroxene, iron–olivine and titaniferous magnetite—but not in ilmenite—as compared with plagioclase and apatite, so that it is of interest to compare the ions Ca^{2+}, Cd^{2+} and Fe^{2+}. The following data are taken from Ahrens (1953):

	Ca^{2+}	Cd^{2+}	Fe^{2+}
Ionization potential I(V)	11·9	16·9	16·24
Radius (Å)	0·99	0·97	0·74

Ahrens (1953, p.10) has defined the ratio of the ionization potentials of two ions of similar radius as the anion affinity index (ϕ), which will have a value near unity for ion pairs showing marked geochemical coherence. For the pair Cd^{2+} : Ca^{2+}, $\phi = 1{\cdot}42$; for the pair Cd^{2+} : Fe^{2+}, $\phi = 1{\cdot}04$, and the slight coherence observed between Cd^{2+} and Fe^{2+} is probably due to similarity in ionization potential, and despite a 25 per cent difference in radius. But the limited results from the Skaergaard intrusion support Rankama and Sahama's general statements (1950, p. 710, 712) that ". . . Cd, together with other elements, remains largely in the residual melts and solutions throughout the main stage of crystallization and the pegmatitic stage" and that "owing to its weaker oxyphile character, cadmium becomes nearly quantitatively enriched in hydrothermal rocks and minerals and its highest concentrations are met in formations belonging to the lowermost temperatures".

Acknowledgements—We wish to thank Mr. A. A. Smales, AERE, Harwell, for suggesting the determination of cadmium as a problem in radioactivation analysis and Professor L. R. Wager for making available the Skaergaard material and for his interest in the work. The necessary irradiations in the Harwell pile B.E.P.O. were arranged through the Isotope Division of the AERE.

References

Ahrens L. H. (1953) The use of ionization potentials—II. *Geochim. et Cosmochim. Acta* **3,** 1-29.

Brooks R. R., Ahrens L. H. and Taylor S. R. (1960) The determination of trace elements in silicate rocks by a combined spectrochemical-anion exchange technique. *Geochim. et Cosmochim. Acta.* **18,** 162–175.

Goldschmidt V. M. (1954) *Geochemistry* (Edited by Muir A.). Clarendon Press, Oxford.

Rankama K. and Sahama Th.G. (1950) *Geochemistry.* Chicago University Press, Chicago.

Sandell E. B. and Goldich S. S. (1943) The rarer metallic constituents of some American igneous rocks. *J. Geol.* **51,** 99-115, 167-189.

Smythe L. E. and Gatehouse B. M. (1955) Polarographic determination of traces of Cu, Ni, Co, Zn and Cd in rocks. *Analyt. Chem.* **27,** 901-903.

Vincent E. A. and Crocket J. H. (1959) Studies in the geochemistry of gold—I. *Geochim. et Cosmochim. Acta.* In press.

Wager L. R. and Deer W. A. (1939) The petrology of the Skaergaard intrusion, Kangerdlugssuaq, East Greenland. *Medd. om Grønland* **105,** No. 4, 1-352.

Wager L. R. and Mitchell R. L. (1951) The distribution of trace elements during strong fractionation of basic magma. *Geochim. et Cosmochim. Acta* **1,** 129-208.

Wager L. R., Vincent E. A. and Smales A. A. (1957) Sulphides in the Skaergaard intrusion, East Greenland. *Econ. Geol.* **52,** 855-895.

Geochimica et Cosmochimica Acta, 1960, Vol. 19, pp. 70 to 79. Pergamon Press Ltd. Printed in Northern Ireland

Argonbestimmungen an Kaliummineralien—VII

Diffusionsverluste von Argon in Mineralien und ihre Auswirkung auf die Kalium–Argon–Altersbestimmung

H. Fechtig, W. Gentner und J. Zähringer
Max-Planck-Institut für Kernphysik, Heidelberg

(*Received* 14 *September* 1959)

Abstract—In calcium-containing minerals Ar^{37} was produced with the aid of a (n, α) reaction and the diffusion of Ar^{37} was measured as a function of temperature. Owing to the high sensitivity of this method it was possible to measure diffusion constants down to room temperature. For fluorite, anorthite, augite and margarite the diffusion constants determined at room temperature are 10^{-21}–10^{-25} cm²/sec. These results are in agreement with those obtained by the potassium–argon age determination. The shape of the curves $D(1/T)$ shows two knees which account for the discrepancy of the values obtained by other methods through extrapolation.

Schon bei den ersten Versuchen, das Alter des Bugginger Salzlagers mit Hilfe des K^{40}-Zerfalls zu bestimmen (Smits und Gentner, 1950; Gentner *et al.*, 1953; Gentner *et al.*, 1954), zeigte sich eine Abhängigkeit der Ar-Konzentration von der Kristallgrösse. Diese Autoren ermittelten aus theoretischen Betrachtungen unter Verwendung ihrer Messergebnisse Diffusionskonstanten für Helium und Argon in diesen Salzen von

$$D_{He}(40°C) = (20 \pm 16) \times 10^{-20}\ \text{cm}^2/\text{sec}$$

$$D_{Ar}(40°C) = (8 \pm 7) \times 10^{-20}\ \text{cm}^2/\text{sec}$$

Diese Abschätzungen konnten für die Diffusion von Helium von Gentner und Trendelenburg (1954) aus massenspektrometrischen Messungen bestätigt werden. Die Autoren konnten die Helium-Gasabgabe des Steinsalzes für Temperaturen oberhalb 500°C messen und daraus die zugehörigen Diffusionskonstanten bestimmen. Der Wert der Diffusionskonstante bei Zimmertemperatur wurde durch Extrapolation gewonnen. Da sich dabei der Wert der Diffusionskonstante um zehn Grössenordnungen ändert, musste ein Messfehler von etwa zwei Grössenordnungen hingenommen werden, wobei vorausgesetzt wurde, dass eine solche Extrapolation erlaubt sei.

Dieselbe massenspektrometrische Methode wurde von Reynolds (1957) zur Bestimmung der Diffusionskonstanten von Argon in einigen Feldspäten und Glimmern angewendet. Reynolds konnte dabei Diffusionskonstanten für Temperaturen oberhalb 400°C messen. Als wesentliches Ergebnis dieser Messungen muss der Verlauf der Diffusionskonstanten in Abhängigkeit von $1/T$ angesehen werden. Der Autor stellt dabei fest, dass es zwei Bereiche mit verschiedener Aktivierungsenergie gibt: zwischen 400 und 600°C die eigentliche Diffusion von Argon, wie sie durch die Beweglichkeit der Argonatome in dem betreffenden Kristallgitter gegeben ist. Oberhalb 600°C ergibt sich eine grössere Aktivierungsenergie, da sich hier nach Flügge und Ziemens (1939) der Einfluss der Beweglichkeit

der Gitterbausteine bemerkbar macht, d.h. die sog. Selbstdiffusion tritt ein. Die für die Altersbestimmung wichtige Diffusionskonstante von Argon in Feldspat bei Zimmertemperatur möchte REYNOLDS (1957) durch Extrapolation des Kurventeiles erhalten, der für Temperaturen unterhalb 600°C gilt. Der Autor erhält auf diese Weise das Ergebnis, dass die Diffusionskonstante von Argon in Feldspat bei $300°K > 10^{-19}$ cm²/sec sein müsste.

Die von uns angewandte Methode zur Bestimmung der Diffusionskonstanten von Argon in Mineralien verwendet das radioaktive Isotop Ar^{37}. Dadurch konnte die Empfindlichkeit des Nachweises soweit gesteigert werden, dass Diffusionskonstanten bis herab zur Zimmertemperatur gemessen werden können.

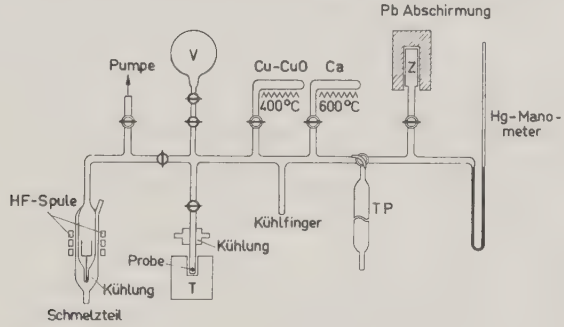

Abbildung 1: Schematische Darstellung der Diffusionsapparatur.

Die radioaktive Methode und geht auf Untersuchungen von RUTHERFORD (1901) zurück. RUTHERFORD untersuchte die Temperaturabhängigkeit der Emanationsabgabe bei Thoriumhydroxyd. Ebenfalls wurde in der HAHNschen Schule von COOK (1939) die Gasabgabe an Eisenhydroxyd mit eingebauter radioaktiver Substanz (Emanation) bei verschiedenen Temperaturen gemessen.

Zur Erzeugung des radioaktiven Ar^{37} in den von uns untersuchten Mineralien wurde eine Anzahl solcher Mineralien im Münchner Forschungsreaktor bestrahlt. Die erste Serie waren die Minerale Flusspat, Anorthit (Ca-Feldspat vom Vesuv), Augit und Margarit (Ca-Glimmer). In solchen Ca-haltigen Mineralien entsteht aus dem Ca^{40} vermöge einer (n, α)-Reaktion der K-Strahler Ar^{37}.

In Abb. 1 ist die Messapparatur schematisch dargestellt. Mit Hilfe eines Temperofens T wird die bestrahlte Mineralprobe auf konstante Temperatur wahlweise zwischen Zimmertemperatur und 1100°C gebracht und das dabei aus der Probe entweichende Gas aufgefangen. Die Wartezeit betrug bei Zimmertemperatur einige Tage, bei höheren Temperaturen 1 Stunde. Mit etwas Trägergas versetzt (Argon aus dem Vorrat V) wird das Gas in Ca- und Cu/CuO-Öfen von den unedlen Bestandteilen getrennt. Mit Hilfe einer Töplerpumpe TP wird es danach in das Zählrohr Z gebracht und gelangt als innere Füllung zur Messung der Aktivität. Zur Bestimmung des Gesamtgehaltes der Probe an Ar^{37} wird eine solche in einem induktiv geheizten Graphittiegel (Schmelzteil) geschmolzen, das entweinde Gas aufgefangen, gereinigt und die vorhandene Aktivität im 4π-Gaszählrohr gemessen.

Die Messergebnisse für die Minerale Flusspat, Anorthit, Augit und Margarit zeigt Abb. 2. Es wurde jeweils die gemessene Aktivität in Abhängigkeit von

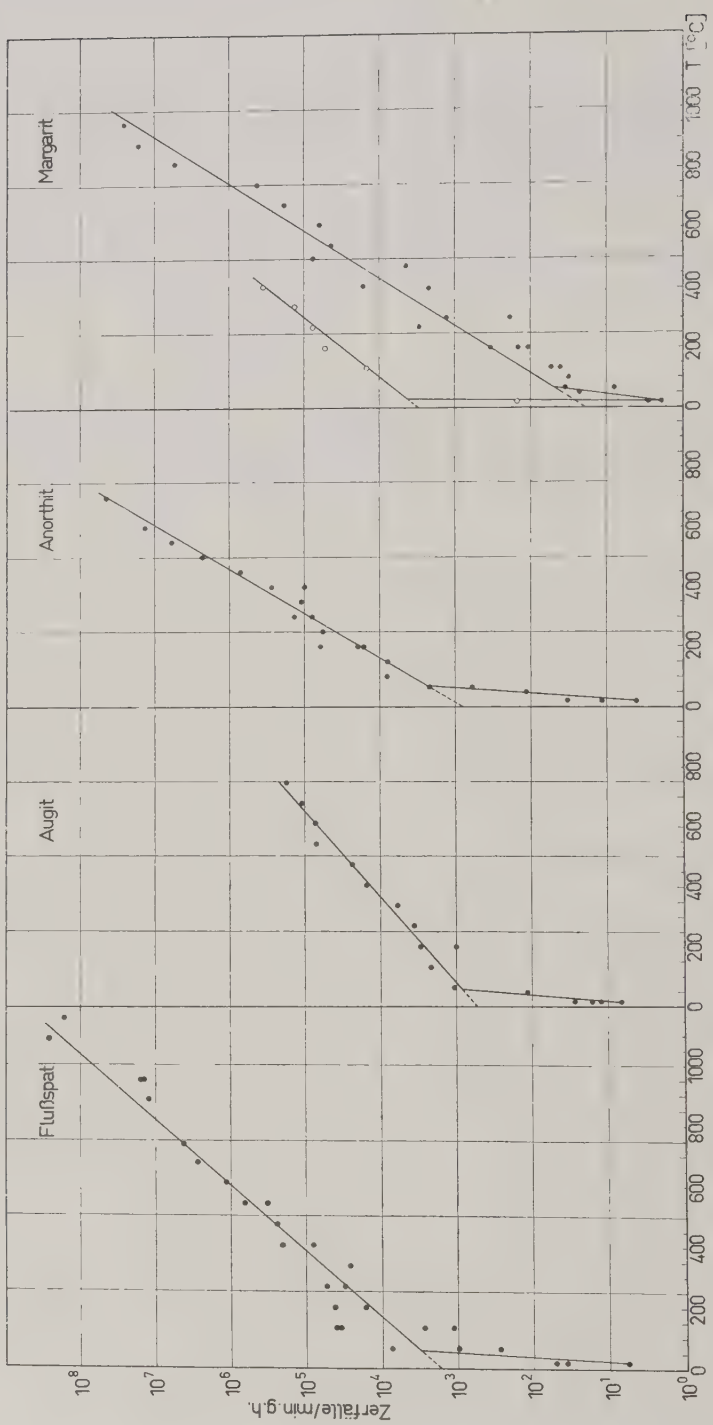

Abbildung 2: Aktivitäten pro g Material und 1 h Diffusionszeit in Abhängigkeit von der Temperatur T.

der Temperatur aufgetragen. Mit Ausnahme von Margarit waren die erhaltenen Kurven mehrmals reproduzierbar. Margarit dagegen zeigte für die erste Messreihe eine Abweichung von den übrigen reproduzierbaren Messwerten. Wir müssen vermuten, dass mit der Austreibung der im Glimmer vorhandenen Feuchtigkeit eine erhöhte Argonabgabe verbunden ist. Die in Abb. 2 dargestellten reproduzierbaren Messkurven zeigen oberhalb einer bei etwa 100°C liegenden Temperatur eine exponentielle Zunahme der gemessenen Aktivität. Unterhalb dieser Temperatur tritt dagegen ein verstärktes Absinken der Aktivität auf. Die hier erhaltene Kurvenform wurde auch von Cook (1939) für den Emanationsverlust aus Eisenhydroxyd beobachtet. Nach Cook (1939) beruht dieser Effekt auf der van der Waalschen Adsorption des Gases und tritt hauptsächlich bei Gasverlusten aus oberflächenreichen Materialien auf.

Bei dem hier eingeschlagenen Weg muss die Frage des evtl. bei der Bestrahlung auftretenden Strahlenschadens aufgeworfen werden. Diese Frage kann im Zusammenhang mit den vorliegenden Messungen noch nicht geklärt werden. Doch lässt sich soviel sagen, dass der Strahlenschaden sich dahin auswirken könnte, dass die Gasverluste und damit die gemessenen Diffusionskonstanten eher zu gross ausfallen müssten. Da die Messreihen mehrere Male reproduzierbar sind, kann man vermuten, dass Strahlenschäden grösseren Ausmasses nicht auftreten. Die Strahlenschäden müssten sich sonst bei Erhitzung des Materials weitgehend erholen. Lediglich im Falle des Glimmers könnten nennenswerte Strahlenschäden vorhanden gewesen sein.

Die Lösung der Diffusionsgleichung wurde von Jost (1952) für den Fall angegeben, dass eine isotrope Volumendiffusion in einer Kugel mit dem Radius a vorliegt. Die Lösung lautet:

$$\frac{C_0 - C}{C_0} = 1 - \frac{6}{\pi^2} \sum_{n=1}^{\infty} \frac{1}{n^2} \cdot \exp\left(-\frac{n^2 \pi^2 Dt}{a^2}\right)$$

wobei C_0 = Gaskonzentration vor der Diffusion;
C = Gaskonzentration nach der Diffusion;
D = Diffusionskonstante;
t = Diffusionszeit.

Für sehr kleine Konzentrationsänderungen, wie sie bei den vorliegenden Untersuchungen in den Proben auftreten, konvergiert diese Reihe sehr schlecht. Deshalb berechneten Carslaw und Jaeger (1947) für diesen Fall und der Bedingung, dass die Diffusionszeit t klein bleibt, den folgenden, mit guter Näherung geltenden Ausdruck:

$$\frac{C_0 - C}{C_0} = \frac{6}{\pi^{1/2}} \cdot \left(\frac{Dt}{a^2}\right)^{1/2} - 3 \cdot \frac{Dt}{a^2}$$

Aus dieser Beziehung wurden für die Minerale Flusspat, Anorthit und Augit mit $a = 5 \times 10^{-2}$ cm und Margarit mit $a = 4 \times 10^{-2}$ cm die Diffusionskonstanten gewonnen. Die Ergebnisse sind in Abb. 3 dargestellt. Die gewonnenen Diffusionskonstanten wurden in Abhängigkeit von $1/T$ aufgetragen.

In Abb. 4 ist der Kurvenverlauf noch einmal schematisch dargestellt. Es lassen sich auch hier mehrere Bereiche unterscheiden: Teil (a): dieser Kurventeil stellt die Diffusion dar, wie sie durch die Beweglichkeit der Ar^{37}-Atome in einem festen Kristallgitter gegeben ist. Teil (b): hier tritt durch die auftretende Selbstdiffusion (Bewegung der Gitterbausteine oberhalb einer gewissen Temperatur (400–600°C)

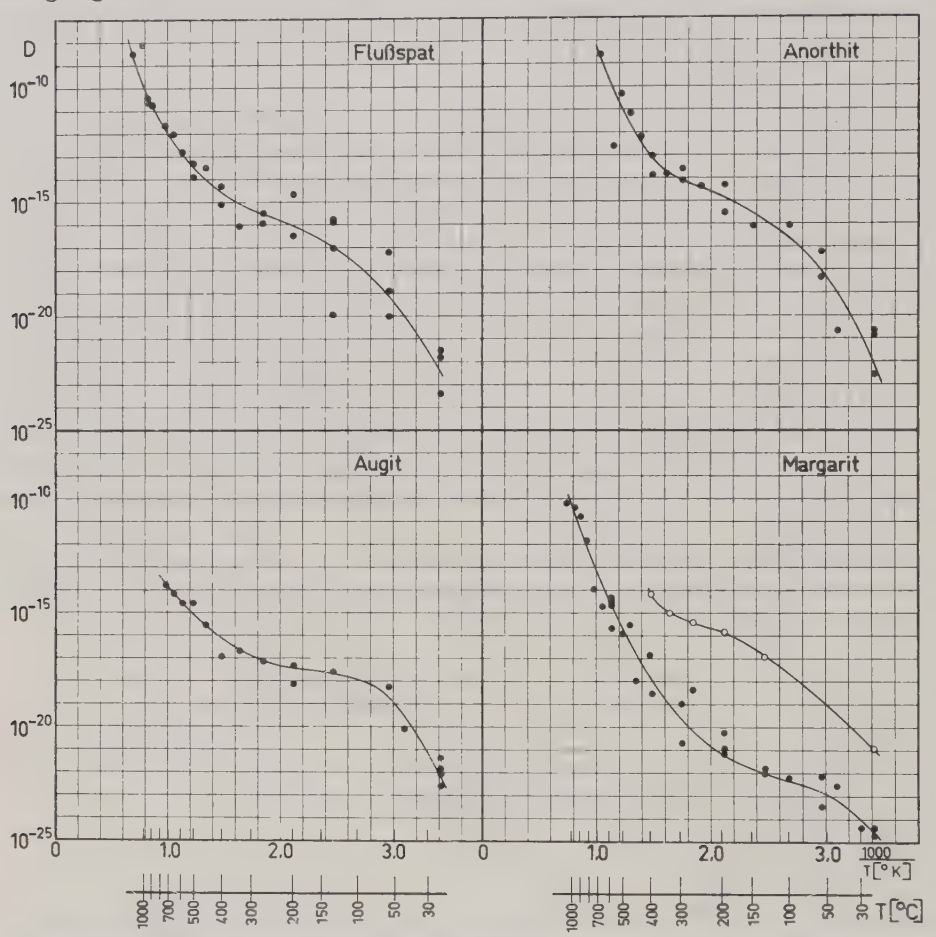

Abbildung 3: Diffusionskonstanten D in Abhängigkeit von der reziproken Temperatur 1/T.

eine Erhöhung der Aktivierungsenergie auf. (Reynolds unterscheidet zwischen diesen beiden Gebieten noch ein übergangsgebiet). Teil (c): Für Temperaturen unterhalb etwa 100°C ist noch ein dritter Kurventeil (c) deutlich zu unterscheiden, der nach Cook (1939) auf die van der Waalsche Oberflächenadsorption des Gases zurückzuführen ist.

Die Kurventeile (a) und (b) wurden auch schon von Reynolds (1957) und neuerdings von russischen Autoren (Amirkhanov *et al.*, 1959) beobachtet. Infolge der für niedrige Temperaturen auftretenden Abweichung ist aber eine Extrapolation der Diffusionskonstanten von höheren Temperaturen auf Zimmertemperatur für die Diffusion von Argon in Feldspäten und Glimmern unzulässig. Reynolds

(1957) gelangt z.B. für die Diffusion von Argon in Feldspat bei Zimmertemperatur zu einem extrapolierten Wert von $D > 10^{-19}$ cm²/sec. Das hier vorliegende Ergebnis für die Diffusion von Argon in Feldspat bei Zimmertemperatur ergibt dagegen einen Wert von $D = 10^{-22}$ cm²/sec.

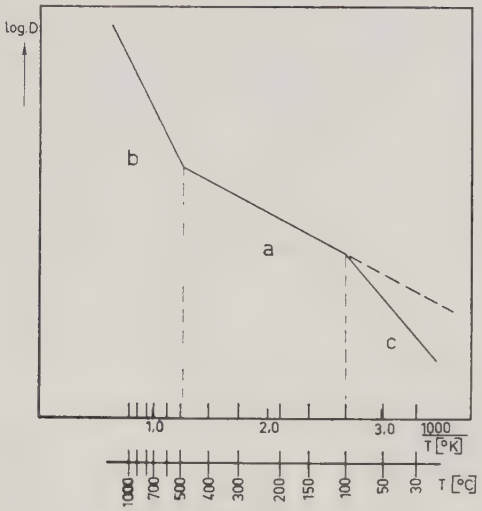

Abbildung 4: Schematischer Kurvenverlauf der Funktion D (1/T).

Die Temperaturabhängigkeit der Diffusionskonstante D ist in den einzelnen Kurventeilen gegeben durch die Beziehung:

$$D = D_0 \cdot \exp\left(-\frac{Q}{RT}\right)$$

wobei D_0 = Konstante mit der Dimension (cm²/sec);
Q = Aktivierungsenergie (cal/mole);
R = 1,9869 (cal/°K mole) = Gaskonstante;
T = absolute Temperatur (°K).

Daraus lässt sich die Aktivierungsenergie Q des Argons in den untersuchten Mineralien berechnen. Die Ergebnisse sind in Tabelle 1 zusammengefasst. Zu

Tabelle 1. Aktivierungsenergien von Argon in verschiedenen Mineralien

Material	Q im Gebiet (a) (kcal/mole)	Q im Gebiet (b) (kcal/mole)	Q im Gebiet (c) (kcal/mole)
Flusspat	8,300	43,500	33,200
Anorthit	10,000	55,900	46,500
Augit	3,200	26,900	38,900
Margarit	6,900	53,700	21,300

ähnlichen Ergebnissen in den höheren Temperaturbereichen kamen auch Gerling (1957) und die oben erwähnten Autoren Amirkhanow, *et al.* (1959).

Belegt man eine Aktivitätsmessung mit einem Fehler von $\pm 10\%$ und die Messung der Korngrösse ebenfalls mit $\pm 10\%$, so ergibt sich für die Diffusionskonstanten ein Messfehler von $\pm 60\%$. Für die Aktivierungsenergie folgt daraus eine Fehlergrenze von $\pm 40\%$.

Die von Gentner *et al.* (1954) an den Bugginger Salzen gewonnenen Ergebnisse können am ehesten mit unseren Messungen an Flusspat verglichen werden. Für das Bugginger Salz (KCl–NaCl–Gemisch) wurde für 40°C eine Diffusionskonstante in der Grössenordnung von 10^{-20} bis 10^{-21} cm²/sec gefunden. Der entsprechende Flusspatwert liegt ebenfalls bei 10^{-21} cm²/sec.

Wie Wasserburg (1957) dargelegt hat, ergibt sich zwischen dem gemessenen A^{40}-Gehalt bei Altersbestimmungen und dem wahren Alter t folgender Ausdruck:

$$\frac{A^{40}}{K^{40}} = \frac{R}{1+R} \cdot \left[-1 + \frac{3}{d^2} - \frac{3 \cdot \cot d}{d} + \frac{6d^2}{\pi^2} \sum_{n=1}^{\infty} \frac{1}{n^2(d^2 - \pi^2 n^2)} \cdot \exp\left\{ \lambda t \left(\frac{1 - n^2\pi^2}{d^2} \right) \right\} \right]$$

wobei $R = 0{,}123$, das Verzweigungsverhältnis;
$d^2 = \lambda a^2/D$ mit $\lambda =$ Zerfallskonstante;
$a =$ Radius der Korngrösse;
$D =$ Diffusionskonstante;

Aus dieser Beziehung lässt sich das wahre Alter t eines Minerals in Abhängigkeit des gemessenen Alters A^{40}/K^{40} auftragen. Es ergibt sich eine Kurvenschar mit dem Kurvenparameter d^2. Dieses wurde von Wasserburg (1957) für Alterswerte bis $1{,}8 \times 10^9$ Jahren ausgeführt. Dasselbe wurde auch schon von Präg (1953) bis 35×10^6 Jahren und von Oser (1954) bis 200×10^6 Jahren bei der Berücksichtigung der Diffusionsverluste von Argon in Salzen durchgeführt. Nicolayson (1957) führte dieses Verfahren für den Uranzerfall aus.

Aus den zitierten Arbeiten geht hervor, dass der Gasverlust nicht allein von der Diffusionskonstante D, sondern von dem Quotienten D/a^2 abhängt. Nach einer der oben zitierten Beziehung ergibt sich D/a^2 zu:

$$\frac{D}{a^2} = \frac{\pi}{36} \cdot \left(\frac{C_0 - C}{C_0} \right)^2 \cdot \frac{1}{t}$$

d.h. D/a^2 ist nur von C, C_0 und t abhängig. Damit ist es aber möglich, ohne Bestimmung der Korngrösse allein aus den Konzentrationen (Aktivitäten) den Quotienten D/a^2 zu bestimmen, womit sich für die Altersbestimmung eine brauchbare Korrektur ergibt. Unter Verwendung der von Nicolayson (1957) gegebenen Werte für den Uranzerfall wurde das wahre Alter in Abhängigkeit vom gemessenen Alter aufgetragen. Das Diagramm ist in Abb. 5 dargestellt.

Die in vorliegender Arbeit gemessenen Diffusionskonstanten haben für Zimmertemperatur die in Tabelle 2 angegebenen Werte; in der letzten Spalte ist der zugehörige Wert für d^2 eingetragen. Nach dem Diagramm der Abb. 5 sind zuverlässige Altersbestimmungen nach der K–Ar–Methode mit diesen Parameterwerten ohne Zweifel möglich. Hervorzuheben ist das Ergebnis des Glimmers Margarit; dafür ist d^2 praktisch ∞, d.h. das Argon wird bei Zimmertemperatur quantitativ

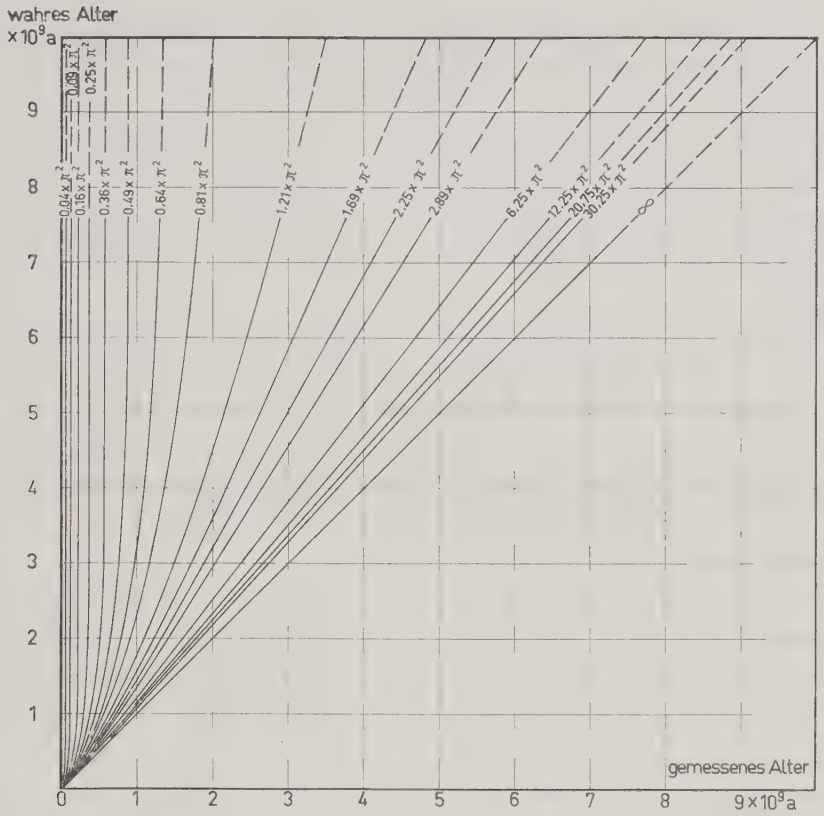

Abbildung 5: Wahres Alter in Abhängigkeit von gemessenen Alter (Parameter d²).

Tabelle 2. Diffusionskonstanten D und Parameterwerte d^2 bei Zimmertemperatur

Material	D bei Zimmertemperatur (cm²/sec)	d^2 für a = 5 × 10⁻² cm
Flusspat	5×10^{-23}	$200 \times \pi^2$
Anorthit	$1{,}5 \times 10^{-22}$	$50 \times \pi^2$
Augit	1×10^{-22}	$50 \times \pi^2$
Margarit	3×10^{-25}	$200.000 \times \pi^2$

festgehalten. Das ist in guter übereinstimmung mit den Ergebnissen der K–Ar–Altersbestimmung an Glimmern, die als die zuverlässigsten angesehen werden.

Gentner und Kley (1957) haben gefunden, dass zwischen gleichaltrigen Glimmern und Feldspäten Altersdifferenzen von *ca.* 5% vorkommen. Aus Tabelle 2 und dem Diagramm der Abb. 5 lässt sich umgekehrt der für die Diffusion verantwortliche Radius a berechnen. Damit hat man eine neue unabhängige Methode zur Abschätzung der in der Natur vorkommenden Kristallgrössen. In der

erwähnten Messung von Gentner und Kley (1957) beträgt a ungefähr 5×10^{-2} cm. Bei diesen Mineralien handelt es sich allerdings um gut ausgesuchte Proben.

Auch lässt sich erklären, dass die relativen Unterschiede der Feldspat- und Glimmeralter nicht vom Alter abhängen. Wie aus Abb. 5 ersichtlich ist, laufen die Kurven für $d^2 > 6{,}25 \times \pi^2$ praktisch linear, d.h. die relativen Altersunterschiede bleiben konstant. Dies ist in Übereinstimmung mit den Altersbestimmungen, wonach bei allen Autoren die relativen Abweichungen der Feldspatalter vom Glimmeralter sowohl bei jüngeren als auch präkambrischen Proben gleich gross sind.

Es sei jedoch darauf hingewiesen, dass die Ergebnisse für die in dieser Arbeit verwendeten Mineralproben nicht ohne weiteres auf alle in der Natur vorkommenden Mineralien übertragen werden können. Wie bereits oben erwähnt, geht die Diffusionskonstante in die Gasverluste linear, die Kristallgrösse quadratisch ein. Die Bestimmung dieser für die Diffusion verantwortlichen Kristallgrösse ist sehr schwierig. Bekanntlich erleiden alle Kristalle mehr oder weniger innere Umwandlungen (bei Feldspäten z.B. Kaolinisierung, Serizitisierung und perthitische Entmischung), die im Innern von Kristallen neue Oberflächen (Korngrenzen) schaffen und die effektive Kristallgrösse herabsetzen.

Gentner und Kley (1957) haben festgestellt, dass bei zunehmender Zerteilung von Varuträsker Feldspäten ein Argonverlust eintritt, der aus inneren Oberflächen und Korngrenzen stammt. Die Verluste setzen bei etwa 100 μ ein und betragen bei *c.* 5 μ etwa 30%. Aus diesen Untersuchungen folgt, dass ein Teil solcher Einschlüsse offenbar von einem geschlossenen Kristallgitter umgeben ist und das Argon vorwiegend durch Volumendiffusion entweichen kann. Die effektive Kristallgrösse wird daher vermutlich oberhalb der Grösse solcher mikroskopischer Bereiche von 100 μ liegen, dürfte jedoch von Fall zu Fall verschieden sein.

Wie bereits erwähnt, besteht der Vorteil dieser Methode darin, dass bei der Ermittlung der durch Diffusion aufgetretenen Gasverluste an natürlichen Kristallen die Bestimmung von Diffusionskonstanten und Korngrössen selbst umgangen werden kann. Soll darüber hinaus noch die Diffusionskonstante bestimmt werden, so muss die Kristallgrösse des betreffenden Minerals ermittelt werden.

Besonderes Interesse in diesem Zusammenhang haben die Diffusionsverluste von Argon in Steinmeteoriten, da solche Meteoriten Alter von einigen Milliarden Jahren besitzen. Über diese Untersuchungen wird in einer getrennten Arbeit berichtet.

Anerkennungen –Herrn Professor Ramdohr und Herrn Dr. Frenzel vom Mineralogischen Institut der Universität Heidelberg danken wir für mineralogische Beratung sowie für Überlassung von Mineralproben. Herrn Professor Maier-Leibnitz und seinen Mitarbeitern, München, danken wir für die Bestrahlung der Mineralproben im Forschungsreaktor München-Garching.

Literatur

Amirkhanov K. I., Brandt S. B. und Bartniski E. N. (1959) Diffusion von radiogenem Argon in Feldspäten. *Dokl. Akad. Nauk.* SSSR 125, 1345.

Carslaw H. S. und Jaeger J. C. (1947) Conduction of heat in Solids. Oxford.

Cook L. G. (1939) Untersuchungen über Chrom- und Eisenhydroxyde und ihre Bedeutung für die Emaniermethode. *Z. phys. Chem.* B **42**, 221.

Flügge S. und Ziemens K. E. (1939) Die Bestimmung von Korngrössen und von Diffusionskonstanten aus dem Emaniervermögen. *Z. phys. Chem.* B **42,** 179.

Gentner W., Goebel K. und Präg R. (1954) Argonbestimmungen an Kaliummineralien—III. Vergleichenden Messungen nach der Kalium–Argon- und Uran–Helium-Methode. *Geochim et Cosmochim. Acta* **5,** 124.

Gentner W. und Kley W. (1957) Argonbestimmungen an Kaliummineralien—IV. Die Frage der Argonverluste in Kalifeldspäten und Glimmermineralien. *Geochim et Cosmochim. Acta* **12,** 323.

Gentner W, Präg R. und Smits F. (1953) Argonbestimmung an Kalium–Mineralien—II. Das Alter eines Kalilagers im Unteren Oligozän. *Geochim et Cosmochim. Acta* **4,** 11.

Gentner W. und Trendelenburg E. A. (1954) Experimentelle Untersuchungen über die Diffusion von Helium in Steinsalzen und Sylvinen. *Geochim et Cosmochim. Acta* **6,** 261

Gerlin E. K. (1957) Argon Method of the Age Determination and its Application in Pre-Cambrian Geology. UNESCO—Konferenz Paris (1957).

Jost B. (1952) Diffusion in Solids, Liquids and Gases, p. 45. New York.

Nicolayson L. O. (1957) Solid Diffusion in radioactive minerals and the measurement of absolute age. *Geochim. et Cosmochim. Acta* **11,** 41.

Oser H. (1954) Argonbestimmungen an Kalisalzen des Zechstein. Diplomarbeit Freiburg i.Br.

Präg R. (1953) Berücksichtigung der Diffusion der Edelgase bei Altersbestimmungen nach der Kalium–Argon-und Uran–Helium-Methode. Dissertation, Freiburg i.Br.

Reynolds J. H. (1957) Comparative study of argon content and argon diffusion in mica and feldspar. *Geochim. et Cosmochim. Acta* **12,** 177.

Rutherford E. (1901) Einfluss der Temperatur auf die "Emanationen" radioaktiver Substanzen. *Phys. Z.* **2,** 429.

Smits F. und Gentner W. (1950) Argonbestimmungen an Kalium-Mineralien—I. Bestimmungen an tertiären Kalisalzen. *Geochim. et Cosmochim. Acta* **1,** 22.

Wasserburg G. J. (1957) $Argon^{40}$: $Potassium^{40}$ Dating. *Nuclear Geology* (Edited by Faul H.) New York.

Geochimica et Cosmochimica Acta, 1960, Vol. 19, pp. 80 to 81. Pergamon Press Ltd. Printed in Northern Ireland

BOOK REVIEWS

K. I. LUKASHEV: **Osnovy Litologii i Geokhimii Kory Vyvetrivaniya (Fundamentals of the Lithology and Geochemistry of the Weathering Zone)**. Izdatel'stvo Akademii Nauk, Belorusskoy SSR, Minsk, 1958. 470 pp., 15 roubles.

SINCE much of the original work on studies of the weathering zone has been done by Soviet workers, it is appropriate that they should also produce the first comprehensive treatise presenting a systematic discussion on all aspects of weathering. In the West many important papers on weathering processes have appeared during the past 40 years. Yet the large number of Russian words adopted in Western soil science and weathering terminology is eloquent evidence of the dominant role Soviet scientists have played and are still playing in this field. Academician LUKASHEV has himself written numerous papers on soils and the geochemistry of the weathering zone. LUKASHEV defines the weathering zone as "the upper part of the lithosphere, in which rocks, air, water and living organisms interact, and in which new organic and mineral groupings are formed by the destruction and rearrangement of substances of deep origin in the upper part of the earth's crust and at the earth's surface."

The first half of the book is devoted to general considerations of the formation of the weathering zone. Physical, chemical and cosmic factors involved are discussed. Ground-water circulation, hydrolysis, oxidation, colloid formation and other processes involved in weathering and the migration, dispersal and concentration of elements receive extensive treatment. "Geoenergetics" is defined as the study of sources of energy in the weathering zone. Geomorphologic considerations such as the effect of relief and climate on specific types of weathering zones follow a discussion of the mineralogy of soils. Clay mineral structures and textures and fabrics of soils are further discussed. The fivefold geochemical classification of the weathering zone used by LUKASHEV consists of the following zones: (1) lithogenic or fragmental (primary minerals little changed by weathering); (2) siallite-clay (hydromicas, kaolin, etc.); (3) siallite–carbonate (calcite, carbonates, gypsum, kaolinite); (4) siallite–chloride–sulphate (halite, anhydrite, thenardite, secondary quartz); (5) iron and aluminium siallite (diaspore, boehmite, gibbsite).

The second part of the book is devoted more specifically to geochemical processes involved in weathering. Sedimentation rates and other geologic processes ordinarily treated in sedimentology texts are mentioned in a discussion of clastic accumulations. LUKASHEV examines the role of a whole series of elements in eluvial processes (which lead to the formation of residual weathering zones). Economic geology is brought in with a discussion of secondary enrichment and the importance of oxidation–reduction reactions. Halogenesis (the process of salt deposition), karst and thermokarst (formation of karst topography by the melting of ice in permafrost zones) processes, and halmyrolysis are discussed.

The chief merit of LUKASHEV's book is not originality of subject matter. What is original is the inclusion in one book of a great amount of material not ordinarily connected with "weathering" in the West. Surveys of weathering such as REICHE (1950) and KELLER (1957) are more limited in scope. LUKASHEV brings together under one cover most of the bits and pieces which certainly apply to "weathering" in the broad sense of the word but are usually found only in texts on geochemistry, economic geology, geomorphology, sedimentology, soil science, soil engineering, and mineralogy. The whole Soviet approach to weathering zone studies is typified by this book, which is indeed a valuable reference. (Of more than incidental value is also the eighteen page list of references at the end of the book.) As a reference, the one major failing of the book, as for most Soviet texts, is the complete lack of indexing.

W. D. ROMEY

Department of Geology
University of California, Berkeley, California.

REFERENCES

REIDE P. (1950) *A Survey of Weathering Processes and Products*. University of New Mexico Press.

KELLER W. D. (1957) *The Principles of Chemical Weathering*. Lucas.

Clays and Clay Minerals: Proceedings of the Sixth National Conference on Clays and Clay Minerals. Edited by Ada Swineford. Monograph No. 2, Earth Science Series. Pergamon Press, London, 1959. 411 pp., 60s. ($8.50).

The Annual Clay Conferences have been bringing together clay mineralogists, agronomists, ceramists and chemists since 1952 to discuss their most recent researches. The proceedings of these meetings have formed an invaluable record of accomplishments in the relatively young field of clay mineralogy. The proceedings of the Sixth Conference (Berkeley, California, autumn 1957) in addition to continuing this important service to clay mineralogists, include an unusual number of reports on subjects that will be equally interesting to silicate mineralogists and colloid chemists whose special fields are not the clay minerals. Although the Conference does not claim to be an international organization, papers are always contributed by foreign laboratories. Mineralogists from Austria, Scotland, Japan and Spain attended the 1957 Conference to discuss their work. All of these reports are included in the Sixth Conference Proceedings.

The volume consists of twenty-eight technical papers and a field trip road log. The first three papers deal with crystal chemistry of micas and feldspars. The question of order in the isomorphous substitution positions within these structures is discussed along with its bearing on polymorphism of the micas that are derived from feldspar. Nine papers treat the general subject of clay mineral genesis by weathering, hydrothermal alteration and diagenetic processes. The direct chemical laboratory approach to the study of clay mineral development is complemented by descriptions of clays actively forming in modern soils and clays in ancient rocks that have been studied geologically. Colloidal chemistry of the clay minerals is the subject of eight other contributions. Two of the eight deal with properties of clay–water suspensions, two with adsorption of water on clays, two with the morphology of clay minerals and chrysotile, and two with the effect of grinding on the colloidal properties of clay minerals. Acid solution of clays is reported in one paper. Four papers are devoted to the petrology of shales and the history (both depositional and post-depositional) that it suggests. Dehydration studies are reported for tobermorite and hectorite in two papers. Sepiolite is the only specific mineral whose structure determination was reported at the Sixth Clay Conference.

It is commonly impossible for the mineralogist to obtain directly data on clay mineral composition and structure in which he is interested. The small particle size of clay minerals limits measurements of their composition and optical properties to aggregates of many crystallites; their occurrence as intermediate phases in rock-forming mineral alterations necessitates considering some clay mineral assemblages to be unstable; their almost universal natural occurrence as mixtures confuses clay mineral classification. For these and other reasons the successful methods of investigation used to study clays are not always those that have been rewarding in other mineralogical systems. The ingenuity used in designing new techniques to measure properties of clay minerals and to present fresh interpretations of available data in terms of clay mineral composition and structure was particularly well displayed at the Sixth Conference. In one of the papers on morphology a relaxation technique was reported that was designed to determine the size and shape of clay crystallites in suspension. This information is a stimulation for the colloid chemist who normally works with particles whose sizes and shapes are poorly defined. Interpretation of the clay mineral content of ancient rocks in terms of the available information on soils and recent marine sediments offers the geologist another basis for depositional environment and source determinations. The exact laboratory studies of mineral dehydration and high-temperature mineral synthesis are useful for the practicing ceramist.

This volume has more than maintained the high level of accuracy and utility established by the other volumes of the series that were previously published by the National Research Council. It has been prepared under the same able editorship as have been the Proceedings of the Second, Fourth and Fifth Conferences. The paper used for printing the text and line drawings has a pleasant semigloss and slight neutral colour which is easy on the eyes but still takes a sharp, clean impression of the type. The only possible objection to the paper is that the printing occasionally shows through the page from the back side. Plates (photographs, electron micrographs, photomicrographs, etc.) are printed on glossy white paper. They provide good detail. The book has a cloth, hard-board binding that is strong but remarkably easy to keep open. The price at $8.50, is somewhat higher per page than the volumes published by the National Research Council.

E. C. Jonas

Geochimica et Cosmochimica Acta, 1960, Vol. 19, p. 82. Pergamon Press Ltd. Printed in Northern Ireland

MEETING ANNOUNCEMENTS

Preliminary Announcement–The Ninth National Clay Conference

The Ninth National Clay Conference, sponsored by the Clay Minerals Committee of the National Academy of Sciences-National Research Council, will be held at Purdue University, Lafayette, Indiana, on October 6, 7 and 8, 1960. In addition a short field trip and laboratory visits are planned for Wednesday, October 5. All those interested in research or technology in fields related to clays or clay minerals are cordially invited to participate.

Program

Two special symposia of invitational papers are planned on the subjects of "Engineering Aspects of Physico-Chemical Properties of Clays" and "Clay-Organic Complexes". The symposium on "Engineering Aspects of Physico-Chemical Properties of Clays" will feature contributions on soil mechanics. The "Clay-Organic Complexes" symposium will be concerned with basic studies of clay-organic systems in the paper and petroleum industries, in soil science, civil engineering, and other areas. In addition, there will be general sessions and original contributions on any aspect of clay mineralogy are invited.

Papers presented at the conference may be published in the Proceedings of the Conference (Clays and Clay Minerals), if accepted by the Board of Editors. The Proceedings will be published by Pergamon Press.

Titles and abstracts of contributions to the general sessions should be submitted to Dr. J. L. White, Agronomy Department, Purdue University, Lafayette, Indiana, by June 1, 1960. Abstracts should be limited to 250 words and should be informative rather than descriptive. Abstracts should be submitted in duplicate.

Field Trip

A short field excursion is planned in the immediate vicinity of Lafayette to examine well-characterized soil profiles and geological features of the area.

Laboratory Visits

Guided tours through the Purdue University Soil Mechanics and Highway Research Project Laboratories as well as the Soil Chemistry and Soil Mineralogy Laboratories of the Agronomy Department are planned for Wednesday, October 5.

Further Details

Dr. J. L. White,
Local Chairman, Ninth National Clay Conference,
Agronomy Department, Purdue University,
Lafayette, Indiana.

Geochemistry Symposium at Helsinki Meeting of IUGG

A programme in Vulcanology, Geochemistry and Petrology is being organized for the Helsinki meeting of the International Union of Geodesy and Geophysics July 25-August 6. Symposia on Geochronology, High Pressure Chemistry, Isotopes Geology, Atmospheric Chemistry, as well as a general programme in geochemistry and petrology, will take place beginning July 24 and going through July 28. Announcement of the detailed programme will be made later this spring.

Geochimica et Cosmochimica Acta, 1960, Vol. 19, p. 83. Pergamon Press Ltd. Printed in Northern Ireland

Papers to be published in future issues

M. A. Van Dilla, J. R. Arnold and E. C. Anderson: Spectrometric measurement of natural and cosmic ray-induced radioactivity in meteorites.

W. H. R. Shaw: Studies in biogeochemistry—I. A biogeochemical periodic table. Studies in biogeochemistry—II. A biogeochemical periodic table. Discussion and references.

A. J. Ellis: Mordenite synthesis in a natural hydro-thermal solution.

G. Jurain: Moyens et résultats d'étude de la radioactivitée due au radon dans les eaux naturelles.

E. W. Heinrich, R. A. Borup and A. A. Levinson: Relationships between geology and composition of some pegmatitic monazites.

C. H. Oppenheimer: Bacterial activity in sediments of shallow marine bays.

R. G. Bader, D. W. Hood and J. B. Smith: Recovery of dissolved organic matter in sea-water and organic sorption by particulate matter.

S. Matthes: Ergebnisse zur Granatsynthese und ihre Beziehungen zur natürlichen Granatbildung innerhalt der Pyralspit-Gruppe.

M. Fornaseri and L. Grand: Flame photometric determination of strontium in silicates. Strontium content of the granite G-1 and the diabase W-1.

F. Frohlich: Beitrag zur Geochemie des Chroms.

S. F. Singer: Production of tritium in nuclear spallations.

Shunji Umemoto: An example of variations in constituents of hot springs.

W. D. Ekman: Nickel in tektites by activation analysis.

R. Park and S. Epstein: Carbon isotope fractionation during photosyntheses.

E. G. Baker: An hypothesis concerning the accumulation of sediment hydrocarbons to form crude oils.

I. A. Breger: Diagenesis of metabolites and a discussion of the origin of petroleum hydrocarbons.

B. Nagy: Review of the chromatographic "plate" theory with reference to fluid flow in rocks and sediments.

G. W. Hodgson, B. Hitchon, R. M. Elofson, B. L. Baker and E. Peak: Petroleum pigments from recent fresh water sediments.

F. J. Stevenson: Some aspects of the distribution of biochemicals in geologic environments.

A. E. Ringwood: Some aspects of the thermal evolution of the earth.

L. G. Stonhill: The estimation of the oxidation state of pitchblende in ores.

R. Kretz: The distribution of certain elements among coexisting calcic proxenes, calcic amphiboles and biotites in skarns.

A. M. Pommer and I. A. Breger: Potentiometric tritation and equivalent weight of humic acid.

INFORMATION FOR CONTRIBUTORS

I. GENERAL

1. Papers on *geochemistry* should be submitted to the appropriate Executive Editor—Prof. L. R. WAGER for papers from the United Kingdom and British Commonwealth, and for papers in English from Europe; Prof. C. W. CORRENS for papers in German or French; Prof. E. INGERSON for papers from the American continents. Papers on *cosmochemistry* should be sent to Prof. W. A. WAHL. Papers submitted for publication will naturally be judged from the standpoint of scientific originality and novelty. Technical details of apparatus used in scientific investigation can, however, be presented in brief notes. Critical comments or preliminary results requiring early publication should be submitted as letters to the editors. Where possible, letters should be confined to 500 words. The preparation of progress reports and review articles will be invited by the editors from time to time. The journal appears as independent and complete numbers, which are combined into volumes of about 300 pages.

2. Only papers which have not been previously published can be accepted. Authors must agree not to publish elsewhere a paper submitted to and accepted by *Geochimica et Cosmochimica Acta*.

3. Fifty reprints of each paper are provided free. Additional copies can be purchased if ordered at the time the first proofs are returned. A reprint order form will accompany first proofs.

II. SCRIPT REQUIREMENTS

1. Scripts must be written in one of the three official languages—English, French or German.

2. The script should be typed (not a carbon copy). The text must be ready for printing and should be carefully checked for errors. Authors will receive proofs for correction.

3. Illustrations should accompany the script, mounted on separate sheets. Line diagrams that require to be redrawn should include all relevant details. Half-tone illustrations should be restricted to the minimum necessary. Photographs should be enlarged sufficiently to permit their clear reproduction and if words or numbers appear on them, two copies should be sent, one clearly printed and the other without inscription. All illustrations should be provided with descriptive legends, which should be given on a separate sheet. Any lettering on diagrams—other than Greek letters, symbols, etc.—should be stencilled and should be sufficiently large and bold to permit reproduction when the diagram has been reduced to a size suitable for inclusion in the journal.

4. References in the text should be given by quoting the author's name and year of publication, i.e. AHRENS (1952). *Full references should be listed at the end of each paper, in alphabetical order, in the following manner*

AHRENS, L. H. (1952). The use of ionization potentials—I. Ionic radii of the elements. *Geochim. et Cosmochim. Acta* **2**, 155–169.

and should include the full title of the article, standard abbreviated title of the journal, year, volume number and inclusive page numbers.

5. The text of articles submitted should be concise and in a readily understandable style. The technical description of the methods used should only be given in detail when such methods are new. The essential contents of each paper should be briefly recapitulated in an abstract in English. Such an abstract, may, however, be submitted by the author in the language of the original typescript for translation into English by the editorial staff.

6. To conserve space, authors are requested to mark less important portions of the paper (such as description of methods, record of experimental results, etc.) for printing in smaller type.

7. Indices of refraction should be denoted by the symbols α, β, γ, ω, ε, n, and vibration directions by X, Y, Z, O and E.

Pergamon Press are also publishers of the following Journals:

JOURNAL OF NUCLEAR ENERGY (*including* THE SOVIET JOURNAL OF ATOMIC ENERGY*). PART A: REACTOR SCIENCE; PART B: REACTOR TECHNOLOGY; PART C: PLASMA PHYSICS—ACCELERATORS—THERMONUCLEAR REACTORS
HEALTH PHYSICS (*The Official Journal of the Health Physics Society*)
JOURNAL OF INORGANIC AND NUCLEAR CHEMISTRY
TETRAHEDRON (*The International Journal of Organic Chemistry*)
TALANTA (*An International Journal of Analytical Chemistry*)
INTERNATIONAL JOURNAL OF APPLIED RADIATION AND ISOTOPES
BIOCHEMICAL PHARMACOLOGY
ARCHIVES OF ORAL BIOLOGY
* BIOPHYSICS
* JOURNAL OF MICROBIOLOGY, EPIDEMOLOGY AND IMMUNOBIOLOGY
* PROBLEMS OF HEMATOLOGY AND BLOOD TRANSFUSION
* PROBLEMS OF VIROLOGY
* PROBLEMS OF ONCOLOGY
* SECHENOV PHYSIOLOGICAL JOURNAL OF THE U.S.S.R.
* PAVLOV JOURNAL OF HIGHER NERVOUS ACTIVITY
* ELECTRIC TECHNOLOGY, U.S.S.R.
* RADIO ENGINEERING
* RADIO ENGINEERING AND ELECTRONICS
* TELECOMMUNICATIONS
* PHYSICS OF METALS AND METALLOGRAPHY
* THE ABSTRACTS JOURNAL OF METALLURGY
* APPLIED MATHEMATICS AND MECHANICS
CHEMICAL ENGINEERING SCIENCE
JOURNAL OF ATMOSPHERIC AND TERRESTRIAL PHYSICS
PLANETARY AND SPACE SCIENCE
ANNALS OF THE INTERNATIONAL GEOPHYSICAL YEAR
SPECTROCHIMICA ACTA
JOURNAL OF THE MECHANICS AND PHYSICS OF SOLIDS
ACTA METALLURGICA (*for the Board of Governors of Acta Metallurgica*)
INTERNATIONAL JOURNAL OF THE PHYSICS AND CHEMISTRY OF SOLIDS
DEEP-SEA RESEARCH
JOURNAL OF NEUROCHEMISTRY
JOURNAL OF PSYCHOSOMATIC RESEARCH
JOURNAL OF INSECT PHYSIOLOGY
INTERNATIONAL JOURNAL OF AIR POLLUTION
INTERNATIONAL ABSTRACTS OF BIOLOGICAL SCIENCES (*for Biological and Medical Abstracts Ltd.*)
RHEOLOGY ABSTRACTS
VACUUM
OPERATIONAL RESEARCH QUARTERLY
ANNUALS OF OCCUPATIONAL HYGIENE
ELECTROCHIMICA ACTA
CHILD PYSCHOLOGY AND PSYCHIATRY
JOURNAL OF SMALL ANIMAL PRACTICE
SOLID-STATE PHYSICS
INTERNATIONAL JOURNAL OF MECHANICAL SCIENCES

* *Translations of Russian journals published on behalf of the Pergamon Institute, a division of Pergamon International Corporation*

Leaflets giving further details and subscription rates of each of these journals are available on request

FILED IN
1960
2
1250 65A

THE GEOCHEMICAL SOCIETY

OFFICERS

TOM F. W. BARTH, President
HAROLD C. UREY, Vice-President

KONRAD B. KRAUSKOPF, Secretary
GEORGE T. FAUST, Treasurer

COUNCILLORS

E. F. OSBORN, 1958–1960
H. G. THODE, 1958–1960
ALBERT E. J. ENGEL, 1959–1961

FRIEDRICH G. HONTERMANS, 1959–1961
RALPH CANNON, 1960–1962
TH. G. SAHAMA, 1960–1962

REGIONAL VICE-PRESIDENTS

LOUIS H. AHRENS
RUI RIBEIRO FRANCO
ING. GEORGES ORDOÑEZ

C. W. CORRENS
J. F. LOVERING
KEN SUGAWARA

COMMITTEES

Auditing Committee:
JOSEPH J. TREGONING, Chairman
WILLIAM L. HILL
C. R. NASSER

Constitution and By-Laws Committee:
MICHAEL FLEISCHER, Chairman
JULIAN R. GOLDSMITH
DENIS M. SHAW

Education Committee:
H. D. HOLLAND, Chairman
J. A. S. ADAMS
D. M. HENDERSON
KURT E. LOWE
G. D. NICHOLLS
HANS P. EUGSTER

Membership Committee:
R. M. GARRELS, Chairman
HARVEY C. DIEBL
CHESTER B. SLAWSON
JAMES E. SLOSSON
IRVING BREGER

Nominating Committee:
WM. T. PECORA, Chairman
T. G. SAHAMA
C. E. TILLEY
G. TUNELL

Programme Committee:
H. T. EVANS, Chairman
GORDON J. F. MACDONALD
H. E. LOWENSTAM

Publications Committee:
E. W. HEINRICH, Chairman
JULIAN R. GOLDSMITH
JOHN C. MAXWELL
N. W. RAKESTRAW
S. C. ROBINSON
L. R. WAGER
EARL INGERSON

Research Committee:
C. G. DODD, Chairman
W. F. BRADLEY
R. A. ROWLAND
T. G. THOMPSON

Russian Translations Committee:
EARL INGERSON

Standards Committee:
ALVIN VAN VALKENBERG, Chairman
MICHAEL FLEISCHER
LOREN STIEFF
GEORGE SWITZER
GEORGE TILTON

Tellers Committee:
CHARLES MEYER, Chairman
HENRY R. CORNWALL
COLIN O. HUTTON